MODELLING OF THE PHASE CHANGE KINETICS OF COCOA BUTTER IN CHOCOLATE AND APPLICATION TO CONFECTIONERY MANUFACTURING

by

BENJAMIN JEAN DIDIER LE RÉVÉREND

A thesis submitted to
The University of Birmingham
for the degree of
DOCTOR OF PHILOSOPHY

School of Chemical Engineering
The University of Birmingham
December 2009

Abstract

Efforts have been devoted over the last decades towards modelling phase change kinetics of fats in chocolate. The fats in chocolate have a number of crystal forms and manufacturers must deliver a product with the right polymorph to the consumer.

In this work a simplified mathematical model was developed that clusters six polymorphs into two, namely *stable* and *unstable*, depending on their Differential Scanning Calorimetry (DSC) and X-Ray Diffraction (XRD) characteristics. This simplification allowed the phase change kinetics to be estimated from a set of DSC experiments conducted at different cooling and heating rates.

The phase change reactions were coupled with the heat transfer equation and used to model temperature profiles and concentration of polymorphs in a model geometry. The model was able to predict both the temperature profiles measured by thermocouples (±2°C) and the fat crystals concentration as measured using XRD (±10%) at various locations in a chocolate slab.

The model was applied to the recently developed processes using very high cooling rates such as the FrozenCone process, to explain their capabilities to produce ”good” chocolate in spite of the high cooling rates used. Such modelling was not possible with existing models, which usually deal with either heat transfer or isothermal crystallisation kinetics.

The main outcomes of this work are (*i*) the coupling of the reactions kinetics with heat transfer which can be expanded to other processes, (*ii*) the novel XRD method and (*iii*) the application to fast cooling processes and their explanation.

à mes amours, Fanny et Grégoire

ACKNOWLEDGEMENTS

I would like to take the opportunity which is given to me here to thank my supervisors, Pr Peter Fryer and Dr Serafim Bakalis for their guidance during my research project and during the writing of this manuscript. My gratitude also goes to Magna Specialists Confectioners Ltd. and EPSRC for their financial support.

I would also like to thank the rest of the research team on Food and Microstructure of Soft Matter Engineering at the Department of Chemical Engineering at the University of Birmingham for their help during the last three years. A special thank goes to Pr Ian Norton for his support.

Je souhaite également remercier mon père, Didier, pour m'avoir orienté vers une carrière d'ingénieur et ma mère, Brigitte, pour ses précieux conseils sur le fonctionnement des industries alimentaires et la valeur d'un doctorat en sciences alimentaires. J'espère qu'ils trouveront dans cette thèse la récompense des efforts consentis pour mon éducation. Je remercie mon frère Guillaume pour avoir su temperer mes ardeurs scientifiques en me rappelant que le chocolat était avant tout un délice.

Enfin, je remercie infiniment ma femme, Fanny, pour sa patience lors de la rédaction de cette thèse et mon fils, Grégoire, pour ses sourires.

NOMENCLATURE

Roman Symbols

$[xxxx]$	Concentration (molar fraction) of phase $xxxx$ (no units)
ΔH	Latent heat of a phase change $(J \cdot kg^{-1})$
$\dot{Q}_{source}$	Source term of the heat transfer equation $(J \cdot m^{-3})$
Bi	Biot number
Cp	Specific heat capacity $(J \cdot g^{-1} \cdot K^{-1})$
Cp_{eff}	Effective specific heat capacity $(J \cdot kg^{-1} \cdot^{\circ} \mathrm{C}^{-3})$
d	Characteristic distance (m)
e	Thickness (m)
Fo	Fourier number
G	Gibbs free energy (J)
H	Molar enthalpy (J)
h	Heat transfer coefficient $(W \cdot m^{-2} \cdot K^{-1})$
K	Kinetic rate of a phase change (maximum value independent of T) s^{-1}
k	Thermal conductivity $(W \cdot m^{-1} \cdot^{\circ} \mathrm{C}^{-1})$

k_{ii}	Kinetic rate of a phase change (dependent of T) s^{-1}
S	Molar entropy $(J \cdot K^{-1})$
stable	Family of crystals consisting of form V and VI of cocoa butter
T	Temperature (K or °C)
t	time (s)
t_f	Freezing time proceeding form the Planck equation (s)
U	Dimensionless temperature
unstable	Family of crystals consisting of form I, II, III and IV of cocoa butter
x	Distance measured from the surface in contact with the plunger (m)

Greek Symbols

$\alpha\ \gamma\ \beta'\&\beta$	Fat polymorphs
α	Thermal diffusivity $(m^2 \cdot s^{-1})$
η	Viscosity of chocolate $(Pa \cdot s)$
Γ	Boundary of a (sub)domain
λ	Wavelength of an X Ray source (Å)
$\nabla \cdot$	Divergence operator div
∇	Gradient operator $\vec{grad}$
Ω	Volume of a (sub)domain
ρ	Density $(kg \cdot m^{-3})$
θ	Diffraction angle of X Rays (°)

Subscripts

ms	Melting of *stable* crystals to *melt*
mu	Crystal growth of *unstable* crystals from *melt*
nuc	Nucleation of *unstable* crystals from *melt*
sm	Crystal growth of *stable* crystals from *melt*
um	Melting of *stable* crystals to *melt*
us	Polymorphous transition from *unstable* to *stable*
CT	Relative to the cooling tunnels
FC	Relative to the cold plunger (FrozenCone)
filling	Relative to the filling of the eggs
Insulator	Relative to the insulator stage side to the PCR
mould	Relative to the egg shell moulds
Peltier	Relative to the Peltier stage side of the PCR
shell	Relative to the egg shells

Acronyms

MAX	Maximum error between the model prediction and experimental data (°C)
$RMSE$	Round Mean Square Error (Deviation)
AMF	Anhydrous Milk Fat
DSC	Differential Scanning Calorimetry
PCR	Peltier Chocolate Rig

SFC	Solid Fat Content
TAG	TriAcylGlycerol
XRD	X Ray Diffraction

TABLE OF CONTENTS

LIST OF ILLUSTRATIONS

LIST OF TABLES

CHAPTER 1

INTRODUCTION

1.1 Context of the study

Chocolate manufacturing is a complex process which combines several unit operations. One of the critical steps is the final cooling step which must be well controlled to ensure that the crystal structure formed throughout the product is stable and will not be altered during storage. Any alteration to the structure is likely to cause blooming (Ali, Selamat, Man et al. 2001, Hartel and Bricknell 1998, Rousseau and Smith 2008), a coating of fat at the surface of the product unappealing to the consumer.

Traditional chocolate cooling is slow and typical cooling rates are between 5°C $\cdot min^{-1}$ at the surface and 0.1°C $\cdot min^{-1}$ at the centre. This difference in cooling rates is due to the low thermal conductivity ($k \approx 0.3W \cdot m^{-1} \cdot^{\circ} \mathrm{C}^{\ -1}$) of chocolate (Stapley, Tewkesbury and Fryer 1999), leading to a typical overall cooling time of several hours.

In the Easter egg manufacturing business, traditional technology can lead to inconsistency in production, in particular in the shapes of the final products (see section 1.2.3). However the slow cooling rates applied ensure proper crystallisation throughout the process.

The company sponsoring this work, Magna, invested in manufacturing lines using the FrozenCone (Aasted, Denmark) (Aasted 2003) process in 2004. This process consists of plunging a cold stamp into molten tempered chocolate cooling it very rapidly. However according to the published literature the cooling rates proceeding from this technique should not lead to the right crystal structure for the cocoa butter present in the chocolate.

Magna produces on some of their lines up to 1,000,000 mini eggs per day. These chocolates are perfectly acceptable to the consumer and exhibit the right crystal structure. In this respect, the conventional view of chocolate manufacture is incorrect, therefore it is a challenge to obtain a fundamental understanding of the process.

1.2 Chocolate processing

1.2.1 History of chocolate processing

It is believed that the Mayas, 2600 years ago, were already drinking chocolate. At this time, chocolate was consumed in America as a sweet and spicy beverage, seasoned with chili pepper, vanilla and pimiento. The beverage was expensive and thus reserved to elites, and cocoa was even often used as a currency. The story of chocolate in Europe begins with the discovery of America and Christopher Columbus brought some chocolate back to Spain for Queen Isabella, but Hernando De Soto introduced it much more broadly (Field-Museum ND).

In the 18th century, a serial of inventions led to the chocolate as we know it today:

- Daniel Peter proposed in 1875, after 8 years of research, his newly developed milk chocolate assisted by his baby food manufacturer neighbour Henri Nestlé;
- Rudolph Lindt invented the conching process, an additional step to decrease the

average size of particles in the blend.

The different tastes and types of chocolate reflect the histories of the industry in different parts of the world, and the tastes of different peoples.

1.2.2 Description of the chocolate process

A list of ingredients for chocolate manufacturing is shown in table 1.1.

One can see that the most basic chocolate recipe is dark chocolate, containing only cocoa solids (mass and butter) and sugar. For the manufacturing of milk chocolate, milk powder, milk fat and eventually vanilla are added. Milk chocolate typically contains more sugar than dark chocolate and therefore contains less cocoa solids. White chocolate is a blend of cocoa butter, sugar and vanilla, which makes it not to be considered as chocolate by connoisseurs due to the lack of cocoa mass. Chocolate also contains emulsifiers to stabilize the blend of the hydrophilic sugar and the hydrophobic fats.

A typical manufacturing process is shown in figure 1.1 (Beckett 2002, Beckett 1989) and can be described as follows:

1. Cocoa beans are first harvested from the cocoa trees.
2. The crops are fermented. During this operation the flavour development is initiated.
3. The fermented cocoa beans are cleaned.
4. The cocoa beans are roasted to continue the flavour development.
5. The shell of the beans is cracked and removed allowing extraction of the cocoa nibs.
6. The cocoa nibs are then finely ground (to achieve a particle size of $150\mu m$). This operation leads to the production of cocoa mass (or cocoa liquor).

7. Three pathways can be used from here:

   (a) The cocoa mass can be pressed to produce cocoa butter and cocoa powder. The filtrate is the cocoa butter and the press cake is broken into lumps and ground to make cocoa powder.

   (b) The cocoa mass can be mixed with other ingredients such as cocoa butter, sugar, vanilla, milk fat, milk powder (or evaporated liquid milk) and an emulsifier (typically soya lecithin and/or PolyGlycerol PolyRicinoleate). A further grinding (refining) and dehydration of the mixture leads to the formation of aggregates called crumb. The chocolate crumb can then be mixed with cocoa butter or another compatible fat to produce chocolate.
   Chocolate crumb has found a wide acceptance in chocolate manufacturing since it just needs to be mixed with cocoa butter to produce chocolate (Lees and Jackson 1979). It was also found that the chocolate made from crumb was harder than chocolate made from the same ingredients without this dehydration process. Reducing reactions during the dehydration process are thought to produce additional flavours. A model of flavour development during the drying process of chocolate crumb has been developed and showed good agreement with experimental data (Edmondson, Grammatika, Fryer et al. 2005).

   (c) The cocoa mass can be mixed with other ingredients such as cocoa butter, sugar, vanilla, milk fat, milk powder and an emulsifier (typically soya lecithin or PGPR). The typical method is to mill the solid ingredients together (sugar, milk powder and/or crumb) and then mix them with the liquid ingredients (cocoa liquor, cocoa butter, milk fat and lecithin). This method leads to different flavours than if all the ingredients are mixed together. Further grinding (refining) and conching operations are required to produce a smooth liquid chocolate having a particle size of $20\mu m$ which is inferior to the minimum size required for detection of particles by the tongue (Vaisey-Genser, Vane and

Johnson 1989).

1.2.3 Chocolate moulding processes

Traditional moulding and cooling towards solidification involves cooling tunnels where cocoa butter is set slowly (usually around 0.5°C $\cdot min^{-1}$) to crystallise under the right microstructure. This process is represented by figure 1.2(a) and consists of the following steps:

1. Freshly tempered chocolate is deposited into the moulds.
2. The chocolate is cooled from the mould side to crystallise at the interface between the mould and the chocolate.
3. The mould is turned upside down and the chocolate which is not set flows to be reworked (molten and tempered).
4. A filling can be injected.
5. Molten (tempered) chocolate is used to close the sweet, or two entities can be stuck together to from an egg.
6. The chocolate is finally set in a cooling tunnel.

This process is not very efficient since most of the chocolate used has to be reworked and the internal shape is controlled by the flow properties of the chocolate at the end of the first step. This can result in under or over filling because the volume of filling required is not constant due to the random character of the shell crystallisation. Moreover it is difficult to maintain the same thickness for the whole shell.

Recently several rapid cooling processes such as FrozenCone (Aasted 2003) have been developed to address these problems. The process is presented in figure 1.2(b).

It consists of a cold press (as low as -30°C) which is stamped into molten chocolate (freshly tempered) for a very short time ($\approx 3s$) to give it the desired shape. The process consists of the following operations:

1. Freshly tempered chocolate is injected into the moulds at a temperature around 30°C .
2. The cold press at a typical temperature of -10°C is applied into the molten chocolate for a short time ($\approx 3s$). This time is enough to cool the chocolate at the surface and crystallise it partially. Using this technique it is possible to give almost any shape to the sweet and to control the external shape (mould) as well as the internal shape (cold stamp).
3. The chocolate is then conveyed in a first cooling tunnel where it sets completely.
4. A filling can then be injected if needed.
5. A second cooling tunnel is used to cool the filling.
6. The sweet is closed either by applying molten (tempered) chocolate at the surface or by assembling two of the entities together (typical of the Easter egg process where the rim is reheated).
7. A final cooling tunnel sets the chocolate used to close the sweet.

The largest application is probably for Easter eggs where half eggs are made using this technique. The advantages of this technique are that the process time are reduced and the volume of the egg shells can be kept constant to very tight tolerances. However as explained below, the crystal structure of cocoa butter is dependent on the cooling rates applied during cooling. As the cooling rates applied are very high (locally up to -100°C $\cdot min^{-1}$), the formation of unstable crystal structures can occur.

1.3 Structure of chocolate

1.3.1 Composition of chocolate

Chocolate is a complex product, as it results from the emulsification of hydrophilic cocoa powder and sugar in a fat matrix (Ollivon 2004). This continuous matrix of fats is responsible for most of the physical (and therefore sensory) attributes of chocolate. The hardness of chocolate can be related to the Solid Fat Content (SFC) of the fat matrix (Braipson-Danthine and Deroanne 2004).

The melting point of the fats are responsible for the smooth texture in mouth or of a certain grittiness if it does not melt at the right temperature, hence the need for the right cocoa butter (or fat mixture) polymorph to be delivered to the consumer in the final product.

1.3.2 Microstructure and polymorphism of cocoa butter

Cocoa butter is a blend of TriAcylGlycerols (TAGs), which result from the triple esterification of glycerol with three fatty acids. A typical TAG molecule is presented in figure 1.3(a) where R1, R2 and R3 represent the different fatty acids attached to the glycerol core.

Due to its homogeneous TAG composition, cocoa butter can almost be considered as a pure material (Ollivon 2004). More than 80% of the total TAGs are mostly symmetric and made of the Palmitic (P) $C16:0$, Stearic (S) $C18:0$ and Oleic (O) $C18:1$ acids which have very similar chain length (Loisel et al. 1998). A typical composition is POS (36.6%), SOS (27.3%) and POP (17.0%).

Cocoa butter and most fats exists under different crystal forms also called polymorphs.

The most stable polymorph for a set of pressure and temperature is the one for which the Gibbs free energy G defined by equation (1.1) is minimal. The free energy (G) is determined by the molar enthalpy (H), the molar entropy (S) and the temperature (T) (Bassani, Liedl and Wyder 2004).

$$G = H - T \cdot S \tag{1.1}$$

The polymorphism of fats in general was extensively studied during the first half of the XX^{th} century (Lutton 1950, Malkin and Meara 1939) using two analytical techniques: Differential Scanning Calorimetry and X-Ray Diffraction.

Differential Scanning Calorimetry (DSC)

DSC is the method typically used to study thermal changes in foods. It has been used to study cocoa butter crystallisation and melting either pure or in chocolate (Cebula and Smith 1991, Dimick and Manning 1987, Fessas, Signorelli and Schiraldi 2005, Md.Ali and Dimick 1994, Merken and Vaeck 1980, Sonoda, Takata, Ueno et al. 2004) (non exhaustive list).

The principle of a power compensation DSC is that a reference pan (containing only air in our case) and a pan containing the sample are kept at the same temperature during an isothermal or temperature ramp experiment. Two separate heaters (one for each pan) and an external cooling system (*e.g.* liquid nitrogen) are used to maintain the pans at the same temperature. A typical compensation DSC layout is presented in figure 1.4.

During a temperature scan experiment without sample phase change, the difference in heat applied to the sample compared to the empty pan is the specific heat capacity of the material ($Cp\,(J \cdot kg{^\circ}\mathrm{C}^{\ -1})$), which can usually be considered constant over a small temperature range (≈ 50°C).

When a phase change (crystallisation, melting or glass transition) occurs, the energy needed to maintain both samples at the same temperature is affected by the latent heat (ΔH) of the phase change, this latent heat can therefore be measured by DSC. If the specific heat capacity is calculated via the built in software, then it is not a constant value, it evolves with temperature and is called effective specific heat capacity (Cp_{eff}).

X-Ray Diffraction (XRD)

XRD has been the method of choice to study the polymorphism of cocoa butter and fats in general (Sato 2001, Schenk and Peschar 2004, Sonoda et al. 2004, Szydlowska-Czerniak, Karlovits, Lach et al. 2005, Wille and Lutton 1966) (non exhaustive list).

The principles of crystallography were initially presented by the Braggs (father and son) and they were attributed the Nobel prize in 1915 *"for their services in the analysis of crystal structure by means of X-rays"* (Bragg 1923). Their idea is that if a monochromatic beam of X-rays, of wavelength λ (nm), under a variable incident angle θ (°), is applied on the parallel and uniformly spaced (d (Å)) plane of a crystal, this beam is diffracted in all directions. (Bragg 1929, Bragg 1913, Bragg and Thomson 1914).

The phase (and therefore the intensity of the diffracted beam) is a function of the incident angle between the beam and the crystal plane. This can be demonstrated mathematically using figure 1.5(b) where the phase between the rays is the difference between the two parallel paths and is:

$$AB + BC - AC'$$

it can be shown using the Pythagorean theorem that:

$$AB = BC = \frac{d}{sin(\theta)} \text{ and } AC = \frac{2 \cdot d}{tan(\theta)}$$

as well as:

$$AC' = AC \cdot cos(\theta) = \frac{2 \cdot d}{tan(\theta)} \cdot cos(\theta).$$

The interference is constructive if the phase is an integer of the wavelength or:

$$AB + BC - AC' = \frac{2 \cdot d}{sin(\theta)} - \frac{2 \cdot d}{tan(\theta)} \cdot cos(\theta) \ = n \cdot \lambda$$

which leads to equation (1.2) which is known as Bragg's equation.

$$2 \cdot d \cdot sin(\theta) = n \cdot \lambda \tag{1.2}$$

where n is the order of diffraction (generally $n = 1$).

Initially, it was thought that there was only three polymorphs (α, β' and β) classified using their respective melting points (Malkin and Meara 1939). However, Larsson (Larsson 1966) showed, using X-Ray diffraction data and thermal analysis techniques, that a fourth "intermediate" form showing similar spacings to β' or β could be determined. He concluded that in complex fat mixtures (such as margarine for example), one should expect four polymorphs named α, β', β_2 and β_1 by increasing order of stability.

The α, β' and β crystal structures are presented in figure 1.3(b) and can be described as:

1. α: H (hexagonal) is the most loose configuration. The acyl groups are oriented at 90° to the plane of the methyl group and rotate freely. A typical XRD pattern shows a dominant peak at ≈ 4.15Å. The TAGs are in the tuning fork configuration which explains the free rotation (Min 2008). This tuning fork configuration is shown for the *alpha* form on figure 1.6.

2. β': $O_{\perp}$ (orthorhombic) where a typical XRD pattern shows dominant peaks at ≈ 4.20Å and ≈ 3.80Å. In this case the acyl groups are tilted by an angle of $68-70°$

to the plane of the methyl group.

3. β: $T_{\parallel}$ (triclinic) is the most ordered and closely packed configuration. A typical XRD patterns show a peak at ≈ 4.60Å and other weaker peaks (hence the need for more than a single β form). In this case the acyl chains are tilted by an angle of 59° to the plane of the methyl end group. The TAGs are usually in the chair configuration as in 1.3(c), which explains the denser packing and smaller mobility.

The crystal structure of PPP (a single TAG) is presented in figure 1.6. Three different polymorphs were found (Sato 2001), as described by Malkin. One can see how the packing increases with the evolution from the least to the most stable polymorphs. The α form is present in a loose tuning fork configuration allowing mobility between the molecules, while β' and β are present in a double chain length packing of chair configuration which is more dense and stable (as expected from the lower G value).

The polymorphism of cocoa butter is also very well documented. It was first proposed by Wille and Lutton (1966) that solid cocoa butter could exist as six different polymorphs, numbered from I to VI. The X-Ray diffraction patterns are shown in figure 1.7. The spacings reported by the authors are presented in table 1.2. The d spacings reported for cocoa butter can be linked to the $2 \cdot \theta$ angle reported on figure 1.7 using the Bragg's equation (1.2).

For example in table 1.2, the d spacings reported for form I of cocoa butter are 4.19 and 3.70Å. Using equation (1.2) one can find that:

$$\theta = asin(\frac{\lambda_{Cu}}{2 \cdot d})$$

which leads to $2 \cdot \theta = 21.2$ and 24.0°, respectively ($\lambda_{Cu} = 1.5405$Å). These values are the ones found on figure 1.7 for form I.

The melting points and enthalpies of the different polymorphs of cocoa butter have been extensively measured (Fessas et al. 2005, Loisel et al. 1998, Wille and Lutton 1966) and are reported in table 1.3 and on figure 1.7. More recently other authors have reported only five different polymorphs, omitting form $\beta' III$ (Schenk and Peschar 2004). One could sum up the polymorphs of cocoa butter as:

- Form I (γ) is the most unstable polymorph ($sub - \alpha$) and melts around 14°C and the XRD pattern shows a very strong peak at 4.18Å.
- Form II (α) melts around 20°C and the XRD pattern shows a very strong peak at 4.20Å.
- Form III (β') is a polymorph thought to be the mixture of form II and IV and melts around 22°C . The XRD pattern shows a very strong peak at 4.20Å. It can be differentiated from form II by the long spacing diffraction pattern.
- Form IV (β') melts around 24°C and the XRD pattern shows two strong peaks at 4.13Å and 4.32Å.
- Form V (β) melts around 29°C and the XRD pattern shows a very strong peak at 4.58Å. It melts easily at mouth temperature and not in the hands and is therefore the preferred polymorph for maximum consumer satisfaction. A method exists to make sure only the form V of cocoa butter is crystallized during the solidification process of chocolate, it is called tempering (*cf.* 1.3.5).
- Form VI (β) melts around 32°C and the XRD pattern shows a very strong peak at 4.59Å and its pattern differs from form V only by the lack of a mid intensity peak at 3.75Å.

1.3.3 Crystallisation of cocoa butter

The solidification of chocolate is due to the crystallisation of cocoa butter. Crystallisation proceeds from two different phases; nucleation and growth.

The nucleation behaviour of fats is heterogeneous (Metin and Hartel 2005) and is promoted by irregularities in the melt (*e.g.* rough surface of the apparatus used, dust particles) that decrease the free energy (activation) required. Secondary nucleation can also occur when a large crystal is fractured during processing.

Over a certain size, nuclei become active growth crystals. Growth of a crystal requires that molecules migrate from the melt to the surface of a the crystal and find its way on the crystal lattice. Growth is therefore resulting in the same release of latent heat as nucleation. This growth phase is slower than the nucleation phase (Metin and Hartel 2005) and this can be explained by two factors:

1. The crystal growth requires the organization of a structure and therefore a long time is needed for the TAG molecule to fit in the crystal lattice.
2. A competition between different TAGs might happen for a similar spot in the crystal lattice. This competition consumes time and this is why multicomponent fats crystallize more slowly than pure compounds (fat eutectic).

When the equilibrium between the solid and the liquid fat is achieved, the growth stops and it is the end of the crystallisation.

As already explained, cocoa butter, once solid, can exist under different polymorphs. It was demonstrated that a fast cooling rate ($> 2°\text{C} \cdot min^{-1}$) leads to the formation of low melting point polymorphs (Stapley et al. 1999). Indeed, fast cooling rates imply a shorter residence time at a given temperature for the crystal lattice to form, resulting in a less structured organization of the TAGs. These low melting point polymorphs can then be reorganized into more stable polymorphs (Himawan, Starov and Stapley 2006, Le Révérend, Bakalis and Fryer 2008). This has been shown using DSC (Fessas et al. 2005) by deconvoluting the enthalpy signal into individual peaks, each peak being attributed to an individual polymorph and by using time and temperature resolved XRD (Loisel et al. 1998).

1.3.4 Impact of fat blending on macroscopic properties

As explained above, cocoa butter is a blend of different TAG. Due to its composition rich in POP, SOS and POS which all have similar chain length, cocoa butter melts and crystallises with very sharp peak when observed using a DSC, as if it was a pure compound. However, cocoa butter with different origins have different TAG composition and this can lead to differences in their phase change properties.

An example of this is illustrated by table 1.4 and figure 1.8. In figure 1.8 one can see that for a given temperature, the Solid Fat Content ($SFC = \frac{\text{mass of crystallised fat}}{\text{total mass of fat}}$) of the Brazilian cocoa butter is always lower than for the Ghanaian and Malaysian. This can be related to the TAG composition of these cocoa butters presented in table 1.4. The Malaysian and Ghanaian cocoa butter are homogeneous and rich in SOS ($[SOS] \approx 84\%$ and $[SOS] \approx 76.8\%$). The Brazilian cocoa butter is more heterogeneous ($[SOS] \approx 63.7\%$ and $[SOO] \approx 17.9\%$). SOO, being liquid at room temperature, contributes to the low SFC of the Brazilian cocoa butter.

Vegetable fats

When different fats are blended, the behaviour of this mixture is not the (weighted) average of the behaviour of the individual components. This phenomenon is illustrated on figure 1.9 which show how the actual SFC of a blend of cocoa butter and filling fat evolves depending on the mass fraction of individual components. Because interactions between the different fats modify the crystallisation properties, the measured SFC (continuous line) is lower than the SFC expected from an ideal mixture (dotted line). Mathematically, this phenomenon can be described by equation 1.3:

$$SFC_{X_{Fat_1}+X_{Fat_2}} \leq X_{Fat_2} \cdot SFC_{Fat_1} + X_{Fat_2} \cdot SFC_{Fat_2} \tag{1.3}$$

where X_i is the mass fraction of component i.

The deviation from the ideal mixture is more pronounced as dissimilar TAGs are used. As such, the fats the more appropriate for blending with cocoa butter should then have a similar TAG composition and crystallising behaviour. The list of the attributes for a typical cocoa butter equivalent was given by Beckett (Beckett 1989):

1. It must have a similar melting range compared to cocoa butter.
2. It should have a similar TAG composition compared to cocoa butter
3. It must be compatible with cocoa butter.
4. It should be processable in the same way as cocoa butter.
5. The fat should crystallize in a β form.
6. Its appearance and resistance to bloom when used in chocolate products should be as good as products made of pure cocoa butter.
7. It should have a stable flavour during processing.

The use of such equivalents in chocolate and cocoa based products is, in the European Union, governed by Directive 2000/36/EC (European Parliament 2000). Replacement of cocoa butter by vegetable fats is authorised up to 5% of the total weight, provided that their labelling indicates that "Contains vegetable fats in addition to cocoa butter". Six vegetable fats (so called cocoa butter equivalents, CBEs), clearly specified in Annex II of the Directive, can be used singly or in blends: illipé (*Shorea spp.*); palm oil (*Elaeis guineensis, Elaeis olifera*); sal (*Shorea robusta*); shea (*Butyrospermum parkii*); kokum gurgi (*Garcinia indica*); and mango kernel (*Mangifera indica*).

A range of studies aiming at the detection of these cocoa butter equivalents in chocolate have been published (Buchgraber, Androni and Anklam 2007, Buchgraber, Ulberth and Anklam 2004). The detection techniques are based on gas liquid chromatography of the melted fat blend to separate the different TAGs. By comparing the TAG composition with reference samples of cocoa butter and the six authorized equivalents, it was possible to detect eventual frauds.

Milk fat

Besides vegetable fats, in typical formulations, milk is added. The impact of milk fats on the cocoa butter crystallization is therefore of great industrial significance. Milk fat has a much more heterogeneous composition than cocoa butter, with a SFC at 20°C of about 20%. At room temperature most of the Anhydrous Milk Fat (AMF) is still liquid, resulting in small interaction with the crystallized cocoa butter (Beckett 1989). Moreover, the high melting fraction of AMF ($\approx 20\%$ solid at room temperature) is rich in P, O and S fatty acids (esterified with glycerol to form TAGs) and has therefore a TAG composition similar to cocoa butter. The solid fraction of milk fat is therefore compatible with cocoa butter while its liquid fraction has little interaction with it.

Because of this low SFC, cocoa butter mixed with AMF exhibits similar properties to the Brazilian cocoa butter mentioned in 1.3.4. It has a lower viscosity and the melting points measured with DSC are reduced (Chapman et al. 1971), as presented in table 1.5.

Due to these properties, milk fat was found to be a good bloom inhibitor (*cf.* section 1.3.6).

1.3.5 Tempering

Tempering is the processing step during which the nuclei of the desired form (form V) of cocoa butter are crystallised from the melt (Loisel, Keller, Lecq et al. 1997a, Seguine 1991). When delivered to the consumer, the cocoa butter contained in chocolate should be in the $\beta(V)$ polymorph, as only this polymorph has the acceptable melting behaviour (Ollivon 2004). Cocoa butter, when crystallized directly from melt without tempering, will crystallise in an α or β' form (Chapman et al. 1971, Loisel et al. 1997a). To ensure only the β polymorph is present, the following steps are commonly used in industry (Beckett 1989):

1. Melt the fats completely, usually by heating the chocolate up to 60°C .
2. Cool the chocolate down to initiate crystallisation by nucleating different polymorphs and beginning crystal growth.
3. Because different polymorphs are randomly nucleated during the cooling stage, it is necessary to heat up the chocolate to a temperature where only $\beta(V)$ crystals will be present (the $\beta(V)$ polymorph is the most stable polymorph crystallizable directly from melt). This will ensure that only $\beta(V)$ crystals will be present in the final product (Chapman et al. 1971, Loisel et al. 1997a).

The process parameters influencing the tempering process are (*i*) the temperature profile and (*ii*) the shear applied to the chocolate (Stapley et al. 1999). It was found that the factors promoting proper tempering are (*i*) a long hold time ($400s$) at the cooling temperature of 22°C , (*ii*) a high shear rate $> 35s^{-1}$ and (*iii*) a reheating temperature below 33°C . Traditional tempering is carried out on a marble table by trained chocolatiers and resembles probably more to art than process engineering. The chocolatiers apply shear to the chocolate by scraping it on the marble. The temperature of the marble is also important since it controls the crystallisation rate.

To reproduce this process on a larger scale, device such as the one presented in figure 1.10 are used, with the following steps:

1. Chocolate is first cooled gently in zone I and a first nucleation occurs ($T \approx 22-24$°C).
2. In zone K, the very low temperature ensures that a consequent number of crystal are formed ($T \approx 16-18$°C).
3. In zone II chocolate is heated to melt the low melting point polymorphs ($T \approx 28-31$°C).

These designs allow industry to produce tempered chocolate quicker by using lower temperatures than traditional marble tempering. One can notice the use of stirring blades to shear the chocolate which is essential for successful tempering. To reproduce this shear on a lab scale, the action of shear during tempering has been extensively studied using concentric cylinders tempering geometries (Bolliger et al. 1998, Loisel et al. 1997a, Stapley et al. 1999).

The typical amount of form V nuclei present in the melt at the end of a tempering process is between 0.5% and 3% (Metin and Hartel 2005).

1.3.6 Blooming

Bloom refers to the white coating at the surface of badly aged chocolate coming from the presence of pure fat crystallised on the surface of the product. Bloom is a defect in the sense that it is visually unappealing to the consumer. Blooming is commonly associated with a lack of tempering but not necessarily. Recent studies have shown that bloom (or dull) can occur for both tempered and untempered chocolate (Lonchampt and

Hartel 2006, Lonchampt and Hartel 2004, Stapley et al. 1999). Examples of bloom are presented on figure 1.11.

For untempered chocolate, the blooming essentially comes from the transition from low melting point polymorphs (thermally unstable crystals α or β') to high melting point polymorphs (usually βVI). During this transition, the material mobility is increased and the migration of fat crystals to the surface is facilitated.

For tempered chocolate the different causes of blooming are (Lonchampt and Hartel 2004):

1. fluctuations of temperature around the melting point of form V;
2. storage to a temperature which is higher than the melting point of form V (31°C);
3. migration of some liquid fat components from the filling in the centre of the product;
4. formulation problems such as the blending of fats which are incompatible (fatty acids with very different lengths).

The mechanisms proposed for the migration of fats to the surface are diffusion and capillary flow (Aguilera, Michel and Mayor 2004). These authors fitted the kinetics of the migration against the Lucas-Washburn equation of capillary rise and good agreement was found between the model and available data. The only explanation for the existence of capillaries in chocolate could come from the appearance of micro-fractures due to thermal stress during the solidification (Tremeac, Datta, Hayert et al. 2007) leading to a network of interconnected pores available for the liquid fat to migrate and crystallise at the surface of the product.

This hypothesis is supported by other studies (Loisel, Lecq, Ponchel et al. 1997b) where a network of cavities occupying between 1% and 4% of the total volume was demonstrated using mercury porosimetry. Such pores have also been investigated at the surface of chocolate using Atomic Force Microscopy (AFM) (Rousseau and Smith 2008). This study showed the existence of a range of cavities in chocolate to support the existence of a capillary flow, but also gave evidence that diffusion was likely to be the cause of blooming in filled chocolates.

The softening effect of milk fats on chocolate could be the cause of the reduction of these fractures explaining the anti-bloom effect of milk fats in chocolate (Lonchampt and Hartel 2004, Walter and Cornillon 2001).

1.4 Description of phase change of fat systems using mathematical models

To simulate phase change kinetics in fat systems, different models have been used, commonly assuming crystallisation as an isothermal transformation.

1.4.1 The Avrami model

The Avrami model (Avrami 1941, Avrami 1940, Avrami 1939) is the most widely used to describe isothermal phase change kinetics. It is a probabilistic model based on the hypothesis that crystallisation occurs because of the presence of crystal nuclei initially present in the melt (in our case these typically proceed from the tempering stage). Nuclei can then:

1. become active growth nuclei with a probability p.
2. be "swallowed" by another active growth nuclei.

Following these assumptions, the fraction of crystallised matter S evolves with time t as follows:

$$S = a \cdot (1 - e^{-k \cdot t^m}) \tag{1.4}$$

where m depends on the growth morphology (linear, plate or spherical), k depends on the nucleation mode and rate and a is the total amount crystallised when equilibrium is reached. m should only take integer values, however when experiments are fitted to the model it is not uncommon to obtain non integer values. Foubert (Foubert 2003) formulated the following hypothesis:

1. nucleation rate is not constant and varies during the process.
2. growth morphology changes during the process.

The dependency of these parameters on external factors such as temperature is possible and can explain the deviations of the model against experimental data.

1.4.2 The Gompertz model

Researchers have also used the Gompertz model, initially developed for microorganism population growth, to model fat crystallisation (Kloek, Walstra and van Vliet 2000). The Gompertz model can be expressed as:

$$S = a \cdot e^{-e^{\frac{\mu \cdot e \cdot (t-\lambda)}{a}+1}} \tag{1.5}$$

where μ is the crystal growth rate and λ the initial time lag.

This model was found to fit the crystallisation kinetics of fully hydrogenated palm oil in sunflower oil mixtures but it fails to provide any fundamental background of the phenomenon.

1.4.3 The Foubert model

The Foubert model has been described extensively in the literature (Foubert 2003, Foubert, Dewettinck, Janssen et al. 2006, Foubert, Dewettinck and Vanrolleghem 2003a, Foubert, Vanrolleghem and Dewettinck 2003b, Foubert, Vanrolleghem, Thas et al. 2005, Foubert, Vanrolleghem, Vanhoutte et al. 2002, Foubert, Vanrolleghem, Thas et al. 2004). This model aims to describe the solid-liquid equilibrium during crystallisation as a chemical equilibrium between two species. Melting is described as a first order reaction and crystallisation as a n^{th} order reaction:

$$\text{Liquid} \underset{K}{\overset{K_n}{\rightleftharpoons}} \text{Solid} \tag{1.6}$$

where K and K_n are the kinetic constants for the reactions. This equation can transformed using kinetic modelling (van Boekel and Tijskens 2001) as:

$$\frac{R}{t} = K_n \cdot R^n - K \cdot R \tag{1.7}$$

where $R = \frac{a-S}{a}$ is the remaining amount of fat to be crystallised. Using fitting on experimental data the values of K_n and K were found to be very similar ($|K_n - K| < 10^{-5}$) and the equation was simplified as:

$$\frac{R}{t} = K \cdot (R^n - R) \tag{1.8}$$

This equation has the advantage of being formulated as an Ordinary Differential Equation (ODE) and could be extended to model non isothermal processes.

Other models have been used to try to model fat crystallisation during non isothermal processes. Other researchers followed a similar route (Fessas et al. 2005) and decided to model the phase change as a set of chemical reactions having their own kinetics. The approach used to get the kinetics was to deconvolve the DSC data to several Gaussian peaks (one per polymorph). The maximum and the area of each peak were respectively set on the melting point and latent heat of fusion of each polymorph from the literature (Loisel et al. 1998). However, the model was not validated against other sets of experimental data.

1.5 Heat transfer in foods

To be able to predict the temperature history of chocolate in an industrial context, the heat transfer equation (Fourier 1822) must be solved with the appropriate initial and boundary conditions as well as physical property information.

1.5.1 Heat transfer equation

The heat flow ($\dot{Q}$) through a surface (A) in a medium where there are no internal movements or moving boundaries can be described as (Incropera and DeWitt 2001, Bimbenet 2002):

$$\dot{Q} = -A \cdot k \cdot \nabla T \tag{1.9}$$

where T is the temperature (K or °C) and k is the thermal conductivity of the material ($W \cdot m^{-1} \cdot K^{-1}$).

Therefore the heat balance in a rectangular parallelepiped of area A (face normal to the heat flow) and thickness dx is:

- the amount of heat going through the face at x is $\dot{Q} = -A \cdot (k \cdot \frac{\partial T}{\partial x})_x$
- the amount of heat going through the face at $x + dx$ is $\dot{Q} = -A \cdot (k \cdot \frac{\partial T}{\partial x})_{x+dx}$
- the amount of heat kept in the volume $A \cdot dx$ is $\frac{A \cdot \rho \cdot Cp \cdot \partial T}{\partial t} \cdot dx$ where t is the time (s), T is the temperature (K or °C), ρ is the density ($kg \cdot m^{-3}$), Cp is the specific

heat capacity ($J \cdot g^{-1} \cdot K^{-1}$).

The heat balance over dt for the volume $A \cdot dx$ is:

$$\frac{A \cdot \rho \cdot Cp \cdot \partial T}{\partial t} \cdot dx = -A \cdot (k \cdot \frac{\partial T}{\partial x})_x - -A \cdot (k \cdot \frac{\partial T}{\partial x})_{x+dx}$$

which gives the heat per unit volume by dividing by $A \cdot dx$:

$$\frac{\rho \cdot Cp \cdot \partial T}{\partial t} = \frac{-(k \cdot \frac{\partial T}{\partial x})_x - -(k \cdot \frac{\partial T}{\partial x})_{x+dx}}{dx}.$$

When dx tends towards 0 the derivative is obtained as:

$$\frac{\rho \cdot Cp \cdot \partial T}{\partial t} = \frac{\partial(k \cdot \frac{\partial T}{\partial x})}{\partial x} = \frac{k \cdot \partial^2 T}{\partial x^2} \text{ if k is constant (isotropic material)}$$

or more generally in 3 dimensions

$$\frac{\rho \cdot Cp \cdot \partial T}{\partial t} = \frac{\partial(k \cdot \frac{\partial T}{\partial x})}{\partial x} + \frac{\partial(k \cdot \frac{\partial T}{\partial y})}{\partial y} + \frac{\partial(k \cdot \frac{\partial T}{\partial z})}{\partial z}.$$

In most processes there is no generation or loss of heat due to internal phenomena but if such processes occur, an additional term $\dot{Q}_{source}$ can be added to obtain the Fourier equation in its most general form. The Fourier equation defines the evolution of temperature in an object (Ω) as:

$$\rho \cdot Cp \cdot \frac{\partial T}{\partial t} = \nabla \cdot (k \cdot \nabla T) + \dot{Q}_{source} \tag{1.10}$$

A set of boundary (Γ) conditions have to be defined to solve equation 1.10. In general two different kinds of boundary conditions are used (Nicolaï, Verboven and Scheerlink 2001):

1. The Dirichlet boundary condition, where the temperature at the boundary (T_Γ) is set:

$$T_\Gamma = T_\infty \tag{1.11}$$

   where T_Γ is the temperature of the boundary (K or °C) and T_∞ is the temperature of the surroundings (K or °C).

2. The Neumann boundary condition is used when the heat flux through the boundary is known:

$$k \cdot \frac{\partial T_\Gamma}{\partial n_\perp} = h \cdot (T_\infty - T_\Gamma) + \epsilon \cdot \sigma \cdot (T_\infty^4 - T_\Gamma^4) \tag{1.12}$$

   where $n_\perp$ is the outward normal to the surface, ϵ is the emission coefficient and σ is the Stefan-Boltzmann constant.

The initial temperature conditions of the system (temperature profile at $t = 0$) must be known to solve equation 1.10.

1.5.2 Application: numerical solutions

Heat transfer is described by the Fourier equation 1.10, which is a Partial Differential Equation (PDE) that can be solved analytically for simple cases (for example infinite plate, semi finite solid, sphere).

For more complex cases, as an analytical solution cannot be obtained, numerical methods have been implemented to approximate temperature profiles. For example finite differences (Ozisik 1994) and finite elements (Gartling and Reddy 1994) have been used to find an approximate solution to equation 1.10. These numerical methods rely on discretizing the geometry using a mesh and solve a system of algebraic equations. These methods have been implemented in commercially available computer codes such as COMSOL Multiphysics, FIDAP and ANSYS Multiphysics that can simplify the solving process.

Heat dissipation and absorption occur as a result of crystallisation and melting of cocoa butter, respectively. The key challenge to predict temperature profiles resides in the estimation of the heat source term. Two different strategies have been used to solve such problems:

Implicit formulation of a source term: the effective specific heat capacity (Cp_{eff})

This approach was used to predict temperature successfully during conventional chocolate cooling (Tewkesbury et al. 2000). For this study, the authors transformed the general Fourier equation 1.10 into a more simple one (1.13), where the source term $\dot{Q}_{source}$ was introduced as part of an effective heat capacity:

$$\rho \cdot Cp_{eff} \cdot \frac{\partial T}{\partial t} = \nabla \cdot k \cdot \nabla T \tag{1.13}$$

The effective heat capacity Cp_{eff} can be calculated as follows:

$$Cp_{eff} = Cp + \dot{Q}_s \cdot \frac{\partial t}{\partial T \cdot \rho} \tag{1.14}$$

using $\dot{Q}_s$ obtained from DSC experiments (Stapley et al. 1999) as a function of temperature and the local cooling rate. The set of experimental data used is presented in figure 1.12

For each time step (t), the temperature (T) and the cooling rate ($\frac{\partial T}{\partial t}$) in each element of the mesh were used to calculate a local $Cp_{eff}(T, \frac{\partial T}{\partial t})$ using the experimental data set (figure 1.12). This Cp_{eff} value was used to calculate the temperature (T) and the cooling rate ($\frac{\partial T}{\partial t}$) for the next time step ($t + dt$). By using this scheme iteratively a solution to the problem can be found. This method is however computationally demanding since the

Cp_{eff} value has to be interpolated for each time step on the whole mesh.

The solution of equation 1.13 using this data set was found to be in good agreement with experimental temperature profiles as presented in figure 1.13. The experiments were designed to simulate the traditional cooling of chocolate in cooling tunnels at relatively low cooling rates ($< 4°\mathrm{C} \ \cdot min^{-1}$). The results presented in figures 1.13(a) and 1.13(b) show that the temperature plateau due to the phase change is accurately predicted.

Explicit formulation of a source term

The source term can also be calculated independently from the physical phenomenon from which it proceeds. This approach was used to predict temperature profiles during the ohmic heating of foods (Alwis and Fryer 1990). In this case the heat generation comes from the applied electrical field E and the current density J due to the electrical resistance of the media. The heat source term was calculated over the volume V as:

$$\dot{Q}_s = \int_v J \cdot E \cdot dv. \tag{1.15}$$

When coupling this ohmic heating process with the Fourier equation, transient evolution of temperature at different locations was calculated and found to be in agreement with experimental data as shown in figure 1.14.

The only available model for heat transfer over a phase change using a source term that was used to predict the cooling kinetics of chocolate was proposed by Franke (1998). The heat source term was a piecewise linear function dependent on time (t) and temperature (T). This function was fitted on temperature profiles recorded during the solidification of chocolate. However this method is useless since the parameters of the source term function do not proceed from a fundamental analysis of the phase change (*e.g.* Avrami or Foubert) and cannot therefore be used to predicted other cooling scenarios.

1.6 Contribution of this project to the field

The microstructure of the cocoa butter in chocolate is, if the tempering process is successful, strongly dependent on the cooling rate applied to the chocolate during processing. Different cooling rates lead to different crystal structures and the system can be simplified as containing only two types of polymorphs (for further explanations see 4.1):

1. The *unstable* crystals family, consisting of γ, α and β' crystals (I to IV) with a strong peak in the XRD short spacing pattern below or around 4.20Å. These are not stable at room temperature (melting point below 30°C) and typically proceed from rapid cooling rates (> 2°C $\cdot min^{-1}$).
2. The *stable* crystals family, consisting of β crystals (V and VI) with a strong peak in the XRD short spacing pattern around 4.60Å. These are stable at room temperature (melting point above 30°C) and typically proceed from slower cooling rates ($<$ 2°C $\cdot min^{-1}$).

For traditional chocolate processing, the cooling rate is relatively low (< 2°C $\cdot min^{-1}$) and therefore the right crystal structure (form V) is easily obtained. However, recent progress in chocolate manufacturing has led to rapid cooling processes (≈ 100°C $\cdot min^{-1}$ at the interface between the chocolate and the plunger), and these fast cooling rates do not necessarily ensure that only the β form V of cocoa butter will be crystallised. The crystallisation of lower stability polymorphs is a problem for the manufacturers since it can lead to an acceleration of the blooming problem (during the polymorphous transition), making the chocolate unacceptable for the consumer.

To model such systems, the heat transfer equation has to be coupled to the phase change kinetics of fats. However such a model has not been published yet.

The model that has been developed (see chapter 4) during this work couples:

1. a kinetic model similar to the one proposed by Fessas (Fessas et al. 2005) containing two polymorphs, *stable* and *unstable*, with phase change kinetics fitted on DSC data.
2. a heat transfer model similar to the one proposed by de Alwis (Alwis and Fryer 1990) using the kinetic model to estimate the heat source term.

The model was used to predict the cocoa butter state and the temperature of the chocolate during processing. The accuracy of the developed model was validated (see chapter 5) against:

1. XRD measurements for the cocoa butter state. Due to the presence of sugar crystals in the chocolate, a novel method has been developed to filter the sugar crystals diffraction from the chocolate XRD data (see chapter 3).
2. temperature profiles for the heat transfer prediction. The small size of the chocolate samples required the development of a rig where the thermocouples could be accurately located (see chapter 2).

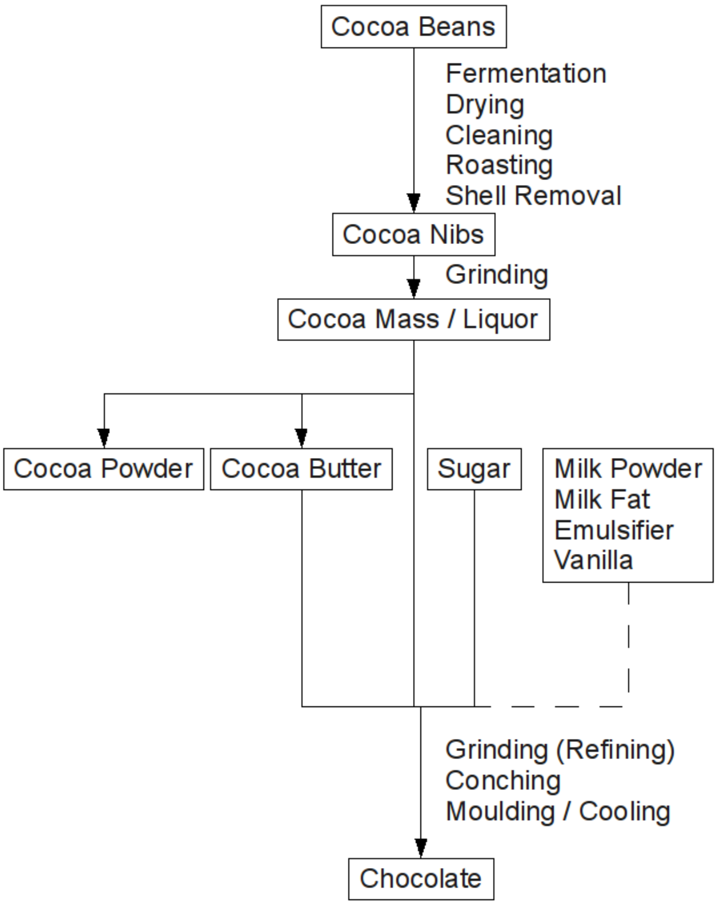

Figure 1.1: Schematic diagram of the traditional chocolate making process (adapted from (Beckett 1989)).

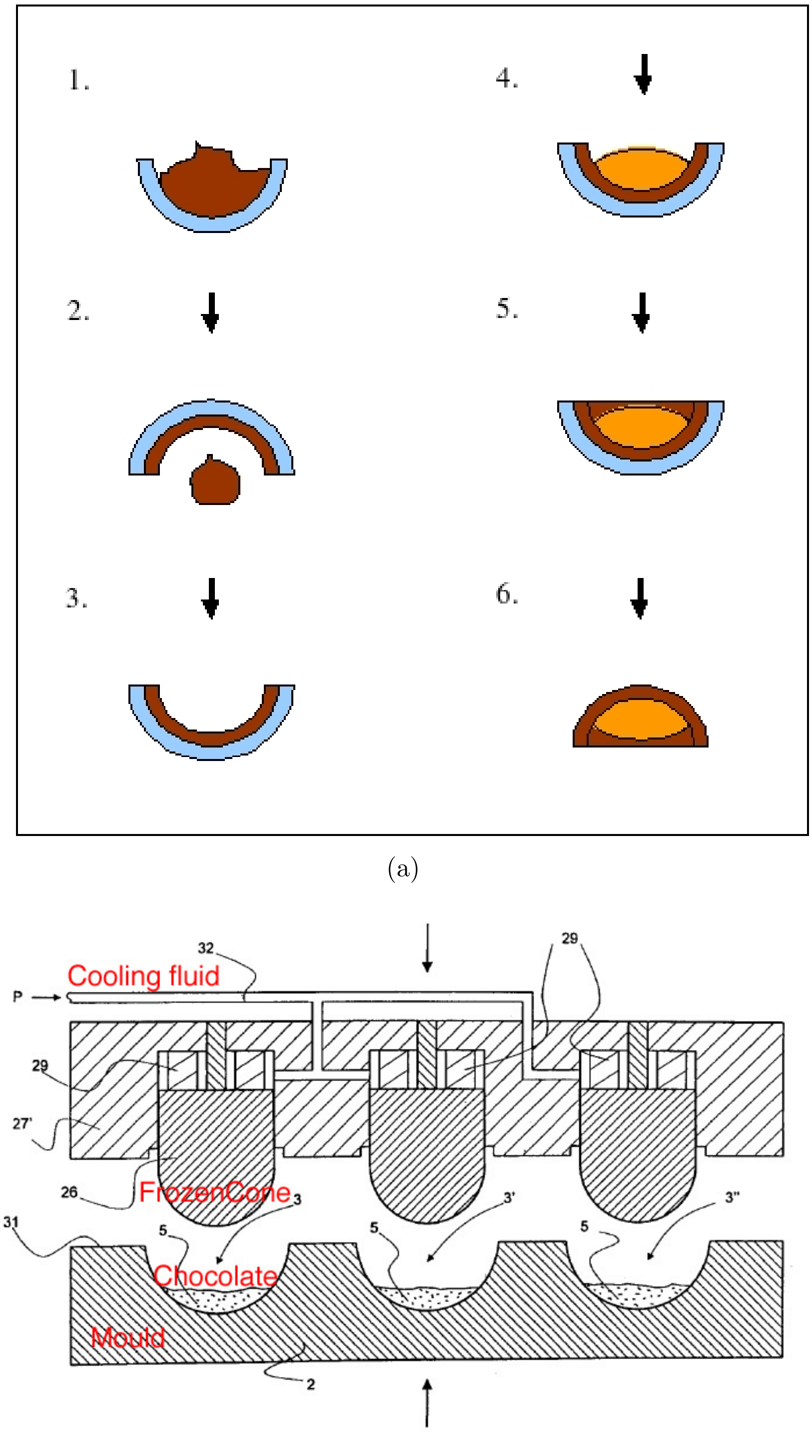

(a)

(b) (Aasted 2003)

Figure 1.2: 1.2(a) shows a typical traditional Easter egg process, in which chocolate is moulded and cooled slowly. 1.2(b) shows the Aasted FrozenCone process, involving rapid cooling of chocolate during moulding.

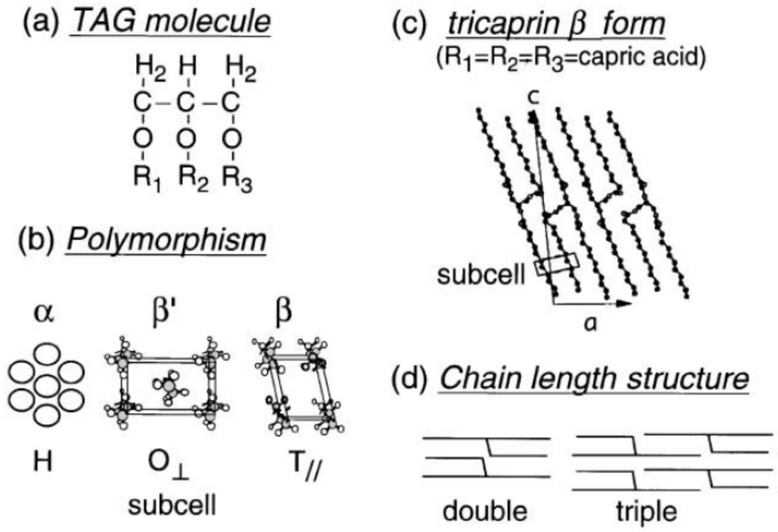

Figure 1.3: A TriAcylGlycerols molecule, polymorphism and subcell structures, chain length structure and unit cell structure of tricaprin β form (Sato 2001).

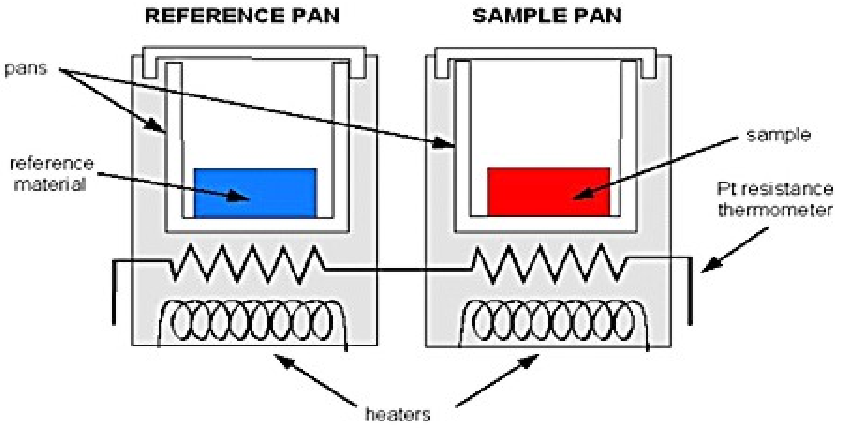

Figure 1.4: Layout of a Differential Scanning Calorimeter (evitherm 2008).

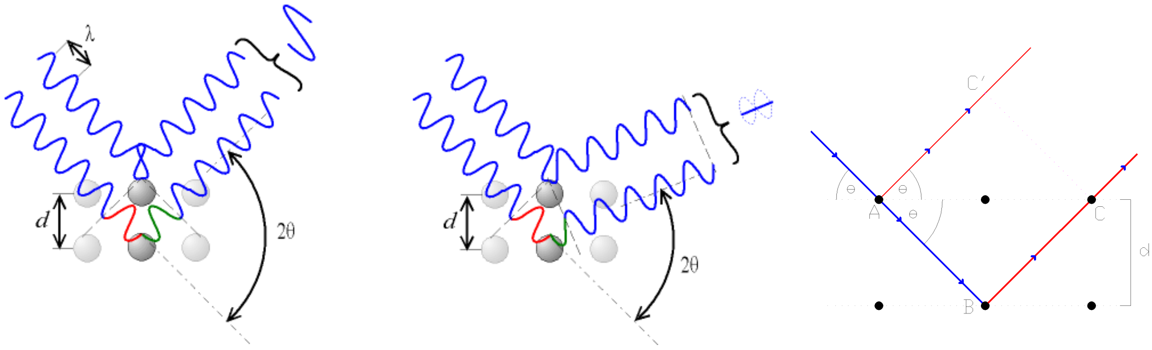

(a) (b)

Figure 1.5: Figure 1.5(a) shows the diffraction of X-rays by the planes of a crystal (Anonymous 2008). A maximum of intensity is reached if the rays are in phase (constructive interference) and a minimum is reached when the rays are out of phase (destructive interference). Figure 1.5(b) shows the geometrical construction of Bragg's law (Anonymous 2008).

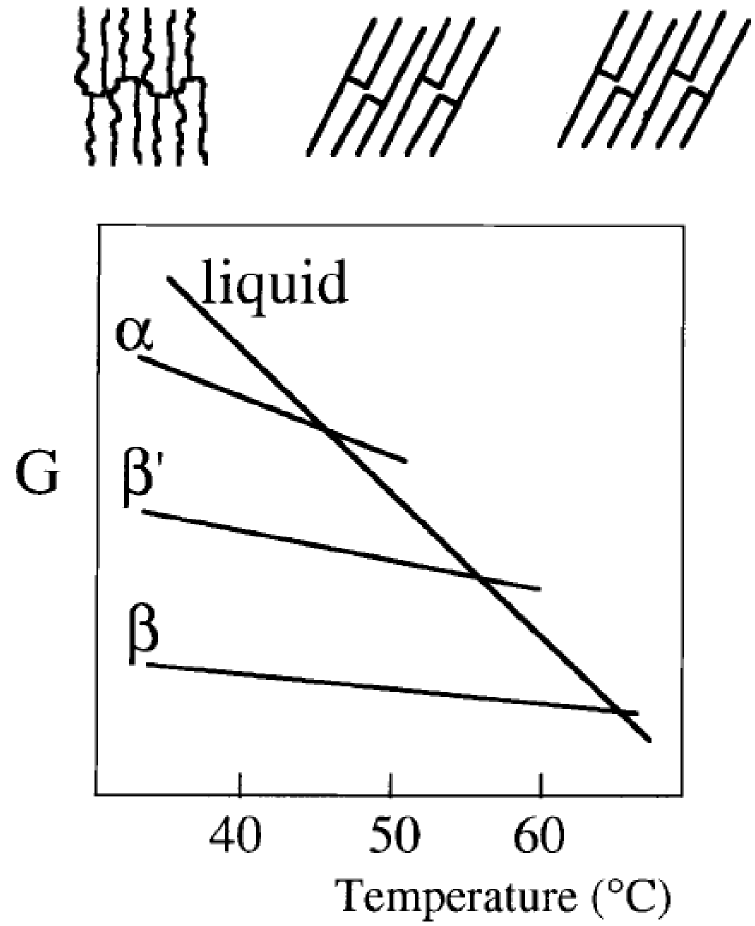

Figure 1.6: $G - T$ relationship for the polymorphs of PPP (Sato 2001).

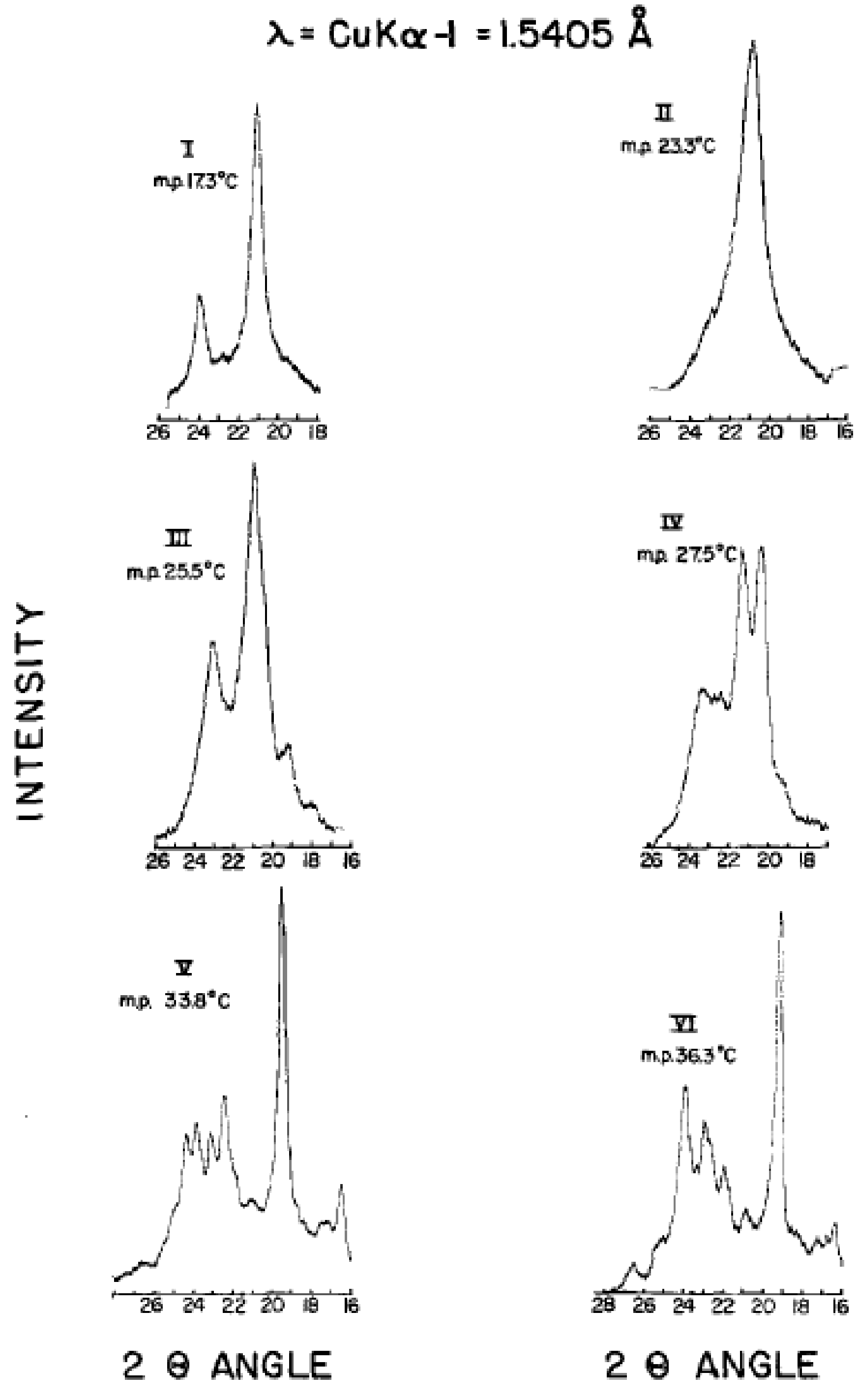

Figure 1.7: Diffractometer short spacing patterns ($2 \cdot \Theta$ angle). (Wille and Lutton 1966) The link between the $2 \cdot \Theta$ angle and the d-spacing is detailed by equation (1.2)

.

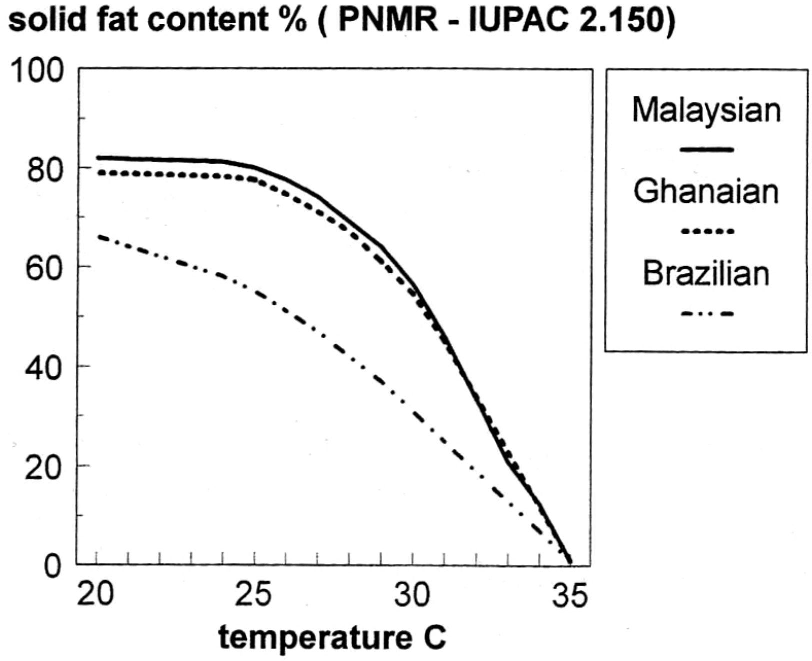

Figure 1.8: SFC of cocoa butters from different growing areas obtained by NMR measurements (Beckett 2002).

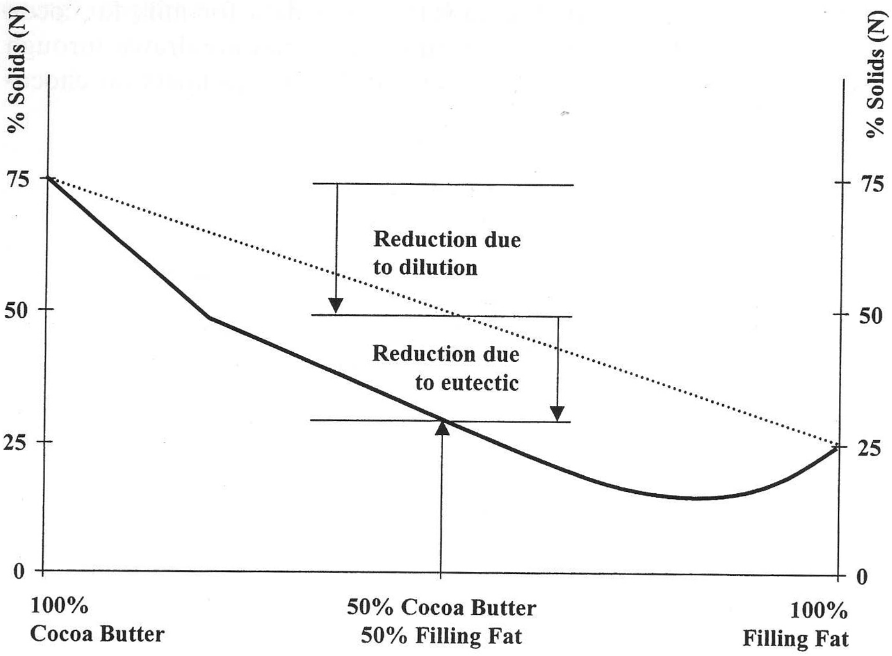

Figure 1.9: Comparison between the expected (ideal mixture) and the measured SFC of mixtures of cocoa butter and a soft filling fat at 20°C (abscissa is the mass fraction). (Beckett 2002)

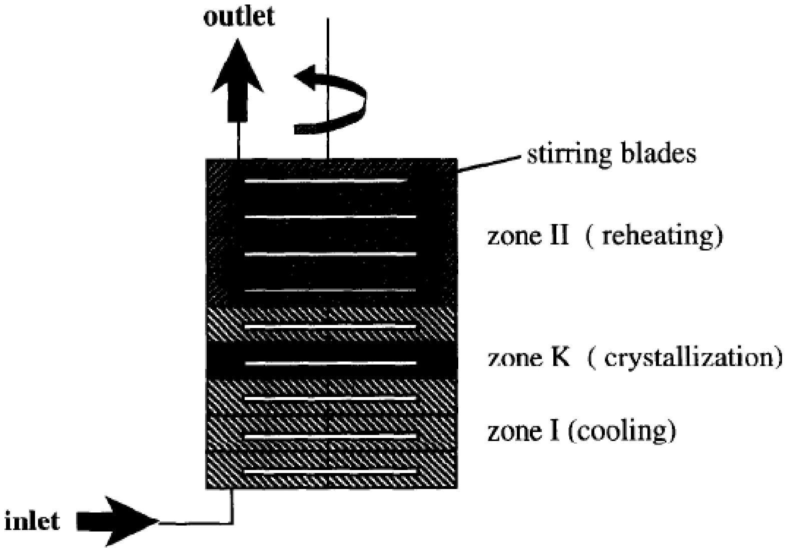

Figure 1.10: Schematic view of an Aasted AMT 250 industrial temperer (Bolliger et al. 1998)

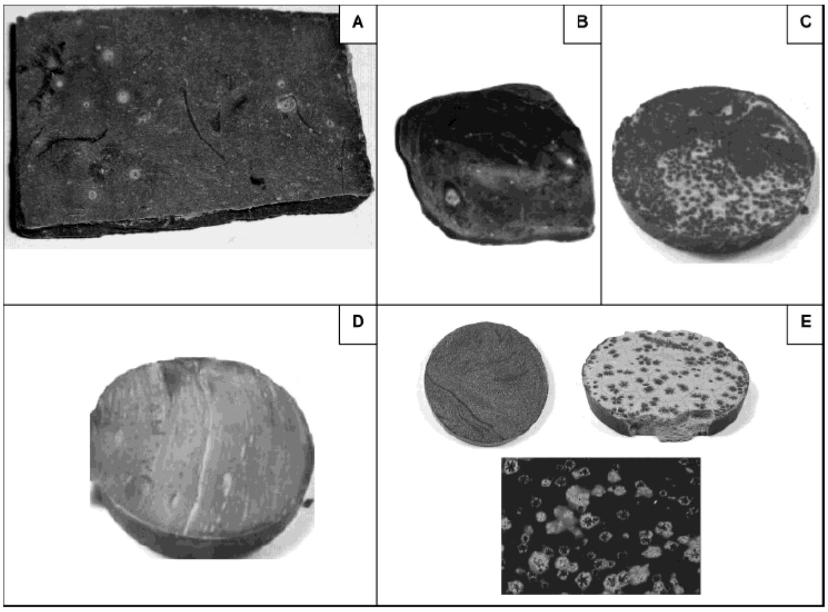

Figure 1.11: Pictures of bloomed chocolate due to (A) storage, (B) fat migration, (C) heat hit, (D) over-tempering, (E) non-tempering. (Lonchampt and Hartel 2004)

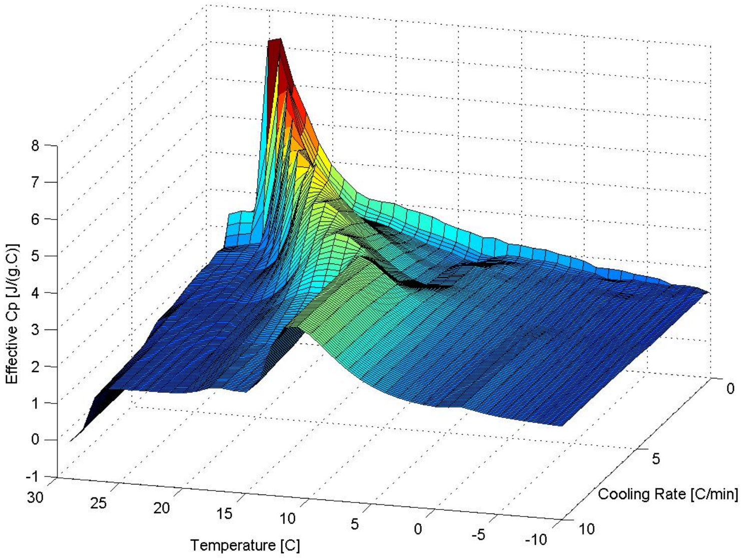

Figure 1.12: Plot of effective specific heat capacity as a function of temperature and cooling rate. (Tewkesbury et al. 2000)

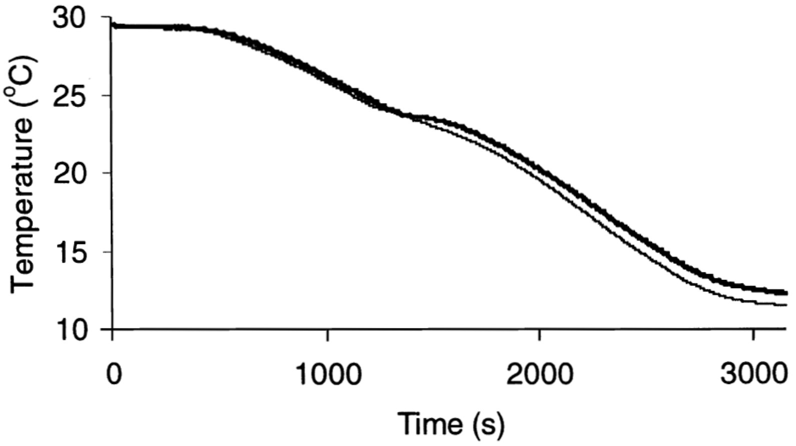

(a)

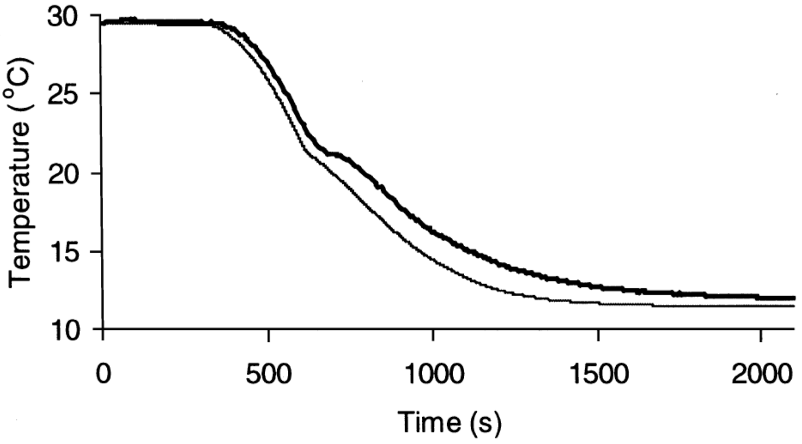

(b)

Figure 1.13: Comparison between calculated and measured temperature profiles in chocolate cooled by forced convection. The nominal cooling rate of the ambient air was 0.5°C $\cdot min^{-1}$ (1.13(a)) and 4°C $\cdot min^{-1}$ (1.13(b)). (Tewkesbury et al. 2000)

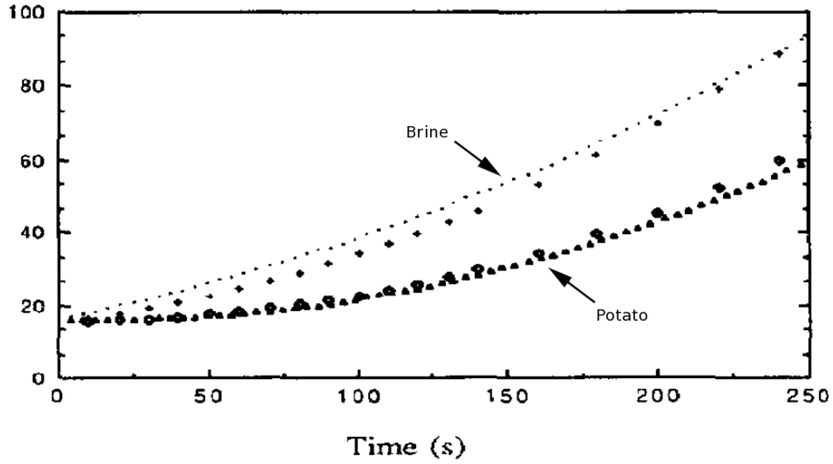

Figure 1.14: Comparison of the ohmic heating of a potato piece (40 x 10 x 20mm, conductivity 0.038 S/m) in brine of conductivity 0.58 S/m, and the modelling of a 40 x 10 mm potato piece. (Experiments are the dotted lines and simulations are the individual points) (Alwis and Fryer 1990)

Table 1.1: The different ingredients involved in chocolate manufacture

	Cocoa liquor	Cocoa butter	Sugar	Milk fat	Milk powder	Vanilla
Dark chocolate	x	x	x	o	o	o/x
Milk chocolate	x	x	x	x	x	x
White chocolate	o	x	x	x	x	x

Table 1.2: Short spacings X-Ray diffraction data for cocoa butter states (W=weak, M=medium, S=strong and V= very). (Wille and Lutton 1966)

Polymorph	*I*	*II*	*III*	*IV*	*V*	*VI*
Short spacings (Å)	4.19 VS	4.24 VS	4.92 VW	4.35 VS	5.40 M	5.43 M
	3.70 S		4.62 W	4.15 S	5.15 W	5.15 W
			4.25 VS	3.97 M	4.58 VS	4.59 VS
			3.86 S	3.81 M	4.23 VVW	4.27 VW
					3.98 S	4.04 W
					3.87 M	3.86 M
					3.75 M	
					3.67 W	3.70 S
					3.39 VW	3.36 VW

Table 1.3: Thermal data on cocoa butter polymorphs according to the literature (Loisel et al. 1998): 1 (Duck 1964) 2 (Wille and Lutton 1966) 3 (Chapman et al. 1971) 4 (Huyghebaert and Hendrickx 1971) 5 (Lovegren et al. 1976) 6 (Merken and Vaeck 1980) 7 (Davis and Dimick 1986)

Polymorph	T (°C) 1	T (°C) 2	T (°C) 3	T (°C) 4	T (°C) 5	T (°C) 6	T (°C) 7
I	18	17.3		14.9-16.1	13	16-18	13.1
II	23.5	23.3		17-23.2	20	20.7-24.2	17.7
III		25.5	20.7	22.8-27.1	23		22.4
IV	28	27.5	25.6	25.1-27.4	25	26-28	26.4
V	33	33.9	30.8	31.3-33.2	30	33.7	34.9
VI	34	36.3	32.3	33.8-36	33.5		

Table 1.4: Triglycerides composition (%) of cocoa butters from different growing areas (Beckett 2002), P is Palmitic acid (C16:0), S is Stearic acid (C18:0), O is Oleic acid (C18:1), L is linoleic acid(C18:2).

TAG	Brazil	Ghana	Malaysia
SSS	1	1.4	2.3
SOS	63.7	76.8	84
SSO	0.5	0.4	0.5
SLS	8.9	6.9	6.8
SOO	17.9	8.4	5.1
OOO	8.0	6.1	0

Table 1.5: Melting points of cocoa butter pure or mixed with milk fat. (Chapman et al. 1971)

Polymorph	IV	V	VI
Melting point pure cocoa butter (°C)	25.6	30.8	32.3
Melting point cocoa butter / MF (°C)	21.9	27.2	30.6

CHAPTER 2

MATERIAL AND METHODS

In this section, a description of the equipment used in this study and the way they were used will be presented. First the formulations used will be presented. In order to measure the right kinetics, this chocolate had to be tempered in the same way as is used in industry. The kinetics of phase change were studied using DSC and a novel method based on XRD. Temperature profiles during the phase change were also recorded in a specially designed rig.

2.1 Chocolate and cocoa butter

Two chocolate formulations were used in this work:

1. The first was a typical milk chocolate formulation from Barry Callebaut (Banbury, UK), this chocolate is a milk chocolate, having a total fat content of 31.7% (19.5% cocoa butter). It contains 56.4% of sugars, which leads to a ratio $\frac{[cocoa\, butter]}{[sugar]}$ of 0.35.
2. The second formulation used in the study was a typical dark chocolate formulation (Taste the Difference, Sainsbury's own brand). It is also free from any vegetable fats except cocoa butter (51.4%), contains 19.2% of sugar, which leads to a ratio

$\frac{[cocoa\,butter]}{[sugar]}$ of 2.68.

The cocoa butter used in the study was supplied by ADM Cocoa (Hull, UK). The capillary melting point (clear point) was measured by the manufacturer to be between 32°C and 35°C .

2.2 Experimental apparatus and methods

2.2.1 Tempering

As detailed in section 1.3.5, tempering is one of the critical steps of chocolate manufacturing.

A Chocovision Revolation 2 (Poughkeepsie, NY, USA) was used to temper chocolate. It consists of a rotating bowl with a fixed (non-rotating) central wall forming two compartments (A and B). A scraper is present at one of the wall ends, allowing material to go in only one of the two compartments (A to B but not B to A). The equipment is shown in figure 2.1. The temperature of the molten chocolate is measured using a PT100 sensor and controlled using an air heater and blower in the base of the apparatus.

Chocolate was tempered using the method suggested by the equipment manufacturer (Chocovison ND); *i.e.* 750g of solid chocolate were melted in the machine (compartment B) and heated up to 42°C for 30 minutes. 110g of solid chocolate (form V) were then used to seed the molten chocolate (compartment A). Whilst the seeds are there to temper the chocolate (mass transfer from A to B), the temperature was dropped from 42°C down to 32°C . When the critical temperature of 32°C was reached the seeds were removed from compartment A and the temperature was then set to reach 30°C .

The temper level of the chocolate was measured using a bench top tempermeter, the

Aasted Mikroverk (Farum, Denmark) Tempermeter PC *II* (Aasted Microverk ND). It consists in a Peltier stage and a temperature measurement sensor (Pt100). The chocolate is poured by the operator into an aluminium cone shaped mould, the cooling stage is similarly shaped to cool the mold. The temperature sensor is located at the centre of the chocolate mass and records the temperature as the chocolate is cooled by the Peltier stage (see figure 2.2).

The analysis of the cooling curve is automatically made by the software to quantify the level of temper. A screenshot from the analysis software can be seen in figure 2.3. First chocolate is cooled down to the crystallisation point, then the phase change occurs around 23.5°C and finally chocolate is cooled as a solid down to a temperature close to the Peltier stage temperature (8°C)

The slope (cooling rate) and temperature values during the phase change are usually used to measure the quality of the tempering (Bolliger et al. 1998). Typically the slope value is in the range -0.5 to 0.5°C $\cdot min^{-1}$ and the temperature in the range 21 to 24°C . The slope obtained in the phase change region using our tempering routine for the milk chocolate on figure 2.3 was -0.045°C $\cdot min^{-1}$ and the temperature was 23.47°C . These values are in agreement with the literature and the industrial data available from Magna.

2.2.2 Differential scanning calorimetry (DSC)

In this study, a Perkin Elmer (Waltham, Massachusetts, USA) DSC 7 (Perkin Elmer 1987) was used, linked to an Intracooler *III* to achieve fast cooling rates. The Intracooler *III* gives the capability to cool down to -50°C with a cooling rate up to -30°C $\cdot min^{-1}$. Nitrogen was used as the purge gas with a standard flow rate of $30ml \cdot min^{-1}$. The samples $(10 - 15mg)$ were sealed in the Perkin Elmer $40\mu l$ aluminium pans using the standard aluminium pan cover.

The objectives of the different DSC experiments were to (*i*) estimate the kinetic rates of the different phase changes occurring whilst heating or cooling, (*ii*) measure the impact of tempering on the crystallisation curves and (*iii*) measure the impact of the cooling method on the microstructure of the product.

In order to address these needs, different types of experiments were performed:

1. Freshly tempered chocolate was cooled from 30°C (temperature of the chocolate out of the temperer) down to −20°C . The cooling rate applied whilst cooling was $-0.1, -0.2, -0.5, -1, -2, -5, -10$ or -20 °C $\cdot min^{-1}$. After cooling chocolate was reheated up to 50°C using a heating rate of $+1$ or $+5$°C $\cdot min^{-1}$.
2. Similar experiments were made on untempered chocolate (from 42°C) to measure the impact of tempering on the crystallisation and melting kinetics.
3. Solid chocolate cooled using various techniques (Magna plant, Birmingham pilot plant and Peltier Chocolate Rig) was reheated from −10°C to 50°C .

Data were processed using the Perkin Elmer Pyris software to correct the slope of the baseline and to calculate the effective Cp:

$$Cp_{eff} = \frac{\dot{Q} \cdot dt}{m \cdot dT}. \tag{2.1}$$

2.2.3 X-Ray diffraction (XRD)

Two different set of experiments were conducted at two different locations.

A first set of experiments was conducted on the single crystal diffractometer Brucker (Coventry, UK) Smart 6000 CCD at the Department of Chemistry at the University of Birmingham. The diffractometer has a detector with high spatial resolution and thus allows data collection for materials with large unit cells. It is also equipped with an

Oxford Cryostreams low temperature device for structural characterization of materials that are unstable at room temperature such as the low melting point polymorphs of cocoa butter present in chocolate. Since the method requires to melt the material, the smaller size of the samples required by single crystal diffractometers appeared adequate compared to the powder diffractometers (XRPD). The wavelength of the copper radiation used in this machine is $\lambda_{\text{Cu}} = 1.54\text{Å}$.

A second set of experiments was conducted at the EPSRC National Crystallography Service located at the University of Southampton. The data were collected using a high brilliance diffractometer. The monochromatic beam of X-Rays brought to the sample came from Molybdenum (Mo) radiation. The X-ray flux at the crystal is approximately six times more than that of a conventional diffractometer. This was achieved by the design and installation of confocal mirrors for Mo radiation. The KappaCCD detector on this diffractometer is a Bruker Apex II detector, giving an additional increase in sensitivity. The wavelength of the molybdenum radiation used in this machine is $\lambda_{\text{Mo}} = 0.71\text{Å}$.

The equipment used in this second set of experiment had a stronger signal than the one used in the first set of experiment. This allowed new experiments needing faster data collection to be performed.

For both sets of experiments, samples of tempered chocolate and molten cocoa butter (supplied by Magna) were crystallized either at room temperature (for the *stable* samples) or as drops on an Aluminium plate kept in a freezer at −25°C (for the *unstable* samples). X ray diffraction patterns were then recorded either solid state at −30°C and liquid state at 40°C . The data was then postprocessed using the DataSqueeze (Heiney 2007) and Powderize (Hooft 1998) softwares. State of the art work using XRD to determine the structure of cocoa butter present in chocolate was previously done by studying pure fat systems (Loisel et al. 1998, Schenk and Peschar 2004). To the best of our knowledge (confirmed by experimental data) sugar crystals generate a strong diffraction signal preventing the use of this technique on raw chocolate. In this work the crystal structure determination was achieved by subtracting the solid and the liquid signal from a chocolate sample cooled using identical processes. Details on the development and accuracy of the method are presented in chapter 3.

2.2.4 Limitations of the DSC and XRD setups

In this work, both techniques have been used to successfully qualify the polymorphous state of cocoa butter. However, it would have been ideal to be able to use both techniques simultaneously using a temperature controlled XRD cell coupled with a calorimeter. This would have allowed a complete characterisation of the system and would have allowed to define both the level of temper applied and the crystallisation kinetics more accurately.

If such a device was to be built, it would be ideal if the source of X-Rays was a synchrotron. Facilities such as the ESRF (Grenoble, France) offer a flux, energy range and resolution unachievable with conventional (laboratory) radiation sources. It would then be possible to monitor the changes in the crystal structure whilst a heat flux is applied, and record the XRD pattern in real time as the high intensity from synchrotron radiation is compatible with short aquisition time.

The extra resolution in the XRD pattern provided by the synchrotron radiation would also be helpful if the model was extended to take into account the six polymorphs of cocoa butter, as they could probably be differentiated in that instrument.

2.2.5 Temperature profiles measurements using a Peltier stage

In order to measure temperature profiles in chocolate in a controlled and reproducible way, a cooling/heating cell shown in figure 2.5(a) was designed. A Linkam (Tadworth, UK) Peltier stage (Linkam Scientific Instruments Ltd ND) controlled via a computer was used to deliver accurate temperature profiles.

The surface available for heat transfer on this stage is $40 \times 40mm = 16cm^2$. The dimensions of the cell are $40 \times 40 \times 11mm$ leading to a weight of $\approx 23g$ for each sample. To maximize the efficiency of the Peltier stage, an insulating cover was made to mould chocolate. A copper plate was used to ensure good contact between the Peltier stage and the chocolate.

Temperature was monitored using K-type thermocouples with a thickness of $0.1mm$ provided by OMEGA Engineering Limited (Manchester, UK). To make sure that the location of the thermocouples was consistent throughout the study, these were guided using syringe needles fixed in the insulating material and linked to a PICO datalogger.

Distances between the surface of copper plate in contact with the Peltier stage and the thermocouples were 2.7, 4.9 and 8.7 mm.

Preliminary numerical simulations of heat transfer were performed using the software COMSOL Multiphysics. The purpose of the simulations was to validate that (*i*) the copper plate used did not affect cooling rates and (*ii*) the heat transfer did only depend on the normal direction to the Peltier stage in the vicinity of the thermocouples.

In this work three representative temperature profiles were applied to the chocolate using the Peltier device (*cf.* figure 2.5(b)):

1. Profile 1 represents a step change down to 0°C (quick cooling)
2. Profiles 2 represents a step change down to 12°C (normal cooling)
3. Profile 3 is more representative of an industrial cooling profile where first a quick cooling step (0°C , similar to a FrozenCone (Aasted 2003) process) is followed by an increase in temperature (12°C , corresponding to the cooling tunnel). Finally temperature was raised up to 60°C to achieve a complete melting of the material.

Figure 2.1: Temperer Chocovision Revolation 2

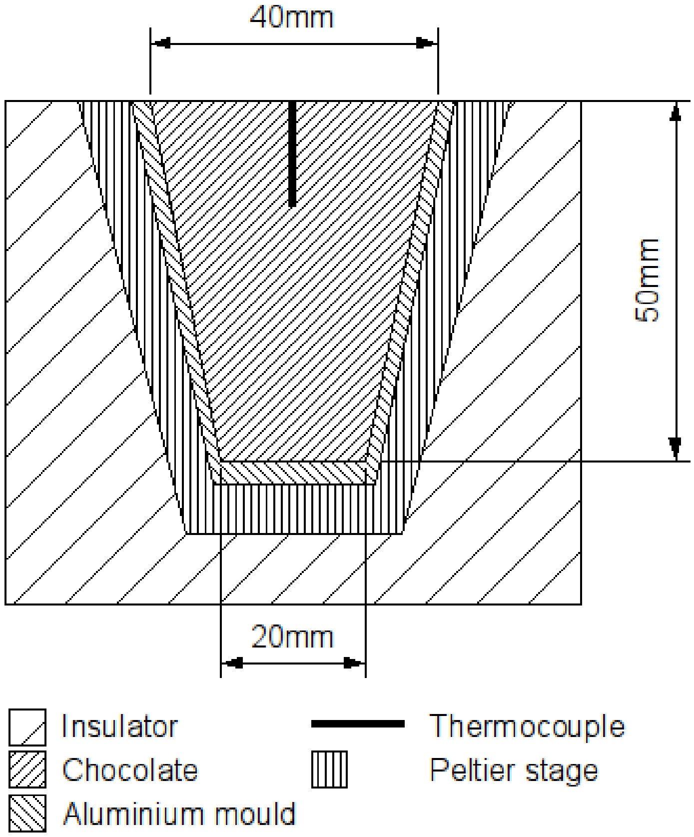

Figure 2.2: Schematic of the Aasted Microverk Tempermeter PC *II* cooling cell

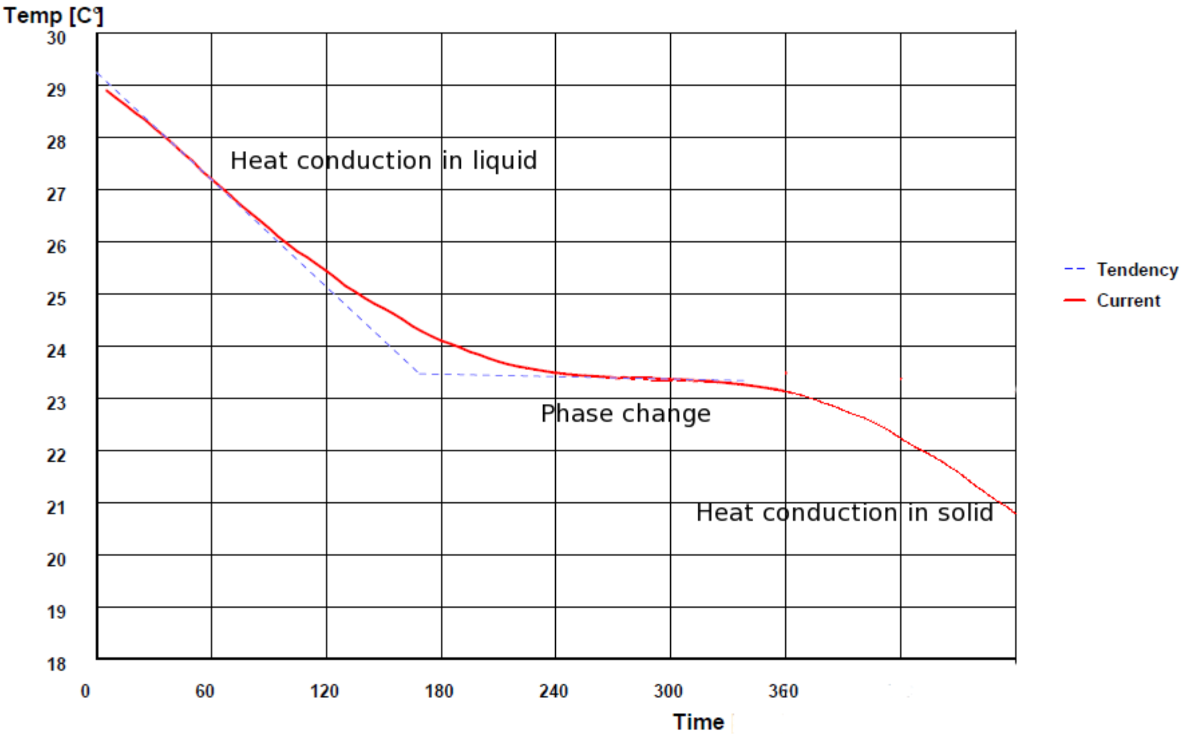

Figure 2.3: Typical tempermeter analysis after tempering in the Chocovision Revolation II.

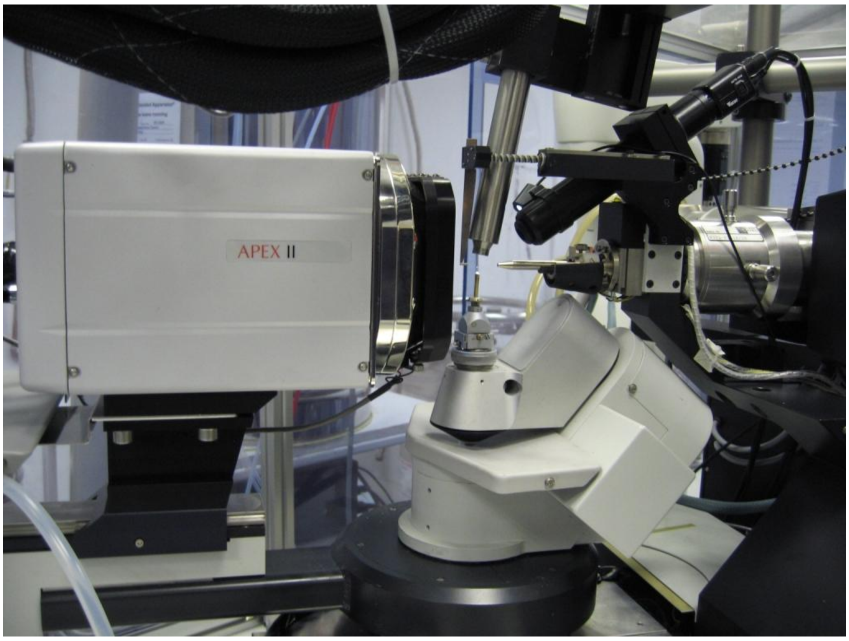

Figure 2.4: Picture of the XRD setup ”Damien” at the EPSRC UK National Crystallography Service.

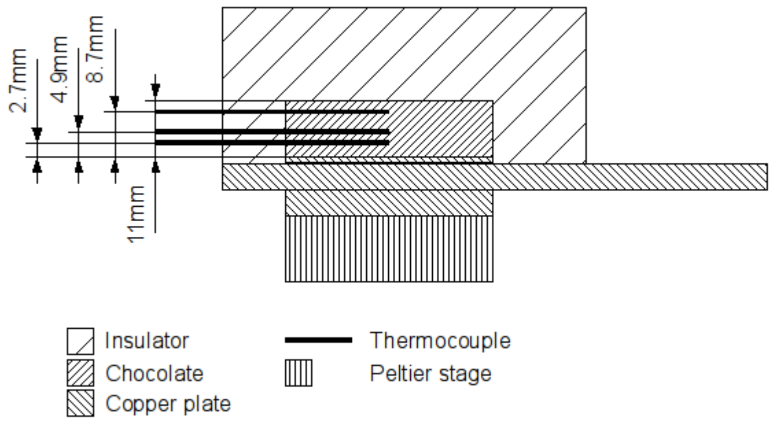

(a)

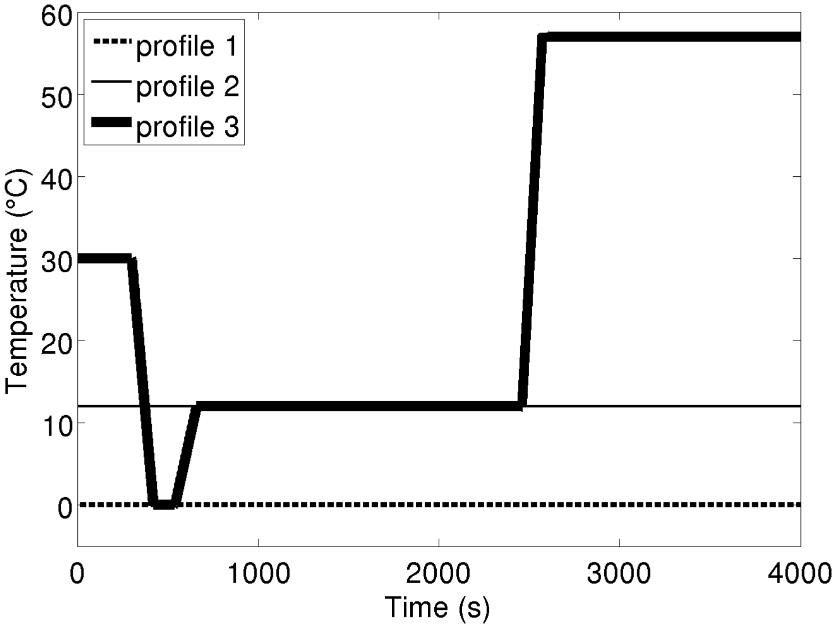

(b)

Figure 2.5: Schematic view of the Peltier Chocolate Rig (2.5(a)) and the temperature profiles programmed to the Peltier stage in order to cool the chocolate (2.5(b))

Table 2.1: Nutrition facts of the two formulations selected for the project

	Milk chocolate	Dark chocolate
Fat content	31.7 %	51.4 %
of which cocoa butter	19.5 %	51.4 %
Moisture	$\leq$ 1 %	$\leq$ 1 %
Energy per 100 g	2250 kJ	2358 kJ
Proteins per 100 g	6.1 g	8.8 g
Total carbohydrates per 100 g	56.4 g	19.2 g

CHAPTER 3

SUGAR CRYSTALS IN CHOCOLATE, A PROBLEM FOR XRD MEASUREMENTS ?

3.1 Limitations to the application of XRD in chocolate

XRD is a method commonly used to characterize the fat crystal structure (Schenk and Peschar 2004, Wille and Lutton 1966, Chapman et al. 1971, Guthrie, Mazzanti and Idziak 2005). The advantage of DSC is that it is directly applicable to chocolate, since other components of chocolate (*e.g.* sugar, cocoa mass and emulsifiers) have little or no heat disturbance during phase change of cocoa butter.

It has been reported that the crystalline sugar present in chocolate has a strong diffracting power on X-Rays and that the pattern of sugar obscures that of cocoa butter (Bricknell and Hartel 1998, Loisel et al. 1997a). Diverse solutions have been proposed and applied to address this problem:

1. The removal of sugar by washing ground chocolate with cold water ($4-6$°C) (Loisel et al. 1997a). The sugar is soluble in water and the chocolate will therefore

be *desugared* and the polymorphic state of cocoa butter can be observed using XRD.

2. Guthrie and others (Guthrie et al. 2005) have proposed that in certain regions of the diffraction patterns, the XRD pattern of cocoa butter could be observed directly. *d*-spacings at 3.98Å and 3.70Å respectively representing form V and VI of cocoa butter were observed and used to measure the polymorphic transition of cocoa butter from form V to VI.

None of these solution is however applicable in our case as the polymorphs to be observed are likely to be III or IV (*unstable*) and V (*stable*). Another approach to qualify the polymorphic state of cocoa butter had to be developed.

3.2 A new approach in using XRD to study cocoa butter polymorphism in presence of sugar

Crystals of sugar in chocolate can cause a dominating XRD signal, with two strong peaks in the region of interest (Kudasheva, Lai, Ulman et al. 2004) located at 4.56Å (overlapping with the main *stable* crystals peak at 4.59Å) and 4.71Å (not overlapping with any reported cocoa butter peaks). In order to study fat polymorphism, it was decided to overcome this problem by measuring the sample at two different states.

Assuming that:

1. sugar is in the same solid state when chocolate is solid (-30°C) and liquid (40°C) and the sugar XRD pattern contribution should be identical in both cases,
2. cocoa butter and sugar are the only species diffracting X-Rays in solid chocolate,
3. liquid cocoa butter does not diffract X-Rays,

the subtraction of the XRD signal of liquid chocolate from the XRD signal of solid chocolate should result in a XRD signal similar to the one of pure solid cocoa butter.

This can be written as:

$$\begin{aligned}XRD_{solid\,chocolate} - XRD_{liquid\,chocolate} &= (XRD_{solid\,cocoa\,butter} + XRD_{solid\,sugar}) \\ &\quad -(XRD_{liquid\,cocoa\,butter} + XRD_{solid\,sugar}) \qquad (3.1) \\ &= XRD_{solid\,cocoa\,butter}\end{aligned}$$

The method proposed in this work to obtain an understanding of the cocoa butter crystal structure in chocolate is to:

1. measure the XRD pattern of solid chocolate (−30°C), when the cocoa butter is completely solid,
2. measure the XRD pattern of liquid chocolate (40°C), when cocoa butter is completely liquid, however sugar is still solid and therefore still diffracts X-Rays,
3. subtract the liquid chocolate pattern (40°C) from the solid chocolate pattern (−30°C) to remove the diffraction pattern caused by the sugar. Collection of data and validation of this method will be presented in this section.

3.3 Method details

Typical data obtained from a milk chocolate system are presented in figure 3.1. All the samples and data presented in this chapter were collected at the EPSRC facility in Southampton. The resolution of the signal is $d\theta = 0.025°$, so all the values for $2 \cdot \theta$ should be read as $2\theta \pm 0.05°$ or $d \pm 0.03$Å in the region of interest.

In figure 3.1(a), a typical XRD pattern for a solid (−30°C) chocolate sample solidified at a cooling rate of 0.5°C $\cdot min^{-1}$ is shown. According to the literature (Stapley et al. 1999), such a sample is expected to contain mainly *stable* crystals, melting over 29°C . The top right quarter shows a magnification of the picture around the area of the expected peak for the *stable* crystals (4.60Å or 8.89° at $\lambda_{Mo} = 0.71$Å). Two rings (4.71Å and 4.56Å) can be seen in this area, the outer (4.56Å) one having a stronger intensity than the inner one (4.71Å).

Consecutively, the sample was melted (40°C) in the diffractometer and a second scan was performed. The X-ray pattern obtained is presented in figure 3.1(b). The two rings are still present but the outer ring is of similar intensity than the first ring. Both of these rings are due to the diffraction of X-Rays by the sugar crystals since they are the only crystalline material present in the melt.

Using the Powderize software (Hooft 1998) which converts the XRD images into an amplitude *vs.* $2 \cdot \theta$ signal, figure 3.2 is generated.

In figure 3.2(a), a main peak can be observed at the right location for *stable* crystals (4.56Å) corresponding to the second of the two outer rings. The shoulder in this peak at 4.71Å accounts for the first of the two rings, which has less intensity. When the sample is liquid, the two consecutive peaks at 4.71Å and 4.56Å in figure 3.2(b) are still present but this time have the same intensity as seen in figure 3.1(b). This implies that both peaks are present in the sugar diffraction pattern. If the two diffractograms are subtracted from one another, the result is a single sharp peak obtained at 4.56Å as presented in figure 3.2(c). This peak is located at the same position as the second peak presented in figure 3.2(a) and 3.2(b). The difference in intensity for this peak measured at 4.56Å, originates from the solid cocoa butter present in the solid sample but absent in the liquid sample. The value $d = 4.56$Å is very close to the "very strong" peak value published in the literature (Wille and Lutton 1966) of $d = 4.58$Å for form V of cocoa butter (see figure 1.7).

The same analysis was conducted for a cooling rate of 5°C $\cdot min^{-1}$. According to previous work (Stapley et al. 1999), this should lead to *unstable* crystals. One can see that the peak resulting from the subtraction (figure 3.3(c)) of the solid (figure 3.3(a)) and the liquid (figure 3.3(b)) sample images is located at a different angle, $d = 4.19$Å. The value $d = 4.19$Å is very close to the "very strong" peak value published in the literature (Wille and Lutton 1966) of $d = 4.25$Å for form III of cocoa butter (see figure 1.7).

If dark chocolate cooled at 0.5°C $\cdot min^{-1}$ is used, the resulting peak (figure 3.4(c)) is located at the same angle as for milk chocolate cooled under the same conditions ($d = 4.56$Å). However, this peak is sharper than the one observed in milk chocolate, further explanations are given below.

These initial results shows that as hypothesized it is possible to obtain an image of the state of cocoa butter using the subtraction of the liquid chocolate signal (XRD of sugar) from the solid chocolate signal (XRD of sugar and cocoa butter). Our approach is to cluster the six crystal polymorphs in two groups, namely *stable* and *unstable* which are typically formed under slow and fast cooling rates, respectively. These measurements seem to confirm that *unstable* crystals are mainly β' and that *stable* crystals are mainly β crystals. This illustrates that different cooling rates lead to different polymorphs of cocoa butter as previously explained in the literature (Stapley et al. 1999).

3.4 Validation of the method

From the above, one can see that it should be possible to use XRD to qualitatively characterize the crystal structure of cocoa butter in chocolate samples. To ensure that the signal obtained from the subtraction method was the one of the cocoa butter present in chocolate, data obtained from this method were compared with the diffraction signal obtained from cocoa butter cooled using the same process.

Figure 3.5 presents the subtracted signals collected from slowly cooled ($0.5°\text{C} \cdot min^{-1}$) tempered milk chocolate and the signal collected from pure cocoa butter cooled under the same conditions. Under these conditions one would expect *stable* crystals to be formed (Stapley et al. 1999). For all the pure cocoa butter samples (triplicate) the maximum recorded peak is $d = 4.56\text{Å}$ which is very close to the expected value according to the literature for form V crystals ($d = 4.58\text{Å}$). Similarly, the maximum recorded peak is $d = 4.56\text{Å}$ for the milk chocolate subtracted signal (triplicate). Moreover the intensity of the peak is very similar for the three replicates of both cocoa butter and chocolate samples proving the reproducibility of the recorded data.

For a second set of experiments, freshly tempered chocolate and molten cocoa butter were cooled very quickly at a cooling rate of about $50°\text{C} \cdot min^{-1}$. The subtracted signal of such chocolate is presented in figure 3.6 compared to the signal for pure cocoa butter cooled under the same conditions. Both pure cocoa butter and subtracted chocolate signal showed a maximum peak located at $d = 4.19\text{Å}$ which is very close to the literature value ($d = 4.25\text{Å}$) for *unstable* crystals which are likely to form at high cooling rates.

Both the *stable* and *unstable* families of crystals, required for the modelling work, can therefore be qualitatively identified in milk chocolate. As expected *stable* (form V) crystals are formed when using a slow cooling rate while a more rapid cooling rate leads to *unstable* (form III) crystals. A more quantitative approach was then implemented to follow *unstable* to *stable* polymorphous transitions.

3.5 Subtraction method to follow the polymorphous transitions of cocoa butter in chocolate

During a typical rapid cooling process (FrozenCone or profile 1 in figure 2.5(b)), chocolate is cooled very quickly to give a shape to the product, then solidified in depth using a cooling tunnel. As a result of the high cooling rate applied to the chocolate, a majority of *unstable* fat crystals is expected. In the cooling tunnel, cocoa butter is likely to transform to the most thermodynamically stable phase, due to the instability of the system after the first rapid cooling step. In this part such transitions are studied and the subtraction method is applied at different temperatures to quantify the evolution of the crystalline state of cocoa butter during an industrial chocolate process.

In figure 3.7, the XRD pattern of pure cocoa butter during heating can be seen. The cocoa butter was originally crystallized at a cooling rate of 50°C $\cdot min^{-1}$:

1. at the initial temperature of 0°C , a peak at $d = 4.19$Å, characteristic of *unstable* crystals, can be seen as expected from the high cooling rate.
2. when heated up in the diffractometer to 15°C at 5°C $\cdot min^{-1}$ it exhibits two peaks at $d = 4.19$Å and $d = 4.56$Å, both of a relative small intensity. This indicates that the *unstable* crystals are gradually replaced by *stable* crystals.
3. finally when reaching 20°C the cocoa butter has completely changed to the *stable* form showing only a peak at $d = 4.56$Å, characteristic of *stable* crystals.

To estimate the concentration of each phase in chocolate samples, the peaks characteristic of each phase have to be integrated, assuming that the area is proportional to the concentration of the phase. The boundaries of each peak (where a peak meets the baseline) had to be defined in order to fix the limits of the numerical integration (trapezoidal Riemann sum).

Using figure 3.7, the boundaries of each peak were defined:

1. for the *unstable* peak at $d = 4.19$Å, the integration limits were set as $d = 4.09$Å for the lower bound and $d = 4.47$Å for the higher bound.

2. for the *stable* crystals peak at $d = 4.56\text{Å}$, $d = 4.47\text{Å}$ was found to be the lower bound and $d = 4.71\text{Å}$ the higher bound.

Similar process of heating an initially *unstable* microstructure was applied to milk chocolate. A freshly tempered sample of milk chocolate was cooled quickly ($50°\text{C} \cdot min^{-1}$) and XRD data was collected at 0, 5, 10, 15, 20, 25, 30, 35 and 40 °C . The signal at 40°C was subtracted from the signals at all the other temperatures to remove the sugar pattern as explained before. The area of each peak was then estimated between the boundaries already defined such as:

$$A_{stable} = \int_{d=4.47\text{Å}}^{d=4.71\text{Å}} I(d) \cdot dd \text{ and } A_{unstable} = \int_{d=4.09\text{Å}}^{d=4.47\text{Å}} I(d) \cdot dd \tag{3.2}$$

where $I(d)$ is the intensity measured by XRD at the d spacing d.

It is reasonable to assume that the size of the peak is proportional to the number of molecules generating the signal. Therefore, the peak area measured was considered to be proportional to the concentration of crystals characterised by the peak integrated (Mazzanti, Guthrie, Marangoni et al. 2007). The signal intensity is also a linear function of the sample mass. Thus XRD signals were scaled so that the peak representative of sugar (common to all milk chocolate samples), would have an arbitrary intensity of 100. Furthermore, data for $A_{unstable}$ and A_{stable} phase concentrations were normalised between 0 and 1 by dividing by the maximum value measured e.g. $A_{unstable}^{max}$ at $T = 10°\text{C}$ for *unstable* and A_{stable}^{max} at $T = 25°\text{C}$ for *stable* crystals (see figure 3.8). An example of this procedure is presented in table 3.1 for *stable* crystals. The area is in the second column while the third column is the area divided by the maximum value recorded; here 0.1142 at 25°C . This effectively normalises the data which are then expressed as a percentage of the maximum value recorded. The objective of this calculation is that data can be looked at quantitatively without having to worry about the size of the sample during the measurement or to be able to compare this with the simulation data (see chapter 5).

The results for the evolution of the amount of cocoa butter in the *unstable* phase are shown in figure 3.8(a). One can see that the normalised concentration gradually decreases from 1 down to 0 between 10°C and 20°C . This is consistent with the hypothesis that *unstable* crystals are mainly form III (according to the XRD measured angle for the strong peak) since form III crystals in a mixture of milk fats and cocoa butter were found to melt completely at 18°C (Chapman et al. 1971).

The amount of cocoa butter in the *stable* state gradually increases between 10°C and 20°C as can be seen in figure 3.8(b). As in figure 3.7 for pure cocoa butter, the cocoa butter in chocolate in the *unstable* state is gradually transformed to the *stable* phase. Finally the *stable* crystals melt between 25°C and 30°C . This is consistent with the hypothesis that *stable* crystals are mainly form V (according to the XRD measured angle for the strong peak) since form V crystals in a mixture of milk fats and cocoa butter were found to melt completely at 27.2°C (Chapman et al. 1971).

Each measurement was performed in triplicate to investigate the repeatability of the results and the low standard deviation is represented by the error bars in figures 3.8(a) and 3.8(b).

In this quantitative study, the *unstable* forms (γ, α and β') have been lumped together but in reality, it is thought that the different crystalline forms have different proportionality coefficients between the area of the peak and the actual concentration in crystals (Mazzanti et al. 2007). For example a value of $1.7\% SFC/nu$ has been reported for form II and $3.2\% SFC/nu$ has been reported for form IV. A small error in the quantification of the *unstable* phase may have therefore been introduced. However, the melting temperature of *unstable* is around 18°C using XRD and DSC (see following chapter), one can assume that *unstable* crystals are typically β' (III or IV) which should have similar proportionality coefficients (both being β').

3.6 Increasing the signal to noise ratio when using dark chocolate

As sugar is crystalline and contributes to the XRD of chocolate samples, one could expect that if the amount of sugar in the samples was reduced, the quality of the signal after subtraction would be improved.

When comparing figures 3.2(a), 3.2(b) and 3.2(c) with figures 3.4(a), 3.4(b) and 3.4(c), the effect of the ratio $[cocoa\ butter]/[sugar]$ on the sensitivity of the method can be observed. As the cooling rate is the same for both samples, similar crystals should be formed and indeed the location of the peak is the same ($d = 4.56$Å). However, the peak attributed to cocoa butter in solid chocolate has a stronger intensity in the case of dark chocolate. The liquid chocolate data is very similar since it is basically the spectrum of the sugar present in both milk and dark chocolate. This translates into a better quality for the peak after the subtraction.

To illustrate this difference in intensity of the diffracted signal, figure 3.9 shows the signal resulting from the subtraction method for slowly cooled (0.5°C $\cdot min^{-1}$) tempered dark chocolate, pure cocoa butter and milk chocolate. The maximum recorded peak for the subtracted signal of dark chocolate subtracted signal is $d = 4.56$Å as well as for the milk chocolate subtracted signal and the pure cocoa butter.

The peak intensity of dark chocolate compared to milk chocolate is higher by a ratio of 4.7 (67 $vs.$ 14). This value is surprisingly close to that expected from the $[cocoabutter]/[sugar]$ ratio, which is higher by 4.66 (2.8 $vs.$ 0.6), as discussed in chapter 2, and explains why the subtraction for dark chocolate is more accurate; the background signal (sugar) represents only a small part one the total recorded data.

When using dark chocolate, the better accuracy makes possible to see even low intensity peaks in the larger angle region ($d = 3.65$Å and $d = 3.98$Å) which has been used to differentiate the form βV from form βVI (Guthrie et al. 2005).

The hypothesis formulated initially; the subtraction of the liquid sample XRD (sugar baseline) from the solid sample XRD (cocoa butter and sugar) could allow the characterization of the cocoa butter state in chocolate, was tested and validated for different cooling rates (and therefore polymorphs) and formulations. This method has therefore been used to validate (in chapter 5) the model proposed in this work (in chapter 4).

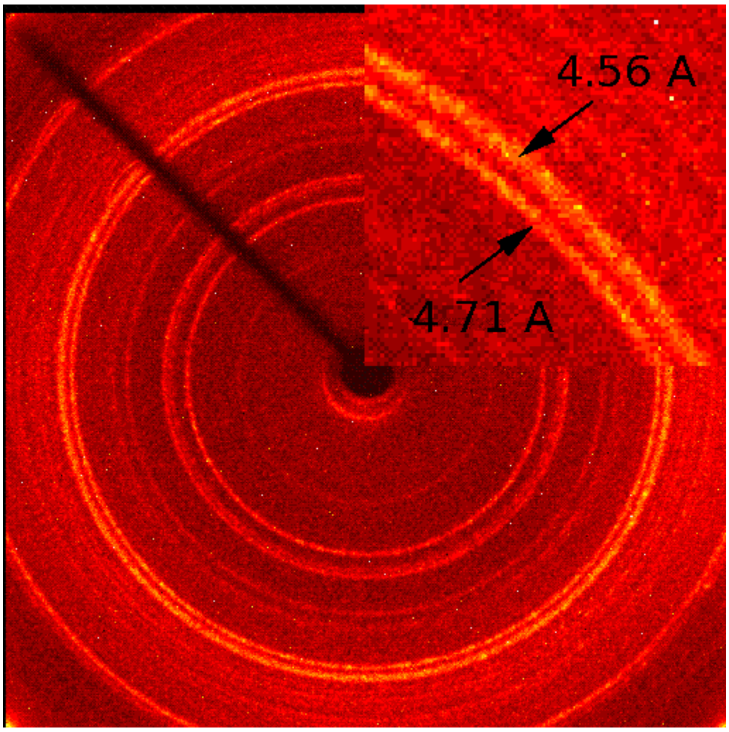

(a)

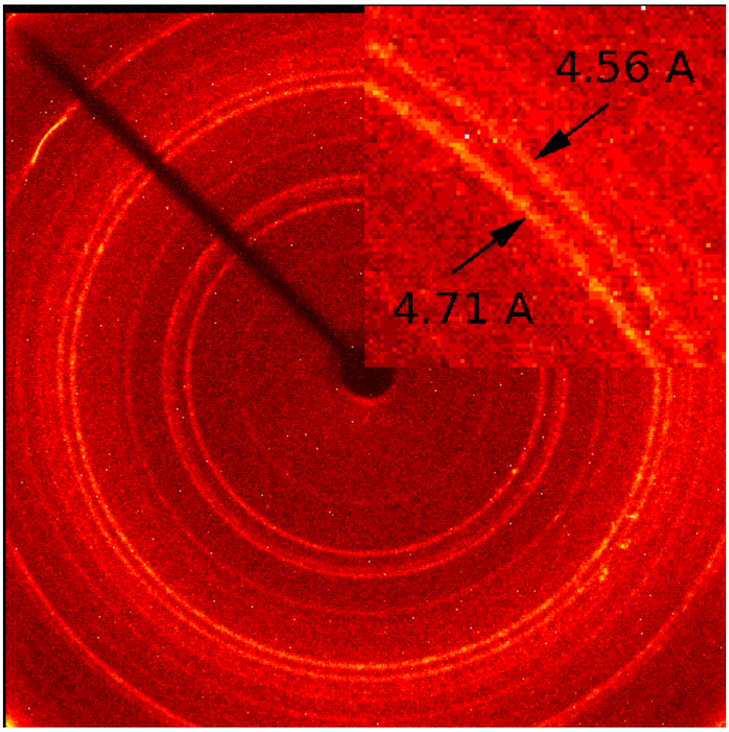

(b)

Figure 3.1: Diffractogram of solid 3.1(a) and liquid 3.1(b) milk chocolate.

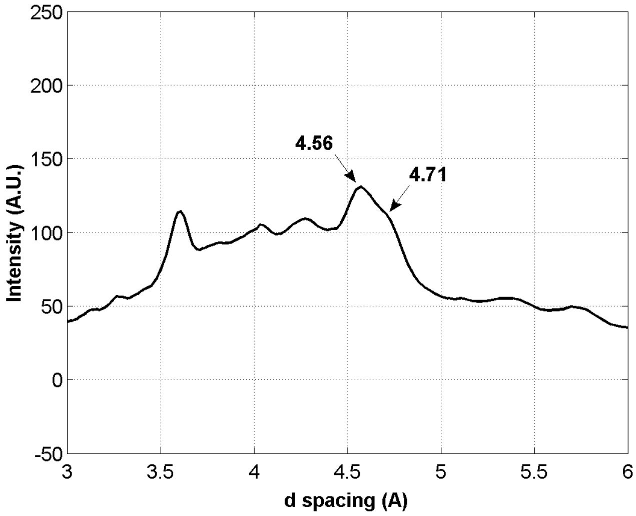

(a) solid milk chocolate cooled at 0.5°C $\cdot min^{-1}$

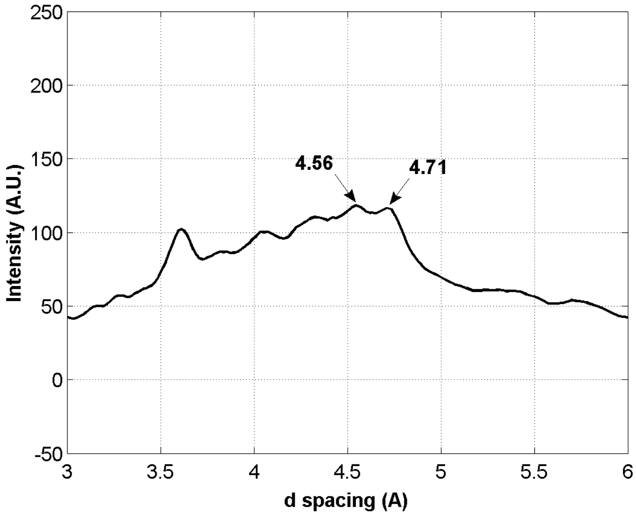

(b) liquid milk chocolate cooled at 0.5°C $\cdot min^{-1}$

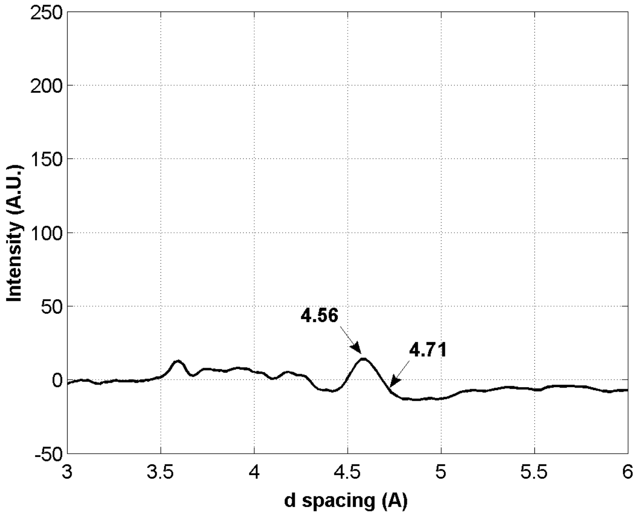

(c) subtraction: 3.2(a)-3.2(b)

Figure 3.2: Powder signal of solid (−30°C) 3.2(a) and liquid (40°C) 3.2(b) milk chocolate cooled at a nominal rate of 0.5°C $\cdot min^{-1}$. The subtraction 3.2(a)-3.2(b) is presented in 3.2(c).

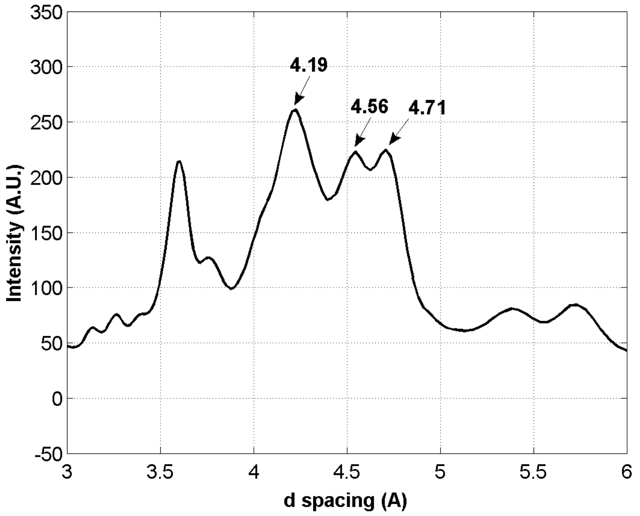

(a) solid milk chocolate cooled at 50°C $\cdot min^{-1}$

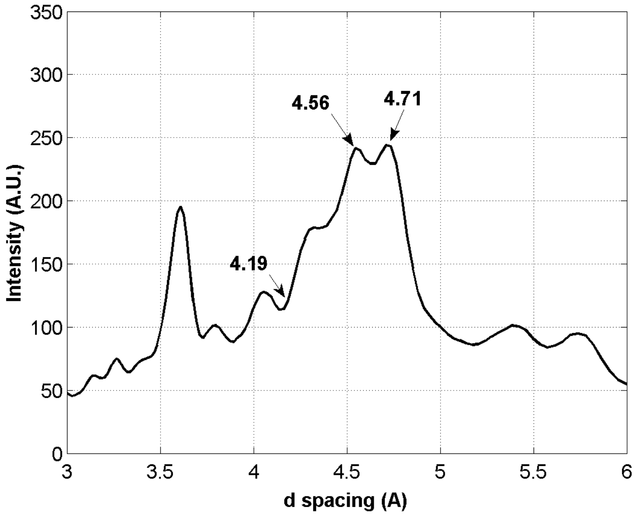

(b) liquid milk chocolate cooled at 50°C $\cdot min^{-1}$

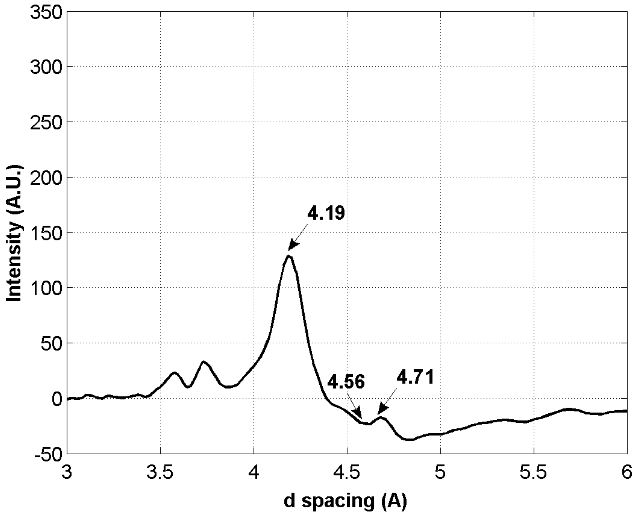

(c) subtraction: 3.3(a)-3.3(b)

Figure 3.3: Powder signal of solid (−30°C) 3.3(a) and liquid (40°C) 3.3(b) milk chocolate cooled at a nominal rate of 5°C $\cdot min^{-1}$. The subtraction 3.3(a)-3.3(b) is presented in 3.3(c).

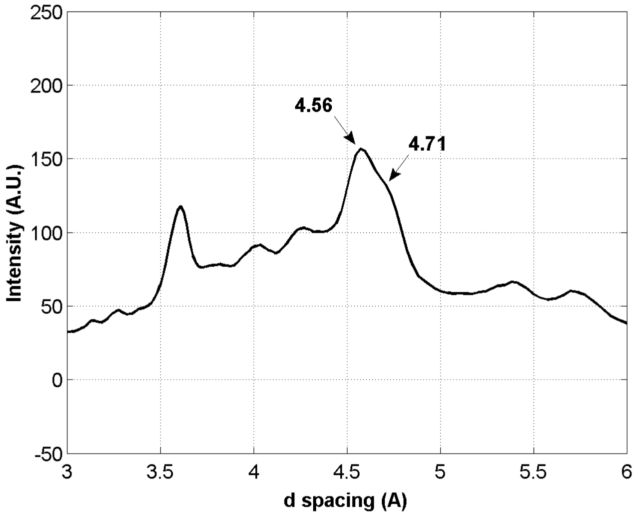

(a) solid dark chocolate cooled at 0.5°C $\cdot min^{-1}$

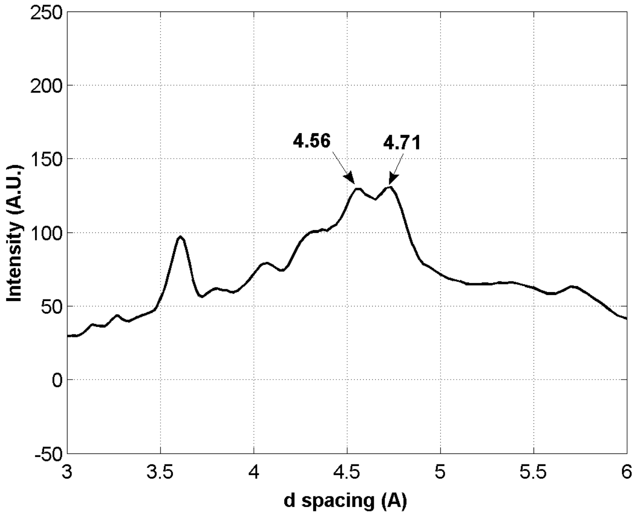

(b) liquid dark chocolate cooled at 0.5°C $\cdot min^{-1}$

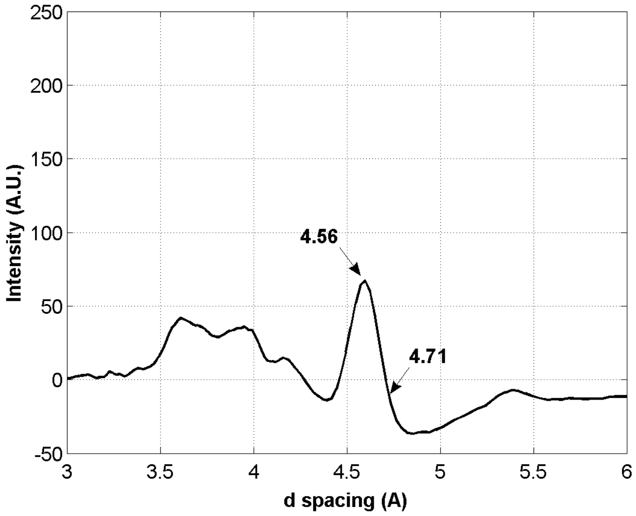

(c) subtraction: 3.4(a)-3.4(b)

Figure 3.4: Powder signal of solid (-30°C) 3.4(a) and liquid (40°C) 3.4(b) dark chocolate cooled at a nominal rate of 0.5°C $\cdot min^{-1}$. The subtraction 3.4(a)-3.4(b) is presented in 3.4(c).

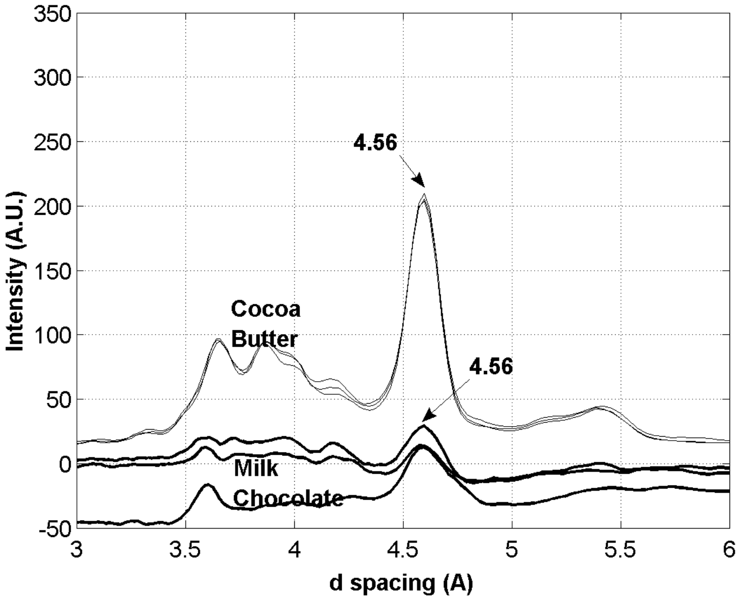

Figure 3.5: Comparison between the XRD diffraction pattern of pure cocoa butter cooled slowly, leading to the formation of *stable* β crystals and the signal obtained from the subtraction of the XRD pattern of liquid milk chocolate from the XRD pattern of solid milk chocolate cooled using the same process as the cocoa butter.

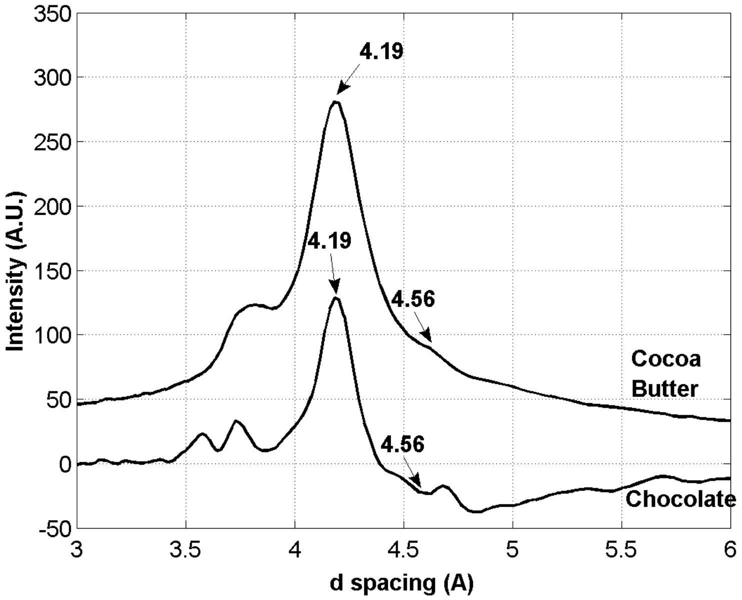

Figure 3.6: Comparison between the XRD diffraction pattern of pure cocoa cooled quickly, leading to the formation of *unstable* β' crystals and the signal obtained from the subtraction of the XRD pattern of liquid milk chocolate from the XRD pattern of solid milk chocolate cooled using the same process as the cocoa butter.

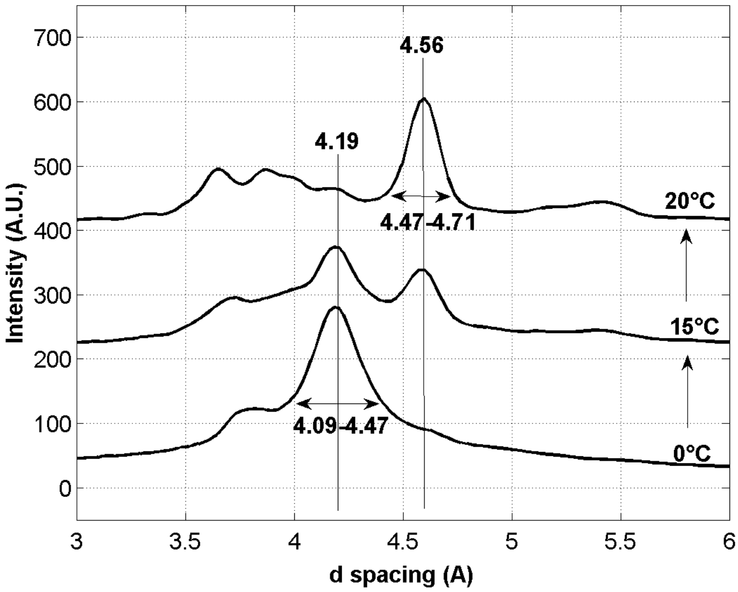

Figure 3.7: Evolution of the microstructure of cocoa butter quickly cooled then slowly heated. The *unstable* β' crystals initially present are gradually replaced by *stable* β crystals. (the curves are separated by 200 arbitrary units for better visualisation)

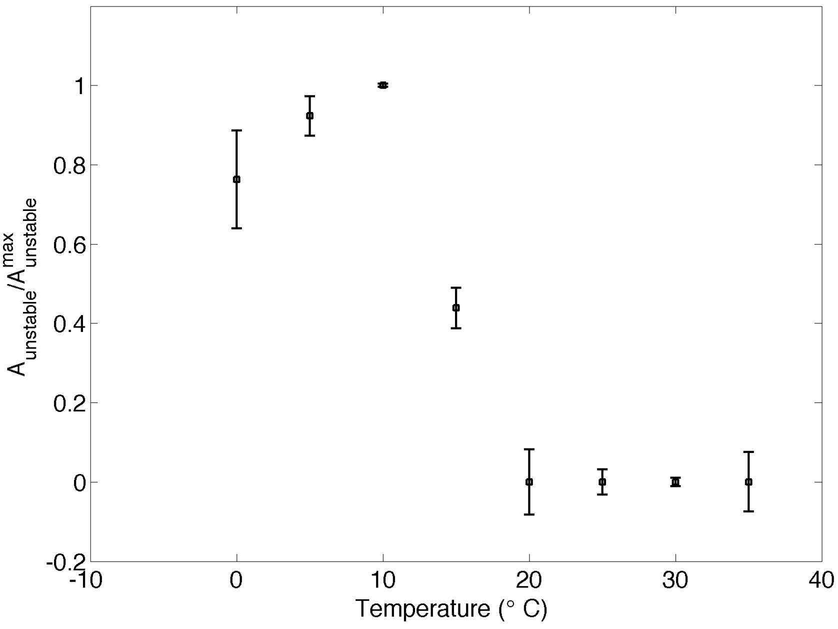

(a)

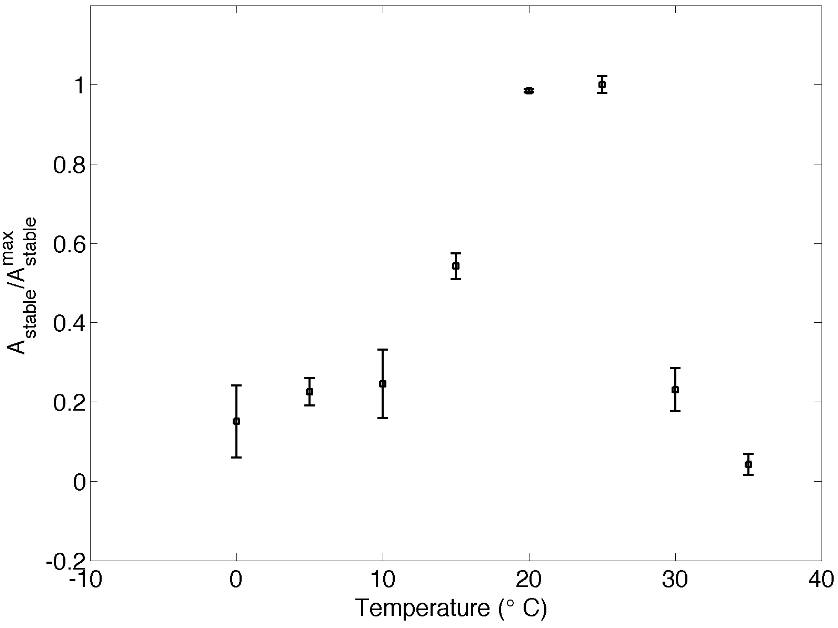

(b)

Figure 3.8: Evolution of the concentration (as measured using XRD) of *unstable* crystals (3.8(a)) and *stable* crystals (3.8(a)) in a sample originally cooled at 50°C $\cdot min^{-1}$.

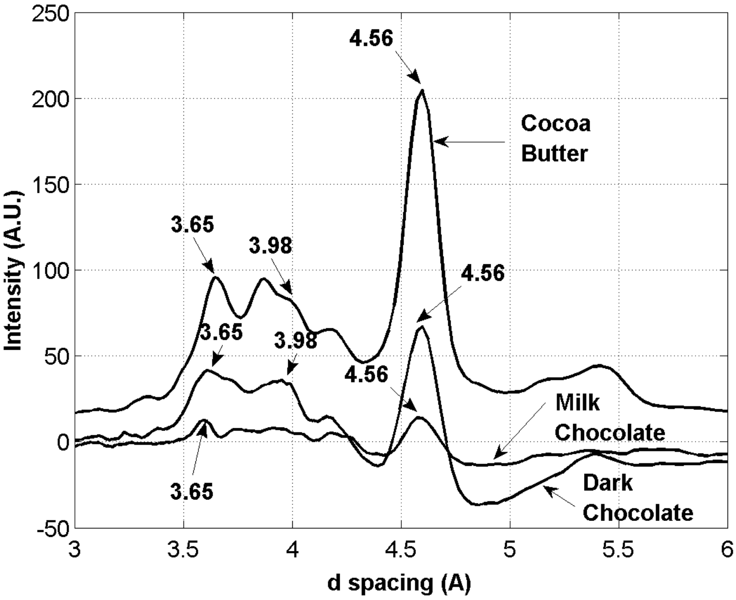

Figure 3.9: Comparison between the XRD diffraction pattern of pure cocoa cooled slowly, leading to the formation of *stable* β crystals and the signal obtained from the subtraction of the XRD pattern of liquid dark (and milk) chocolate from the XRD pattern of solid dark (and milk) chocolate cooled using the same process as the cocoa butter.

Table 3.1: Evolution of the area of the peak characteristic of *stable* crystals ($d = 4.56\text{Å}$) during reheating of chocolate cooled using profile 1

T	A_{stable}	$\frac{A_{stable}}{A_{stable}^{max}}$
0	0.0097	0.0849
5	0.026	0.1979
10	0.0207	0.1813
15	0.0636	0.5569
20	0.1104	0.9667
25	0.1142	1.0000
30	0.0303	0.2653
35	0.0026	0.0228
40	0	0

CHAPTER 4

MODEL DEVELOPMENT

In order to understand the physical phenomena occurring during the solidification of chocolate, a model of the crystallisation of cocoa butter has been developed. It is divided in two parts:

1. a kinetic model which emulates the system by considering a set of reactions between different polymorphs and the melt. The rates of the reactions were set to be dependent on temperature, as crystallisation occurs when the melt is supersaturated (function of temperature) (Decloux 2002) and melting occurs when enough energy (as heat) is transferred to the system.
2. a heat transfer model which heat source term is estimated from the results of the kinetic model.

Since the kinetic model depends on the temperature and the heat transfer model depends on the kinetics, a coupled approach had to be used to solve the problem. This was possible using the COMSOL Multiphysics software.

4.1 Development of a simplified mathematical model to describe the phase change of fats

Cocoa butter is the main functional material in the phase change of chocolate, as verified in chapter 3 using the XRD subtraction method. As described in chapter 1, there are six polymorphs for cocoa butter, so the solidification of chocolate in the correct form is a complex operation. The crystal form preferred by consumers is form V since it melts around 31°C meaning that it will melt easily at mouth temperature but will not melt in the hand.

The details of the six polymorphs were already presented in section 1.3.2. According to literature data, it was decided that polymorphs could be grouped in:

1. The *unstable* crystals, consisting of γ, α and β' crystals (I to IV) with a strong peak in the XRD short spacing pattern below or around 4.20Å and are not stable at room temperature (melting point below 30°C).
2. The *stable* crystals, consisting of β crystals (V and VI) with a strong peak in the XRD short spacing pattern around 4.60Å and are stable at room temperature (melting point above 30°C).

Because of the difference of melting points, the two families can be easily distinguished using DSC data. The results of initial experiments are reported in figures 4.1 and 4.2 and show that two temperature ranges for the melting peaks can be identified.

It is generally accepted that two factors controlling the crystal structure (*stable* or *unstable*) of the final product are (*i*) tempering (Afoakwa, Paterson, Fowler et al. ND, Loisel et al. 1997a, Loisel et al. 1997b, Lonchampt and Hartel 2006, Lovegren et al. 1976) and (*ii*) the cooling rate (Stapley et al. 1999) applied during the solidification. The influence of these factors was investigated using DSC.

In figure 4.1, the effect of tempering on crystallisation as measured by DSC is shown by comparing the crystallisation and melting behaviour of a tempered and an untempered sample of the same milk chocolate formulation. When chocolate is untempered the crystallisation curve has a peak (B) at 14°C whereas for the tempered crystallisation curve, the peak (A) reaches its maximum at 21°C. This is due to the presence of form V crystals in the melt of the tempered chocolate, form V is a high enthalpy (H) state and therefore has a high crystallisation point. The untempered chocolate crystallises in a non controlled way leading to α and β' polymorphs.
During reheating the untempered chocolate melts (C) at a low temperature (19.5°C) due to the unstable polymorphic state of the cocoa butter. Tempered chocolate melts (D) around 29°C which confirms that the polymorph formed during cooling was form V (β).

In figure 4.2 the effect of two different cooling rates on the phase changes in tempered chocolate is shown by comparing the crystallisation and melting behaviour of a tempered sample of the same milk chocolate formulation cooled at 1°C $\cdot min^{-1}$ and 10°C $\cdot min^{-1}$. When a relatively slow (1°C $\cdot min^{-1}$) cooling rate is applied to tempered milk chocolate, the crystallisation occurs (A) around 21°C which is similar to the values obtained in the literature (Stapley et al. 1999, Tewkesbury et al. 2000). When a quick cooling rate (10°C $\cdot min^{-1}$) is applied to tempered milk chocolate, the crystallisation occurs (B) around 12°C similarly to the crystallisation curve of untempered chocolate in figure 4.1. One can assume that crystals α or β' are formed during this quick cooling as they are for untempered chocolate since the crystallisation temperature is similar. The rapid cooling probably induces kinetic limitations in the development of βV crystals. During reheating the slowly cooled chocolate melts (F) at 29°C, as (D) in figure 4.1. An interesting phenomenon occurs for the quickly cooled chocolate:

1. quickly formed crystals melt (C) first around 18°C, same as (C) in figure 4.1.

2. recrystallisation or solid-solid transition happens, as shown by the exothermic peak

(D) at 21°C (same temperature than slow cooling crystallisation (B) from melt).

3. more stable crystals formed during reheating (and/or partially present initially) melt (E) at 29°C (same as (F)).

It is interesting to notice that this polymorphous transition only occurs when the chocolate was initially tempered as no transition is seen in the reheating curve of the untempered chocolate in figure 4.1. The need for tempering is therefore essential whether rapid or slow cooling is to be applied to the chocolate.

These experimental observations indicate that:

1. Two main peaks can be seen for crystallisation at 12°C or 21°C and two main peaks can be seen for melting at 18°C or 29°C . Thus the six polymorphs can be clustered in two groups.
2. *unstable* crystals form either when cooling untempered chocolate or by rapid cooling of tempered chocolate.
3. *stable* crystals form either by slow cooling of tempered chocolate or by reheating of rapidly cooled tempered chocolate.

These observations are consistent with the findings reported in chapter 3 using XRD data. The presence of a peak at $d = 4.19$Å can be linked with the low melting point (18°C) of *unstable* (form III) crystals for high cooling rates (> 2°C $\cdot min^{-1}$) while the presence of a peak at $d = 4.56$Å can be linked with the high melting point (30°C) of *stable* (form V) crystals for low cooling rates (< 2°C $\cdot min^{-1}$). As discussed in the introduction (section 1.4.3), a model considering more polymorphs has been published (Fessas et al. 2005) by deconvolution of the DSC signal in individual peaks but no kinetic rates have been reported in the paper suggesting a failure in the parameter identification step, probably caused by the complexity of the system.

For our simplified system, six essential reactions can describe the system by linking the three different phases (*stable*, *unstable* and *melt*) to one another:

$$\begin{array}{cc}
\text{Nucleation of}\, unstable & melt \xrightarrow{k_{nuc}} unstable \\
\text{Growth of}\, stable & melt \xrightarrow{k_{ms},\, stable^c} stable \\
\text{Growth of}\, unstable & melt \xrightarrow{k_{mu},\, unstable^c} unstable \\
unstable\,\text{to}\, stable & unstable \xrightarrow{k_{us},\, stable^c} stable \\
\text{Melting of}\, stable & stable \xrightarrow{k_{sm}} melt \\
\text{Melting of}\, unstable & unstable \xrightarrow{k_{um}} melt
\end{array} \tag{4.1}$$

In order to be able to calculate the amount of crystals present during cooling or heating of chocolate, the reactions presented in (4.1) were formulated as mass balances:

$$\begin{aligned}
\frac{d[stable]}{dt} &= k_{ms} \cdot [melt] \cdot [stable]^c + k_{us} \cdot [unstable] \cdot [stable]^c - k_{sm} \cdot [stable] \\
\frac{d[unstable]}{dt} &= k_{nuc} \cdot [melt] + k_{mu} \cdot [melt] \cdot [unstable]^c - k_{um} \cdot [unstable] - k_{us} \cdot [unstable] \cdot [stable]^c \\
\frac{d[melt]}{dt} &= -k_{ms} \cdot [melt] \cdot [stable]^c + k_{sm} \cdot [stable] - k_{nuc} \cdot [melt] - k_{mu} \cdot [melt] \cdot [unstable]^c \\
& \quad + k_{um} \cdot [unstable]
\end{aligned} \tag{4.2}$$

To simplify the model, each of the kinetic parameters were considered constant over the range of temperature applicable (higher or lower than the phase change temperature). They were therefore modelled as sigmoid functions (in this case logistic functions) dependent on the difference between the temperature and the crystallisation (solidus) or melting (liquidus). For example, during the crystallisation of stable crystals from the melt, the rate of the reaction $k_{ms} = 0 s^{-1}$ if the temperature is higher than the crystallisation temperature (solidus) $T_{ms} = 21$°C and $k_{ms} = K_{ms}\, s^{-1}$ if the temperature is lower. The use of the logistic function helps to smooth the step change around the critical temperature to avoid any numerical discontinuity.

The *unstable* phase nucleation kinetic rate k_{nuc} was modelled as a piecewise linear function of temperature since it seemed fair to assume that the supercooling $(T_{nuc} - T)$ was the driving force for nucleation.

Overall, the model requires estimation of six constants; K_{ms}, K_{sm}, K_{mu}, K_{um}, K_{us} and K_{nuc}; to be fitted on experimental data.

$$k_{ii} = \begin{cases} \frac{K_{ii}}{1-e^{+(T-T_{ii})}} & \text{for } k_{us}, k_{um} \text{ and } k_{sm} \\ \frac{K_{ii}}{1-e^{-(T-T_{ii})}} & \text{for } k_{mu} \text{ and } k_{ms} \end{cases} \tag{4.3}$$

$$k_{nuc} = \begin{cases} K_{nuc} \cdot (T_{nuc} - T) & (T < T_{nuc}) \\ 0 & (T \geq T_{nuc}) \end{cases}$$

The shape of the sigmoid functions was fixed as described in (4.3) and only the maximum value was to be estimated.

The temperature at which the transformations occur were obtained by measurement of the crystallisation and melting temperatures for the stable and the unstable phase using preliminary obtained DSC data. The values used are presented in table 4.1. The temperatures presented for the melting of *stable* (form V) is lower than the temperature reported for pure cocoa butter due to the influence of milk fats (Chapman et al. 1971).

4.2 Fitting of the kinetic model to DSC data

DSC can be used to measure the heat flow generated during a phase change, as discussed in section 1.3.2. This heat flow can also be calculated theoretically by solving the system of ODEs and using the following equation:

$$\dot{Q}_{source} = \Delta H_{stable} \cdot \frac{\partial[stable]}{\partial t} + \Delta H_{unstable} \cdot \frac{\partial[unstable]}{\partial t} \tag{4.4}$$

To be able to estimate $\dot{Q}_{source}$, ΔH_{stable} and $\Delta H_{unstable}$ were measured using the Perkin Elmer software. Using the built-in numerical integration routine for the melting peaks area, it was found that $\Delta H_{stable} \approx 22000 J \cdot kg^{-1}$ and $\Delta H_{unstable} \approx 19000 J \cdot kg^{-1}$.

One could have also obtained these values using the ΔH values for form V ($\approx 136000 J \cdot kg^{-1}$) and III ($\approx 117000 J \cdot kg^{-1}$) of pure cocoa butter (Loisel et al. 1998). Considering a maximum Solid Fat Content $SFC_{max} = 80\%$ (as in figure 1.8) and the concentration in cocoa butter in the chocolate used $[cocoa\,butter] = 19.5\%$, and that only cocoa butter contributes to the phase change peak, one would obtain:

$$\Delta H_{stable} = \Delta H_{formV} \cdot SFC_{max} \cdot [cocoa\,butter] = 21200 J \cdot kg^{-1} \tag{4.5}$$

$$\Delta H_{unstable} = \Delta H_{formIII} \cdot SFC_{max} \cdot [cocoa\,butter] = 18250 J \cdot kg^{-1}. \tag{4.6}$$

which is very close to the numbers obtained from chocolate in the DSC.

To obtain the K_{ii} values, the system 4.2 of Ordinary Differential Equations (ODEs) was solved using MATLAB's `ode23` solver and the solution was fitted on a set of DSC experiments using the MATLAB optimization routine `fmincon` used to minimize the quantity $\sum(Cp_{eff_{experiment}} - \frac{\dot{Q}_{source_{model}}}{\rho \cdot \frac{dT}{dt}})^4$ ($\dot{Q}_{source}$ calculated as in equation 4.4). The use of the power 4 rather than the more often used power 2 (commonly referred as sum of squares) allowed to give more weight to the peaks rather than to the baseline of the DSC signal.

Kinetic rates k_{ms}, k_{mu} and k_{us} were assumed to be dependent on the amount of crystals present in the system. This hypothesis originates from the fact that tempering is a requirement to the crystallisation of *stable* crystals from the melt (Le Révérend et al. 2008). Similarly the presence of *unstable* crystals would increase the crystallisation rate of the *unstable* phase. However, recent experimental work (Yasuyoshi and Hartel 2008) has reported that the actual amount of seeds required was not of significant importance, as long as some were present. Thus a parameter c, representing the weight of the concentration of crystals already present in the system on the kinetic rates (k_{ms}, k_{mu} and k_{us}) was therefore set to a small value ($c = 0.1$).

The cooling rates used in the set of DSC experiments to fit the parameters were 0.5, 1, 2, 5, 10 and 20°C $\cdot min^{-1}$ and the reheating rates was fixed at 5°C $\cdot min^{-1}$. The quantity $\sum(Cp_{eff_{experiment}} - \frac{\dot{Q}_{source_{model}}}{\rho \cdot \frac{dT}{dt}})^4$ was summed for each of these experiment. Typical results of the optimization routines can be seen on figure 4.3. At the end of the optimization routine, a set of parameters for the kinetic model was obtained, this set is presented in table 4.1. As expected the *stable* crystals take longer to form than *unstable* crystals ($K_{ms} = 0.005 s^{-1}$ vs. $K_{mu} = 0.08 s^{-1}$) while the melting of both crystal forms follow similar kinetics. The *unstable* to *stable* transition is very fast compared to the *melt* to *stable* reactions and this is consistent with the published data (Mazzanti, Marangoni and Idziak 2005) where the authors found this reaction dominant at 22°C which is close to the temperature where k_{us} starts to increase ($T_{us} = 25$°C). A general view of the kinetic rates in function of temperature can be seen in figure 4.4.

4.3 Coupling of the kinetic model to the heat transfer equation

When there is a spatial distribution of temperature (like on the Peltier stage cell or in industrial processes), the heat transfer equation 4.7 has to be solved.

$$\rho \cdot Cp \cdot \frac{\partial T}{\partial t} = \nabla \cdot (k \cdot \nabla T) + \dot{Q}_{source} \tag{4.7}$$

As discussed in section 1.5, boundary and initial conditions used have to be defined as well. The boundary conditions are dependent on the equipment used. The behaviour of the specifically designed rig has been investigated.

4.3.1 Determination of the thermal behaviour of the Peltier Chocolate Rig (PCR)

The model will be validated using the PCR, thus the relevant boundary conditions experienced in the PCR had to be estimated.

Preliminary experimental data showed that the temperature set on the Peltier stage was never recorded by the thermocouples in the chocolate, even when steady state was reached. This suggests that there is a deviation from a perfect contact (Dirichlet condition) at the Peltier stage cooling surface and that some heat is lost on the insulated surface. To define the boundary conditions, it was also necessary to estimate the heat transfer coefficients on both surfaces.

This was achieved by fitting experimental temperature profiles to a theoretical model of heat conduction in a material with known thermal properties (conductivity k, density ρ and heat capacity Cp). An agar gel ($0.5\%\,w/w$) having the thermal properties of water of $k = 0.57 W \cdot m^{-1} \cdot K^{-1}$, $\rho = 1000 kg \cdot m^{-3}$ and $Cp = 4180 J \cdot kg^{-1} \cdot K^{-1}$ was used (Le Maguer 1986). The temperature profiles were obtained over a range of experimental conditions.

Four experiments were conducted:

1. cooling the gel from 60°C down to 30°C

2. cooling the gel from 20°C down to 0°C
3. heating the gel from 0°C down to 30°C
4. heating the gel from 40°C down to 60°C

In each case, the equation for conduction heat transfer (4.7) was solved with $\dot{Q}_{source} = 0$, since no phase change occurred within the temperature range. As already explained, at the center of the cell (where the thermocouples are located) heat transfer can be considered unidirectional. Thus, to decrease computational cost without compromising accuracy a 1D finite difference model was used.

The sum of squares between the experimental and the numerical data (4 experiments, 3 thermocouples each) were minimized during the fitting process to find the best couple $(h_{insulator}, h_{Peltier})$ to satisfy the experimental data. The values found were:

1. $h_{Peltier} = 150W \cdot m^{-2} \cdot K^{-1}$ which is typical for heat transfer between food in contact with solids (Wichchukit, Zorrilla and Singh 2001).
2. $h_{insulator} = 7W \cdot m^{-2} \cdot K^{-1}$ which means that the insulation used could have been thicker since this value is relatively high (natural convection provides $h \approx 20W \cdot m^{-2} \cdot K^{-1}$).

Typical examples of the fitting results are presented in figure 4.5.

4.3.2 Determination of the thermal properties of chocolate

Further to boundary conditions the thermal properties of chocolate were also required for the model.

The density ρ was measured gravimetrically by weighting a known ($100ml$) volume of liquid chocolate, it was found that for the formulation used $\rho = 1300kg \cdot m^{-3}$. The specific heat capacity Cp was measured by using DSC data in the region where there was no phase change. The values $Cp_{solid} = 2000\,J \cdot kg^{-1} \cdot K^{-1}$ and $Cp_{liquid} = 1500\,J \cdot kg^{-1} \cdot K^{-1}$ were measured. These values are very similar to the ones found in precedent studies (Tewkesbury et al. 2000).

Only the thermal conductivity k had to be estimated. As the heat transfer coefficients for the system were known from section 4.3.1, the thermal conductivity k has been estimated by fitting the model on experimentally obtained temperature profiles where no phase change could be observed. For solid chocolate the range was $0 - 20$°C and for liquid chocolate the range was $40 - 60$°C . This curve fitting process lead to $k_{solid} = 0.25 W \cdot m^{-1} \cdot K^{-1}$ and $k_{liquid} = 0.35 W \cdot m^{-1} \cdot K^{-1}$. These values were of similar order compared to the values found in the literature (Tewkesbury et al. 2000). A typical example of the fitting result is presented in figure 4.6.

One can appreciate that the quality of the fit in figure 4.6 is not as good as in figure 4.5. This can be attributed to the fact that chocolate is a more complex system than the agar gel and that the thermal properties over the temperature scan are not really constants. Given the number of polymorphs in the system, it is likely that transitions occur in the system, therefore defining a single k is difficult. However it was considered that the correlation coefficient $r^2 = 0.965$ was good enough to carry on with this assumption and the values found.

4.3.3 Application modes, geometry, mesh and solver

To couple different physical phenomena in COMSOL, it is necessary to define different `Application modes` which describe the physics applied to the system. The `Application modes` used in our case were:

1. Transient conduction heat transfer (T) with the following properties:

Thermal conductivity (estimated by curve fitting in 4.3.2) $k = k_{solid} \cdot [unstable + stable] + k_{liquid} \cdot [melt]$.

Density (measured gravimetrically in 4.3.2) $\rho = 1300 kg \cdot m^{-3}$.

Specific heat capacity (measured by DSC in 4.3.2) $Cp = Cp_{solid} \cdot [unstable + stable] + Cp_{liquid} \cdot [melt]$

Source term (ΔH measured in 4.2) $\dot{Q}_{source} = \Delta H_{stable} \cdot \frac{\partial [stable]}{\partial t} + \Delta H_{unstable} \cdot \frac{\partial [unstable]}{\partial t}$.

Boundary conditions (estimated by curve fitting in 4.3.1) $h_{Peltier} = 150 W \cdot m^{-2} \cdot K^{-1}$, $T_{Peltier}$ is the temperature of the Peltier stage during the profile, $h_{insulator} = 7 W \cdot m^{-2} \cdot K^{-1}$, $T_{ext} = 23°\text{C}$ is the external temperature around the insulator and insulation $\nabla T \cdot n = 0$ elsewhere. These boundary conditions are specified on the geometry in figure 4.7(b).

Initial condition $T_0 = 30°\text{C}$ which is the temperature of the chocolate at the end of the tempering process.

The evolution of the phases within each element of the mesh was described using the Convection Diffusion application mode by setting the diffusion rate to 0. This effectively enables us to solve the ODE system with a temperature dependence for the kinetic rates within each mesh element.

2. Convection Diffusion ($[stable]$) with the following properties:

Reaction rate (k_{ii} estimated by curve fitting in 4.2) $k_{ms} \cdot [melt] \cdot [stable]^c + k_{us} \cdot [unstable] \cdot [stable]^c - k_{sm} \cdot [stable]$.

Boundary conditions Insulation $\nabla [stable] \cdot n = 0$.

Initial condition $[stable]_0 = 0.03$ which is the relative concentration in *stable* crystals of the chocolate at the end of the tempering process (Metin and Hartel 2005).

3. Convection Diffusion ($[unstable]$) with the following properties:

   Reaction rate (k_{ii} estimated by curve fitting in 4.2) $k_{nuc} \cdot [melt] + k_{mu} \cdot [melt] \cdot [unstable]^c - k_{um} \cdot [unstable] - k_{us} \cdot [unstable] \cdot [stable]^c$.

   Boundary conditions Insulation $\nabla[unstable] \cdot n = 0$.

   Initial condition $[unstable]_0 = 0$ which is the relative concentration in *unstable* crystals of the chocolate at the end of the tempering process.

4. Convection Diffusion ($[melt]$) with the following properties:

   Reaction rate (k_{ii} estimated by curve fitting in 4.2) $-k_{ms} \cdot [melt] \cdot [stable]^c + k_{sm}[stable] - k_{nuc} \cdot [melt] - k_{mu} \cdot [melt] \cdot [unstable]^c + k_{um} \cdot [unstable]$.

   Boundary conditions Insulation $\nabla[melt] \cdot n = 0$.

   Initial condition $]melt]_0 = 0.97$ which is the relative concentration in *melt* material of the chocolate at the end of the tempering process (Metin and Hartel 2005).

Since it was found using a preliminary FEM model that the heat transfer was unidirectional in the vicinity of the thermocouples, only a narrow 2-D shape was modelled. The experimental 3-D system ($40 \times 40 \times 11mm$) was simplified to a 2-D ($5 \times 11mm$) surface. The system was also solved in a 1-D geometry ($11mm$) but no significant differences in the computational time ($25s$) were found. This is due to the COMSOL GUI being the limiting factor in simple problems.

To solve the set of equations numerically, the computational domain was discretized using the integrated meshing capabilities of COMSOL algorithms. The meshing must however be handled with great care since the accuracy of the solution can be greatly improved by a fine mesh but too fine a mesh will significantly increase the computing time for only a small improvement in accuracy. Since chocolate has a low thermal conductivity, heat transfer in the material is slow, implying that a relatively coarse mesh can be used.

However, at the interface with the Peltier stage some large temperature (and therefore crystallinity) gradients can be observed, hence a finer mesh was used on the boundary where the chocolate is in contact with the Peltier stage.

To find out rigorously what was the best compromise between the required computational time and the accuracy of the solution, the mesh dependency of the solution was investigated. The criterion used was the amount of *unstable* crystals at $200\mu m$ from the Peltier stage after $120s$ of profile 1 (*cf.* figure 2.5(b)). The solution stabilizes around 0.64 as the quality of the mesh (number of elements) increases as seen in figure 4.7(a). As suspected, it was found that a high number of elements at the interface with the cooler and a coarser mesh elsewhere was the best compromise between speed and accuracy of the solution. This was achieved by using the `Normal` free mesh mode and with the maximum element size set to $100\,\mu m$ on the boundary in contact with the Peltier stage. The mesh proceeding from these settings consists of 923 elements and is presented in figure 4.7(b). The computational time required to solve the problem is $203s$. On figure 4.7(a), one can see that this is the mesh providing the stable solution using the lowest number of elements.

Several solvers are available to the user in COMSOL Multiphysics. The solver used in this case is the default UMFPACK, typically used for solving any sparse matrix LU factorization problems (Davis 2004, Davis and Duff 1997). The time step setting was set to `strict` and the solver was allowed to use complex solutions since the exponent $c = 0.1 < 1$ could result in a solver crash if [*stable*], [*unstable*] and [*melt*] were to reach very small negative values ($> -10^{-5}$) as it is often the case in diffusion problems.

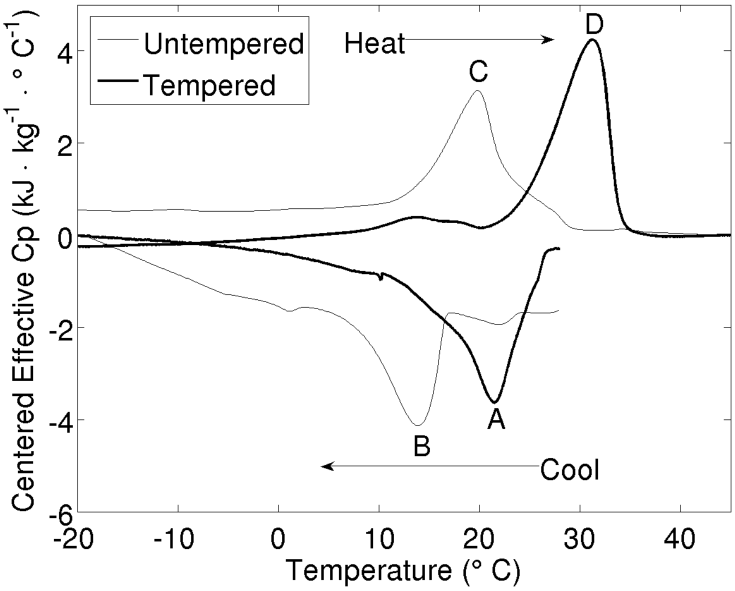

Figure 4.1: DSC curves for tempered and untempered chocolates cooled from 30°C at 1°C $\cdot min^{-1}$ (bottom) and reheated to 40°C at 5°C $\cdot min^{-1}$ (top)

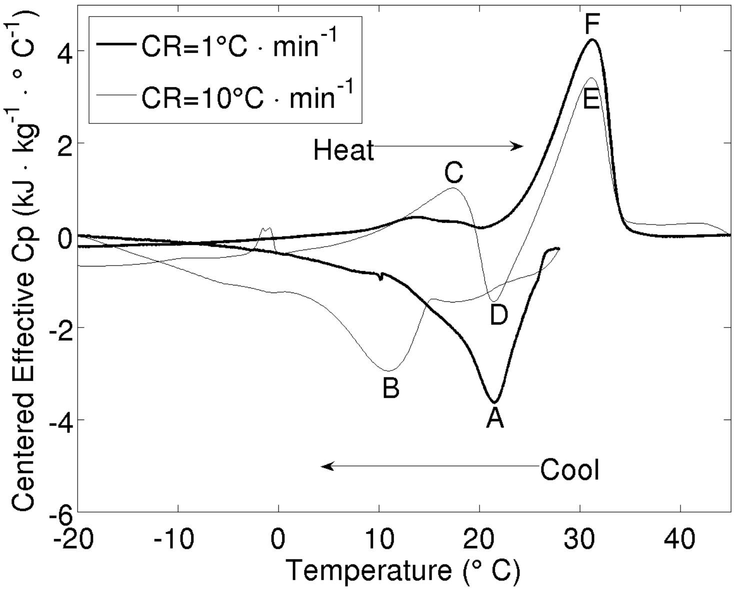

Figure 4.2: DSC curves for tempered chocolates cooled from 30°C at 1°C $\cdot min^{-1}$ and 10°C $\cdot min^{-1}$ (bottom) and reheated to 40°C at 5°C $\cdot min^{-1}$ (top)

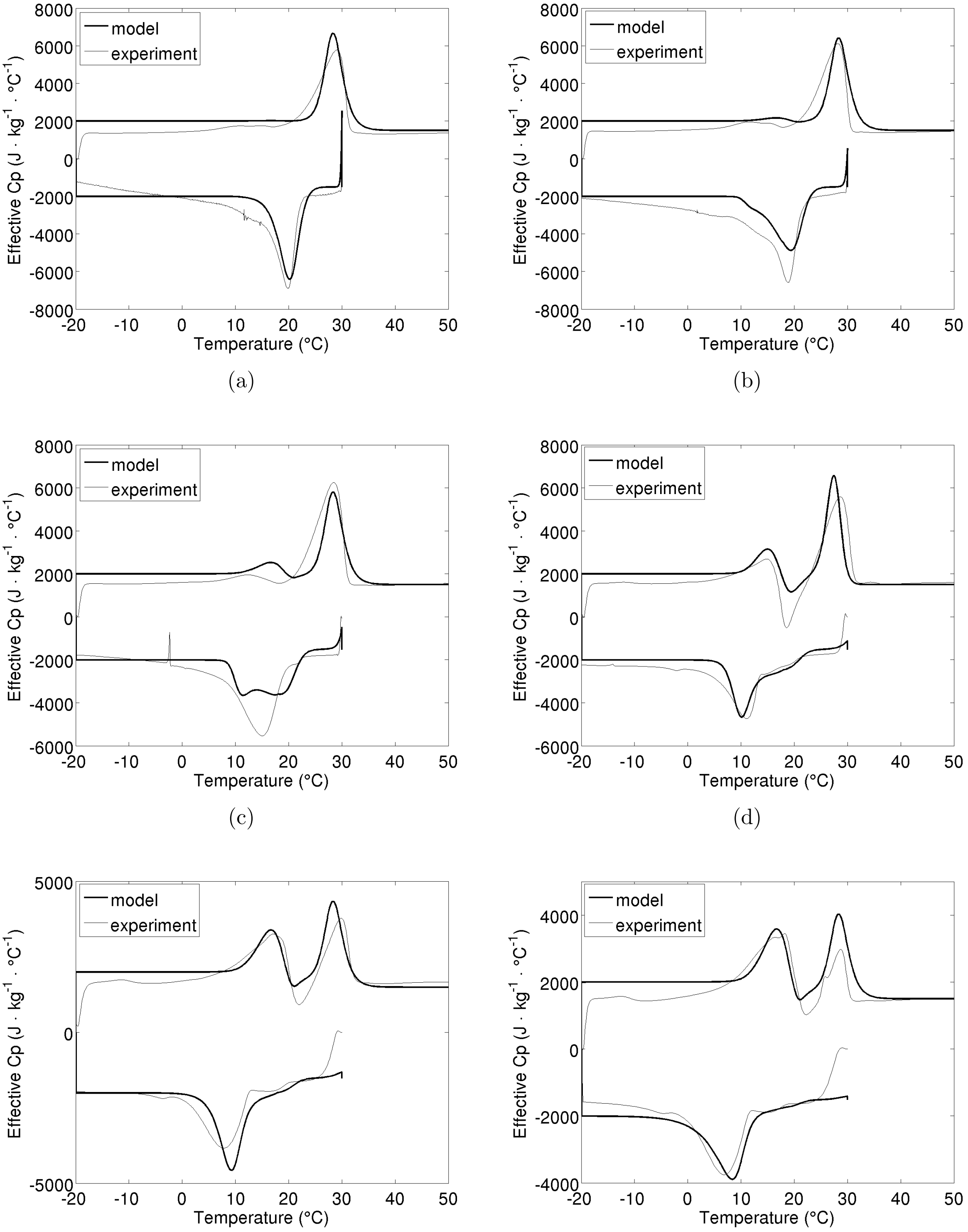

(a) (b)

(c) (d)

(e) (f)

Figure 4.3: Comparison between calculated and measured DSC profiles for cooling rates of 0.5°C $\cdot min^{-1}$ (4.3(a)), 1°C $\cdot min^{-1}$ (4.3(b)), 2°C $\cdot min^{-1}$ (4.3(c)), 5°C $\cdot min^{-1}$ (4.3(d)), 10°C $\cdot min^{-1}$ (4.3(e)) and 20°C $\cdot min^{-1}$ (4.3(f)) after fitting of the kinetic parameters.

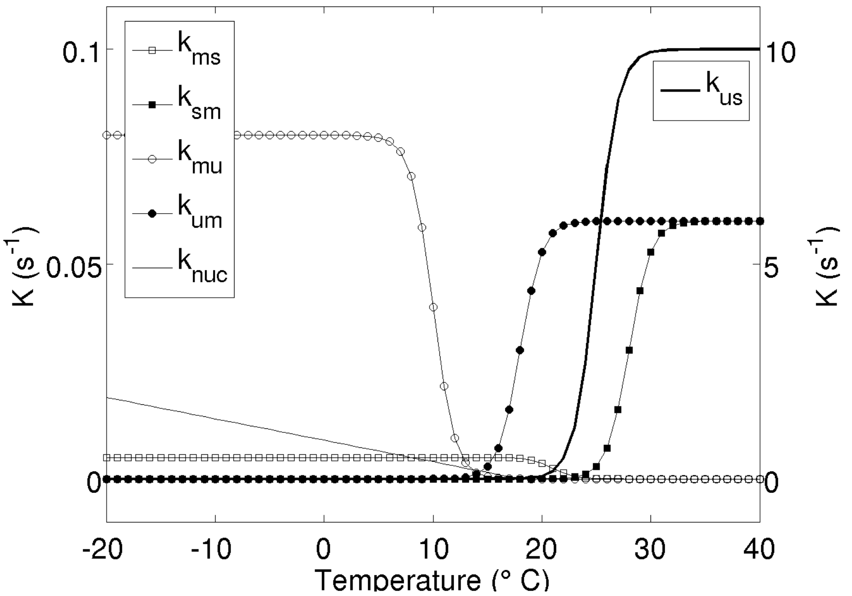

Figure 4.4: Kinetic parameters for the different phase changes in function of temperature. k_{ms}, k_{sm}, k_{mu}, k_{um} and k_{nuc} are on the left axis. k_{us} is on the right axis.

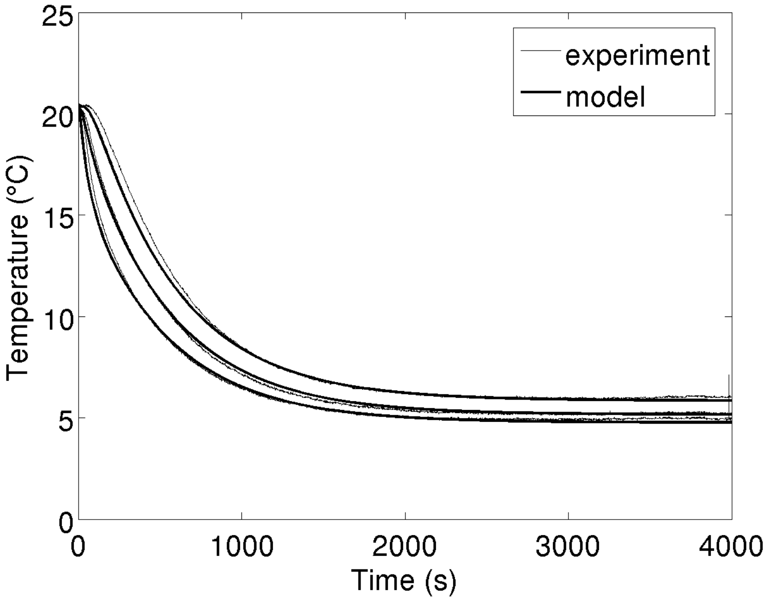

Figure 4.5: Comparison between fitted and measured temperature profile using thermocouples (K) during the cooling of an agar gel (0.5% w/w) in the PCR.

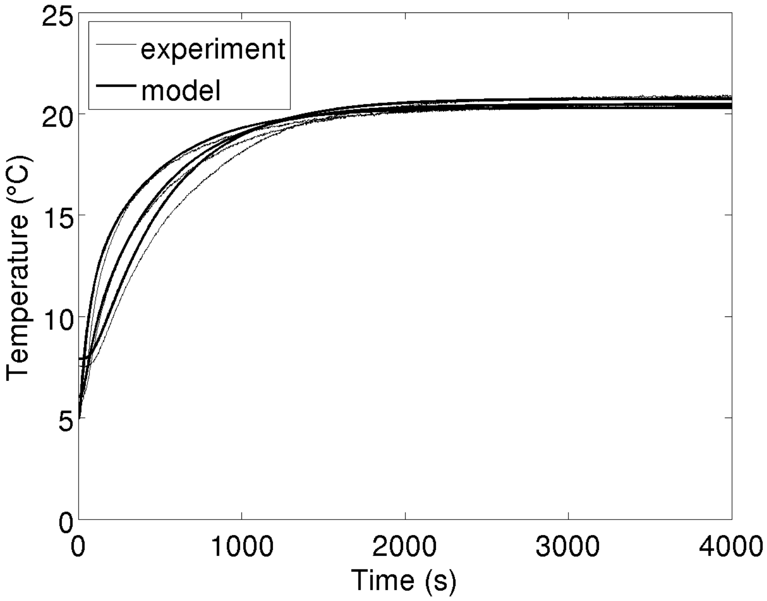

Figure 4.6: Comparison between fitted and measured temperature profile during the heating of solid chocolate in the PCR.

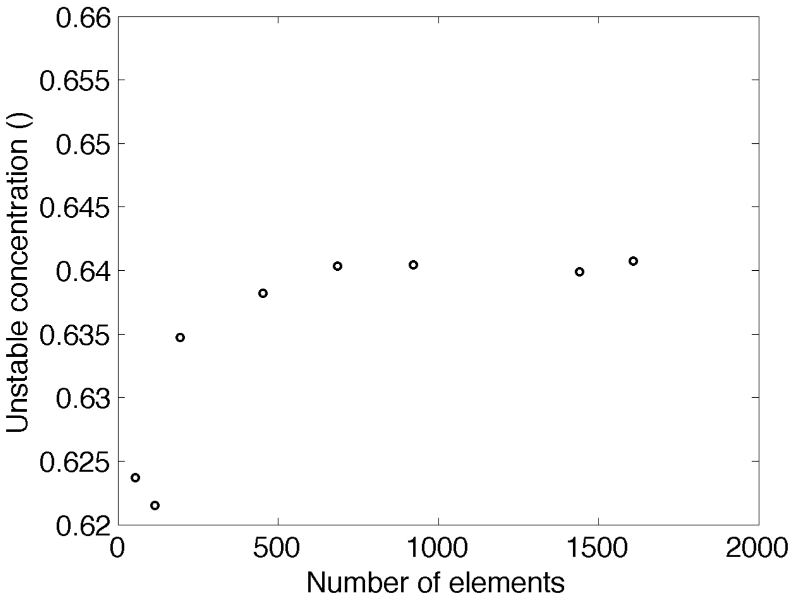

(a)

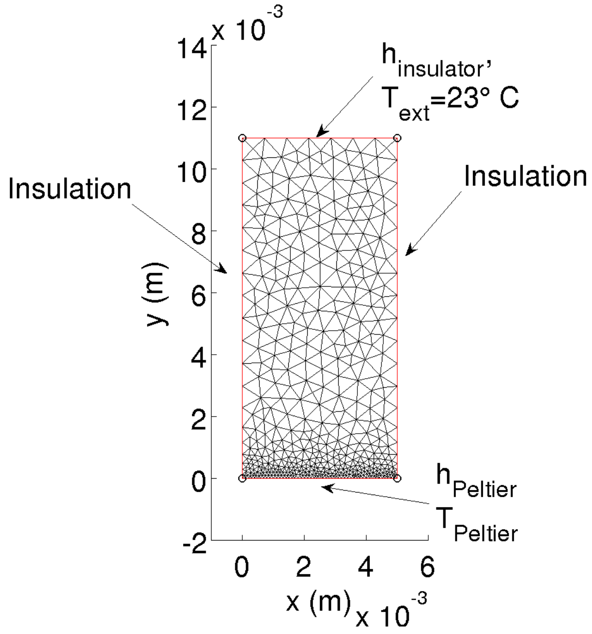

(b)

Figure 4.7: Mesh dependency of the solution ([*unstable*] crystals at $200\mu m$ from the Peltier stage after $120s$ of profile 1) (4.7(a)) and the mesh which was used for further study (4.7(b)).

Table 4.1: Parameters used to model the phase change

Variable	Max. value (K_{ii})	Temperature (T_{ii})
K_{ms}	0.005 s^{-1}	21 °C
K_{sm}	0.06 s^{-1}	28 °C
K_{mu}	0.08 s^{-1}	10 °C
K_{um}	0.06 s^{-1}	18 °C
K_{us}	10 s^{-1}	25 °C
K_{nuc}	0.0005 s^{-1}	18 °C

CHAPTER 5

VALIDATION OF THE MODEL

The objective of the model developed in chapter 4 is to predict the microstructure and the evolution of the temperature during chocolate processing, including FrozenCone processing. Typical steps include a wide range of cooling rates ($0-50$°C $\cdot min^{-1}$) depending on the technology used, but also heating in case a warm filling is injected.

Validation of the model was performed using both temperature profiles and crystal structure information. The Peltier stage cell was used to deliver a range of temperature profiles to the chocolate during solidification and the crystal structure of the solidified chocolate was measured using the XRD method described in chapter 3.

5.1 Prediction of the temperature profiles and microstructure in chocolate when cooled using profile 1

5.1.1 Temperature and prediction in a quickly cooled chocolate (profile 1)

The model was first used to simulate the cooling and phase change kinetics occurring when a high cooling rate (> 2°C $\cdot min^{-1}$) is used (profile 1 as in figure 2.5(b)).

In figure 5.1, experimental and numerical temperature profiles can be compared. Experiments were performed in triplicates and error bars represent one standard deviation of the experimental data. The quality of the model was quantified using the Root Mean Square Error ($RMSE$) defined by equation 5.1. The maximum (MAX) of the difference $|T_{model} - T_{experiment}|$ was also reported. The results of this analysis are presented in table 5.1.

$$RMSE = \sqrt{\frac{\sum_{i=0}^{n}(T^{i}_{exp} - T^{i}_{model})^2}{n}} \tag{5.1}$$

Far from the surface of the Peltier stage, *i.e.* $x = 8.7mm$, after approximately 500 seconds, a plateau in temperature, characteristic of a phase change, can be observed. Similar profiles are reported in the literature (Franke 1998, Tewkesbury et al. 2000) and exhibit the same plateau. The temperature at which the phase change occurs (22°C) indicates that *stable* crystals are formed, since it is the temperature at which the crystallisation peak for *stable* crystals occurs in a DSC (as in figure 4.2). Once crystallization has been completed the temperature gradually decreases to finally reach steady state. Due to heat losses to the environment this temperature is somehow higher ($\approx$ 5°C) than the actual temperature of the Peltier stage. The $RMSE$ was found to be 1.27°C which is the same order as the standard deviation of the experimental data.

From the experimental data it can be calculated that at $x = 2.7mm$ cooling rate is about 1°C $\cdot s^{-1}$ while at $x = 8.7mm$, it is 0.01°C $\cdot s^{-1}$. Therefore, based on DSC results and previous work on the relationship between cocoa butter polymorphism and rate of cooling (Stapley et al. 1999), one would expect more *stable* crystals to be formed further from the Peltier stage.

Closer to the boundary of the Peltier stage, *i.e.* $x = 4.9\,\text{and}\,2.7mm$, a plateau similar to the one observed at $8.7mm$ cannot be seen. This does not imply that there is no phase change, rather that any heat generated during crystallization is rapidly transferred to the Peltier stage. One can see that there is also a good agreement between the model and the experimental data, since the $RMSE$ was found to be 0.84°C and 0.80°C which is less than the standard deviation of the experimental data.

The relatively high values of the maximal error in profile 1 (2, 1.5 and 1.8°C) are reached at the end of the profile, in the steady-state region, which should be easiest to model. This difference can probably be explained by the fact that when close to 0°C condensation and ice crystals develop on the Peltier stage limiting the heat transfer, a phenomenon not considered by the model. However rapid cooling systems in industry operate in moisture controlled environments to avoid this problem.

The quality of the prediction can be assessed by the fact that the model is within one standard deviation (error bars) from the average recorded temperature over three repetitions. To monitor the quality of the phase change modelling, one can use the local cooling rate $\frac{\partial T}{\partial t}$ as presented in figure 5.1(b). When the phase change occurs, the heat generated balances with the heat transferred to form the plateau observed in the temperature curve, translating as a peak in the cooling rate (negative values) towards 0°C $\cdot s^{-1}$ at around $400s$. In figure 5.1(b), one can see the experimental cooling rate profiles and the prediction of the model, for $x = 8.7mm$. One can see that the peak in the cooling rate profile is predicted accurately in time at $t = 400s$ (x axis) and in intensity at $\frac{\partial T}{\partial t} = 0.008$°C $s^{-1} = 0.48$°C $\cdot min^{-1}$ (y axis). The model was found to predict phase change very well, within the experimental variation over the three replicates.

5.1.2 Microstructure modelling of after rapid cooling (profile 1)

As described in section 2.2.3, XRD measurements of cocoa butter in chocolate were performed at two different facilities (University of Birmingham and University of Southampton). Similar results were observed with both experimental set ups. The objective of this part was to verify that the amount of *stable* and *unstable* crystals predicted by the model was comparable to the amount measured using X-Ray diffraction data.

Chocolate was cooled using profile 1 (*cf.* figure 2.5(b)) and was analysed using the XRD subtraction method developed in chapter 3. A first set of experiments was conducted at the University of Birmingham XRD facility. The chocolate slab was sampled at distances of $1mm$, $2mm$ and $5mm$ from the Peltier stage. Similarly the model was run using profile 1 as the $T_{Peltier}$ boundary condition.

The crystal structure profile predicted by the model is presented in figure 5.2. As expected, further away from the Peltier stage, more *stable* crystals form, since the cooling rate is lower at $x = 5mm$ (about 2°C $\cdot min^{-1}$) than at $x = 1mm$ (about 10°C $\cdot min^{-1}$). The values predicted by the model for this setup are presented together with the experimental data identified using XRD in table 5.2. It is important to notice that the amount of *unstable* crystals is never higher than 50%, as chocolate cannot be cooled as quickly using this method (maximum cooling rate of about 10°C $\cdot min^{-1}$) as it is possible with the DSC (20°C $\cdot min^{-1}$ giving almost 100% *unstable* crystals) .

The phase change described by these figures can be linked with the slope change in the temperature profiles presented in figure 5.1. The phase change predicted is the source of the heat generation which gives rise to the plateau present on the temperature curves recorded during cooling.

In figure 5.3 results obtained from XRD measurements collected at Birmingham are shown. A chocolate slab cooled using profile 1 in the PCR was sampled at $1mm$, $2mm$ and $5mm$ from the Peltier stage, just after the end of the profile. The area of these peaks in the subtracted signal (figure 5.3) were estimated using a trapeze integration method to obtain the concentration of the different phases, *stable* and *unstable* at different locations ($1mm$, $2mm$ and $5mm$) in the slab of chocolate.

One can see that the area of the peak characteristic of *stable* crystals is maximum when chocolate is sampled at $5mm$ from the Peltier stage and is minimum when chocolate is sampled at $1mm$ from the Peltier stage. On the other hand, the area of the peak characteristic of *unstable* crystals is maximum when chocolate is sampled at $1mm$ from the Peltier stage and is minimum when chocolate is sampled at $5mm$ from the Peltier stage. The areas of each peaks are also reported in table 5.2 to be compared with the model data.

These observations are qualitatively consistent with the literature and the model predictions since closer to the Peltier stage, cooling rates are higher and higher levels of *unstable* cocoa butter should be formed.

The peak area measured was considered to be proportional to the concentration of crystals (Mazzanti et al. 2007). However the coefficient of proportionality seems to be different depending on the polymorph observed, which is not surprising. The areas cannot therefore be compared to one another directly and had to be normalised before further analysis could be undertaken.

The data for the *unstable* and *stable* phase concentrations were normalised between 0 and 1 by dividing by the maximum value measured e.g. the maximum value for *unstable*, $[unstable]_{max}$ is that found at $1mm$ for $[unstable]$ and thus for $[stable]_{max}$ at $5mm$ for $[stable]$. The model data was normalized in the same way to be able to compare model and experimental data. For a more complete explanation of the calculation, please see section 3.5. In figure 5.4, the experimental data measured with the XRD subtraction method and predicted by the model are shown. The different symbols for each points are used to follow which simulation (figure 5.3) and experimental (figure 5.2) data are compared. The model compares favorably with the experimental data and no significant differences can be observed. The correlation coefficient between the experimental data and the model is $r^2 = 0.98$ ($p = 0.00095$), the correlation is therefore very significant and points are close to the $y = x$ line ($experiment = model$).

Similar data were collected using the EPSRC facility in Southampton. The chocolate was cooled in the same way (using profile 1) and it was decided to investigate different levels in the slab. The concentration of *unstable* crystals directly at the point of contact between the stage and the chocolate were not measured in the first set of experiments (University of Birmingham). However, they are critical for rapid cooling processes such as the FrozenCone technology because the cooling rates are very high (about 20°C $\cdot min^{-1}$). Therefore, for this set of experiments slices at $0mm$ (collected by carefully scaping at the point of contact between Peltier stage and chocolate), $1mm$ and $5mm$ were used and compared to the numerical prediction proceeding from the model for the same locations.

On figure 5.4, one can see that, as in the first experiment, the model agrees favorably with the experimental data ($r^2 = 0.978$). The model slightly over estimates (+20% maximum) the amount of both phases when their concentrations are low; this might also be due to a lack of sensitivity of the experimental measurement.

5.1.3 Prediction of the microstructure evolution during reheating of a rapidly cooled chocolate

The mathematical model presented in this work was applied to the same experiment described in section 3.5 to evaluate its abilities to predict polymorphous transitions:

1. Chocolate was sampled from the interface ($0mm$) with the Peltier stage at the end of profile 1.
2. Chocolate was reheated at a nominal cooling rate 5°C $\cdot min^{-1}$, from 0°C to 40°C .
3. Every 5°C , the temperature was kept constant for $1\,min$, in order to allow the XRD measurement to be collected at constant temperature.

Thus the (T, t) profile is as shown on figure 5.5(a)). This was simulated for the model as well to make sure that the data were comparable.

As already discussed in 3.5, to compare between the model and the experimental data, both were normalized by dividing by the maximum concentration recorded, e.g. $[unstable]_{max}$ at 10°C for $[unstable]$ and $[stable]_{max}$ at 25°C for $[stable]$ for the experimental data. For a more complete explanation of the calculation, please see section 3.5. Both the experimental and the simulation data is shown in figure 5.5(b). One can see the comparison between experimental data and theoretical predictions for the concentration in *unstable* and *stable* crystals.

During reheating, one can see that the amount of *unstable* crystals decreases from $unstable = 1$ to $unstable = 0$ between 10°C and 15°C . This corresponds to the melting temperature range of the *unstable* crystals observed using DSC. The *unstable* to *stable* transition is accurately predicted by the model, which is important since this feature will be used when predicting the evolution of the polymorphs occurrence during a rapid cooling process. The amount of *stable* crystals increases from 0.2 to 1 from 10°C to 15°C . From 20°C onwards, the amount of *unstable* crystals is null whereas the amount of *stable* crystals decreases between 25°C and 35°C which is consistent with the experimental DSC data. In general, there is a good agreement between the experimental and the model predicted data and many features are predicted. The main error from the model is that the melting of *stable* crystals is predicted to occur at slightly lower temperatures than the ones observed experimentally. This can be explained by the fact that the experimental sample is measured as a series of steady states (due to the $1min$ wait for the measurements) whereas the model was fitted on a dynamic DSC experiments (constant heating rate of $5°\text{C} \cdot min^{-1}$). The steps at constant temperature would help to increase the stability of the system marginally increasing the melting point by a few degrees. One can see on figure 5.5(b) that the model predicts plateaus during reheating, these plateaus are due to the temperature being kept constant for $1min$ to make sure that the measurement occur at steady state and have a duration of $60s$.

5.2 Prediction of other temperature profiles

Temperature profiles 2 and 3 (see figure 2.5(b)) were also applied using the Peltier Stage to the milk chocolate formulation. The model was used to predict the temperature and the occurrence of each of the crystal forms during the cooling or heating of chocolate in the device. The temperature profiles applied with the Peltier stage are presented in figure 2.5(b) and replotted on the different graphs as $T_{Peltier}$. For the model, the geometry used is described in figure 2.5(a) and the temperature profile was used as the external temperature $T_{Peltier}$ for the Neumann boundary condition on the Peltier stage side.

On figure 5.6(a) the temperatures experimentally measured and predicted by the model when profile 2 is used are shown.

For $x = 8.7mm$ a similar plateau to that observed for the same location in figure 5.1(a) is observed. The duration of this plateau is longer than in figure 5.1(a) as would be expected due to the slower cooling rate. The model predicts a longer phase change than observed experimentally by $\approx 600s$. This is probably due to the fact that during the phase change, a very slow cooling rate is achieved ($\frac{\partial T}{\partial t} < -0.2°\text{C} \cdot min^{-1}$), as seen in figure 5.6(b), which is out of the range of the fitted DSC data ($0.5 - 20°\text{C} \cdot min^{-1}$). The model is better optimized for faster kinetics and therefore underestimates the phase change when kinetics are very slow as in this case. This overestimation of the phase change duration (underestimation of the kinetics) is quite clear on figure 5.6(b), where the peak location is well predicted ($\approx 600s$ after the beginning of the experiment) but is much broader in the model prediction than in the experimental data. The values of the cooling rates being mispredicted are however very low ($\frac{\partial T}{\partial t} < -0.2°\text{C} \cdot min^{-1}$) and these errors do not make any significant difference to the quality of the temperature predictions.

The temperature prediction of the model is good for the profile 2 and the values for $RMSE$ (0.30°C) and the maximum error (1.07°C) were reasonably low. This demonstrates the ability of the model to predict slow cooling processes which is important since most chocolate products are still manufactured this way.

The temperature profile at $x = 2.7mm$ is well predicted, with a low $RMSE$ (0.7°C), and the good fit on the steady state region confirms our hypothesis about the error made by the model on the steady state region when using profile 1.

Only two different locations were reported as the relatively slow cooling makes the temperature profiles at $x = 2.7mm$ and $x = 4.9mm$ too close to each other (± 1°C) to be distinguished. Figure 5.7(a) compares temperatures recorded experimentally and those predicted by the model when chocolate is cooled in the Peltier stage device using profile 3 (see $T_{Peltier}$ on figure 5.7(a)). Typical processing in a FrozenCone involves (i) a quick cooling step over a short time when the plunger is applied ($2 - 5s$) and (ii) a longer process time as the product passes through a cooling tunnel at 12°C ($20min$). Melting can eventually occur if a warm filling is injected or when the half shells are joined during the process, for which a local remelting of the material is used to seal the two halves together. Profile 3 was used to simulate a situation similar to this process.

During cooling at $x = 8.7mm$, cooling rates are of similar magnitude as when profile 2 is applied ($\approx 0.2°\text{C} \cdot min^{-1}$). This resulted in a similar cooling curve with a plateau characteristic of the phase change at $t = 600s$. During heating, the phase change plateau is located at ($t = 2700s$). There is a good agreement between the model and the experiment ($MAX = 1.81$°C). Figure 5.7(b) shows that away from the Peltier stage (at $x = 8.7mm$), a low heating rate (≈ 3°C $\cdot min^{-1}$) is generated, and the melting phase change plateau ($t = 2700s$) is accurately predicted. This can be explained by the fact that the model was optimized for relatively slow heating (5°C $\cdot min^{-1}$ during the DSC fitting)

For the temperature profiles at $x = 2.7mm\,\text{and}\,x = 4.9mm$, one can see that the temperature decreases until $t = 600s$ when the phase change starts to occur. A new feature in the profiles can be seen; the temperature increases by 2°C at $x = 2.7mm$ and by 1°C at $x = 4.9mm$. One can see that the Peltier stage temperature $T_{Peltier}$ is raised from 0°C to 12°C at $t = 600s$ but this cannot explain the increase of temperature in the vicinity of the thermocouples. Indeed the phase change occurs at a temperature higher than 12°C (17°C at $x = 2.7mm$ and by 21°C at $x = 4.9mm$) and therefore one would still expect the temperature to decrease (according to Fourier's law). The reason for this is that the heat generated during the phase change is higher than that transferred to the Peltier stage. The raise of $T_{Peltier}$ promotes crystallization and the cocoa butter sets rapidly, generating a large amount of heat in a very short time, resulting in this unintuitive increase of temperature, which is however accurately predicted by the model. The temperature then decreases slowly and stabilizes to reach steady state. The high values for the maximum error for profile 3 are encountered in the melting region, since high heating rates are applied (up to 11°C $\cdot min^{-1}$) and the model has not been optimized for that (5°C $\cdot min^{-1}$ during the DSC fitting).

Overall, in the geometries and experimental conditions used, the model was found to give an accurate prediction (±2°C and $RMSE < 1.3$°C), of the three different temperature profiles applied. It was therefore decided to extend it to an industry like geometry for the rapid cooling of Easter eggs.

5.3 Sensitivity analysis of the model to different parameters

The model requires a range of chemical and physical parameters. These parameters and their method of acquisition/estimation are detailed in the model description in section 4.3.3. It was decided to investigate the effect of the variation of a number of parameters on the temperature and phase change kinetics predictive abilities of the model to identify the level of accuracy required for each of the parameters.

5.3.1 Influence of the number of DSC curves fitted to obtain the kinetic parameters

Six DSC curves (cooling rate between $0.5 - 20°\text{C} \cdot min^{-1}$) were used to obtain the kinetic parameters for the model by curve fitting. For practical purposes obtaining six DSC curves might not always be feasible. It was decided to test the result of the same model if only two DSC curves are used.

The DSC experiments needed for the fitting should demonstrate the formation of *stable* and *unstable* crystals when cooling and the solid-solid (polymorphous) transition occurring when *unstable* crystals are reheated. Therefore both slow ($-1°\text{C} \cdot min^{-1}$) and fast ($-10°\text{C} \cdot min^{-1}$) cooling rates are required. The heating rate can be kept constant $+5°\text{C} \cdot min^{-1}$ as it was assumed that this heating rate was slow enough for all reactions to happen (Stapley et al. 1999). The kinetic parameters obtained using the same fitting method as presented before are shown in table 5.3. The values of the parameters obtained using only two curves are of similar magnitude as the parameters obtained using six curves (±40%) except for K_{us}, for which a significantly different value ($1.5 vs. 10$) was obtained; this is still two to three orders of magnitude higher than the other parameters.

Figure 5.8, compares model A (data from 6 curves) and model B (data from 2 curves) and the experimental data collected with a cooling rate of 5°C $\cdot min^{-1}$. In black, the model A compares very well with the experimental data ($RMSE = 478 J \cdot kg^{-1} \cdot ^{\circ}\text{C}^{-1}$) which is expected due to the fact that this curve was actually part of the fitting process. However when only two curves were used (-1 and -10°C $\cdot min^{-1}$) for the fitting routine, the model B (in red) still compares very well with the experimental data ($RMSE = 487 J \cdot kg^{-1} \cdot ^{\circ}\text{C}^{-1}$).

Because of this similarity, it is possible in the future that only five parameters need to be fitted and that any large number can be used for K_{us} ($K_{us} > 5 s^{-1}$). The difference in K_{us} between models A and B does not give rise to a greatly different shape of the polymorphous transition peak in the heating curve (K_{us} is the kinetic rate for the *unstable* to *stable* transition).

To assess the sensitivity of the temperature predictions on these kinetic parameters, model B was also used to predict the temperature profiles in the PCR system when simulating profile 3 (*cf.* figure 2.5(b)). Model B was not found to be significantly less accurate than model A. In figure 5.9, one can see that the predicted curves (A and B) are very close to the experimental data; ±1.81°C for model A and ±1.89°C for model B. In table 5.4 the $RMSE$ and maximum error (MAX) values for the three locations studied are reported. Model B tends to be slightly less accurate (±1°C at $x = 2.7 mm$) but no major differences could be observed.

The predictions obtained for the evolution of [*stable*] and [*unstable*] concentrations obtained using model B were also found to compare favorably against XRD data. In figure 5.10(a), one can see that model A and B are not significantly different from one another. The main difference is that melting of *unstable* crystals is faster ($[unstable]_{T=12^{\circ}\text{C}} \approx 0.7\, vs.\, [unstable]_{T=12^{\circ}\text{C}} \approx 0.9$) because of the higher K_{um} in the model B compared to model A. This can be related to the faster formation of *stable* crystals shown in figure 5.10(b) as more *melt* material is available to recrystallize. Due to the higher K_{sm}, *stable* crystals also appear to melt more rapidly $[stable]_{T=28^{\circ}\text{C}} \approx 0.2\, vs.\, [stable]_{T=28^{\circ}\text{C}} \approx 0.3$ in the model B compared to model A.

Overall, the sensitivity study demonstrated that the kinetic parameters used in the model can be estimated by using only two DSC curves (-1 and $-10^{\circ}\text{C} \cdot min^{-1}$) selected to include the crystallisation of *stable* and *unstable* material as well as the *unstable* to *stable* transition. Similarly, it was found that the kinetic constant K_{us}, which is two orders of magnitude higher than the rest of the parameters, does not need to be fitted and can just be fixed to a large value compared to the rest of the other kinetic parameters (anything higher than $K_{us} = 1$ makes it one order of magnitude higher than the rest). The potential gain in time could be considerable if this kinetic model had to be fitted on more formulations, and fitting on only two DSC curves seems sufficient for most industrial requirements.

5.3.2 Influence of thermal parameters on the model

The different parameters tested during this sensitivity analysis were either material properties: k_{solid}, k_{liquid}, Cp_{solid}, Cp_{liquid}, ΔH_{stable}, $\Delta H_{unstable}$, and ρ or process parameters: $h_{Peltier}$, $h_{Insulator}$ and $[stable]_0$ (level of temper).

To evaluate the changes due to these parameter variations, the temperature and concentrations of the different phases (*stable*, *unstable* and *melt*) were monitored at $t = 600s$ during the simulation of profile 3 at three different locations ($x = 2.7mm$, $x = 4.9mm$ and $x = 8.7mm$). Each of the parameters were varied from -50% to $+50\%$ of the experimentally measured value.

Influence of the density (ρ)

The density ($\rho_{exp} = 1300 kg{\cdot}m^{-3}$) impacts the thermal diffusivity $\alpha = \frac{k}{\rho \cdot Cp}$ of the material. One can calculate that $0.5 \cdot \rho_{exp} \leq \rho \leq 1.5 \cdot \rho_{exp} \Leftrightarrow 2 \cdot \alpha_{exp} \geq \alpha \geq 0.66 \cdot \alpha_{exp}$. On figure 5.11, one can see the effect of changing ρ (or α) on temperature, $[stable]$, $[unstable]$ and $[melt]$. On figure 5.11(a),it can be seen that the density has a significant impact on the temperature predicted by the model. For example, when ρ increases from $\rho = \rho_{exp} = 1300 kg \cdot m^{-3}$ to $\rho = 1.5 \cdot \rho_{exp} = 1950 kg \cdot m^{-3}$, at $x = 2.7mm$, T increases from $\approx$ 15°C to $\approx$ 17.5°C which shows that the temperature prediction is quite sensitive on the variation of ρ. Due to the changes in the temperature the different phases concentrations are significantly affected by the variation of ρ. On figure 5.11(b), the *stable* crystals concentration decreases when the density increases to the point where no *stable* crystals are crystallized when $\rho = 1950 kg \cdot m^{-3}$ at $x = 2.7mm$ from the Peltier stage. The higher temperature related to a higher density also decreases the amount of *unstable* crystals and therefore increases the amount of *melt* in the system.

Influence of the temper level ($[stable]_0$)

As measuring the level of temper is challenging, the values used were obtained from published data (Metin and Hartel 2005). Values between 0.5% and 3% are reported . The latter value was used in the model ($[stable]_{0_{lit}} = 0.03$). On figure 5.12 the temperature and concentration of *stable* are shown, when the temper level is varied in the domain $0.5 \cdot [stable]_{0_{lit}} \leq [stable]_0 \leq 1.5 {\cdot} [stable]_{0_{lit}}$. One can see that this value has little impact on the temperature and the phases concentrations predicted by the model. Similar results were obtained for the *unstable* and *melt* concentrations. These results are in agreement with experimental studies conducted recently by seeding different levels of cocoa butter using $\beta(V)$ crystal seeds and measuring the crystallisation kinetics (Yasuyoshi and Hartel 2008). For the model, this can be explained by the fact that crystal growth does not have a strong dependence on the amount of crystals present in the melt, as demonstrated by the low value for c ($c = 0.1$) used in the model (see section 4.2).

Overall, the developed mathematical model was found to be accurately predicting both temperature profiles and concentrations of *stable* and *unstable* polymorphs during various processing conditions. A sensitivity analysis showed that the kinetic parameters fitting step could be done on only two DSC curves rather than six. It was also found that ρ, k_{solid}, k_{liquid}, Cp_{solid}, Cp_{liquid} and $h_{Peltier}$ have a high impact on the temperature predicted by the model and therefore on the different phases concentrations in the phase change region. It was found that $stable_0$ had little effect as $h_{Insulator}$, ΔH_{stable} and $\Delta H_{unstable}$.

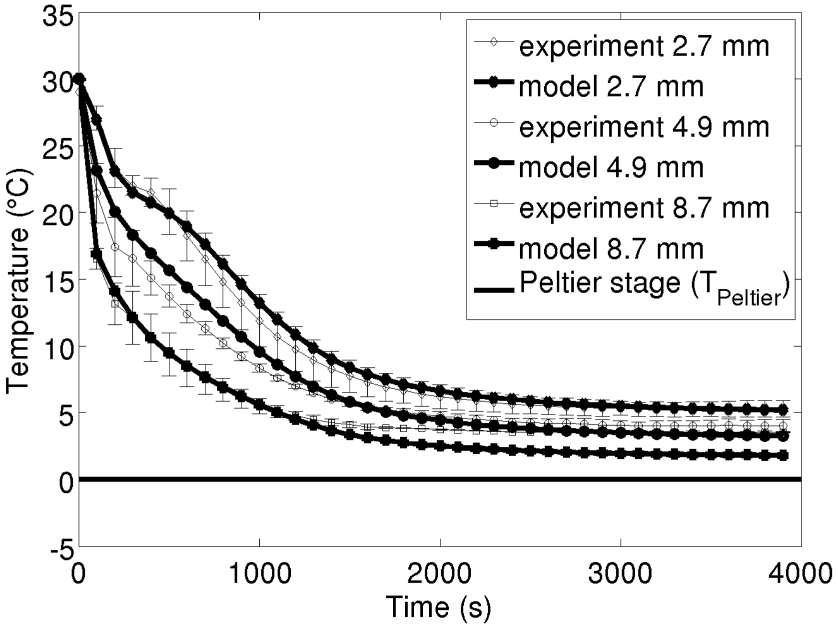

(a)

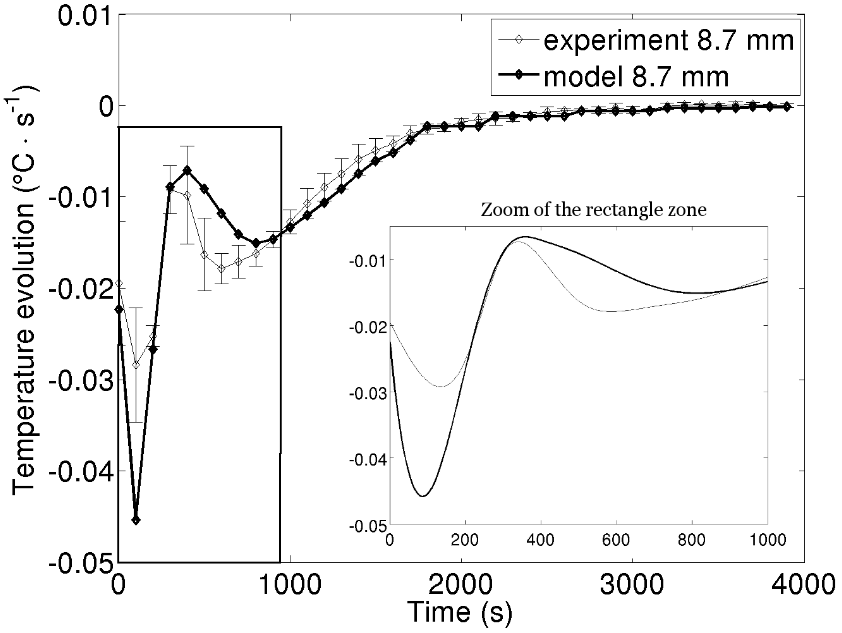

(b)

Figure 5.1: Experimental and simulation data compared for chocolate cooled using profile 1 (*cf.* figure 2.5(b)), temperature profiles (5.1(a)) and cooling rate at $8.7mm$ (5.1(b)).

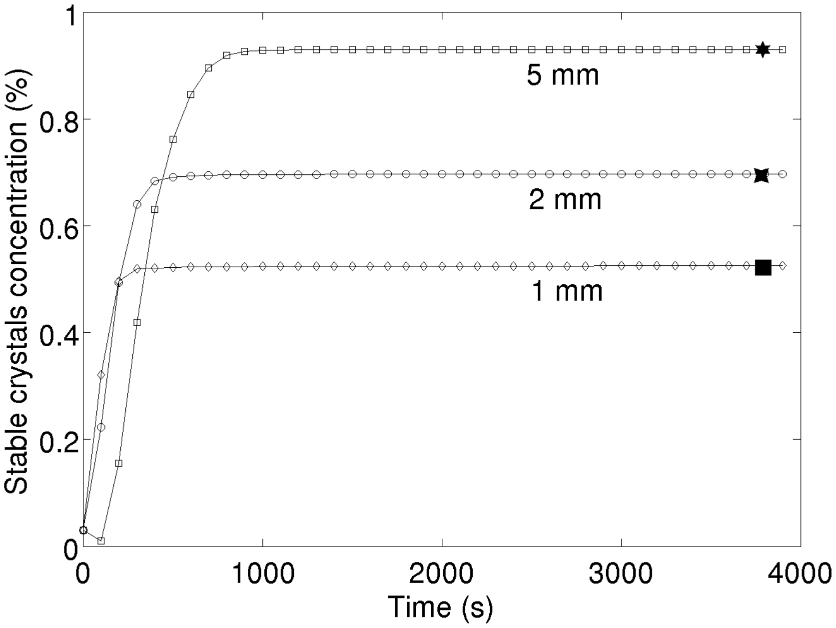

(a)

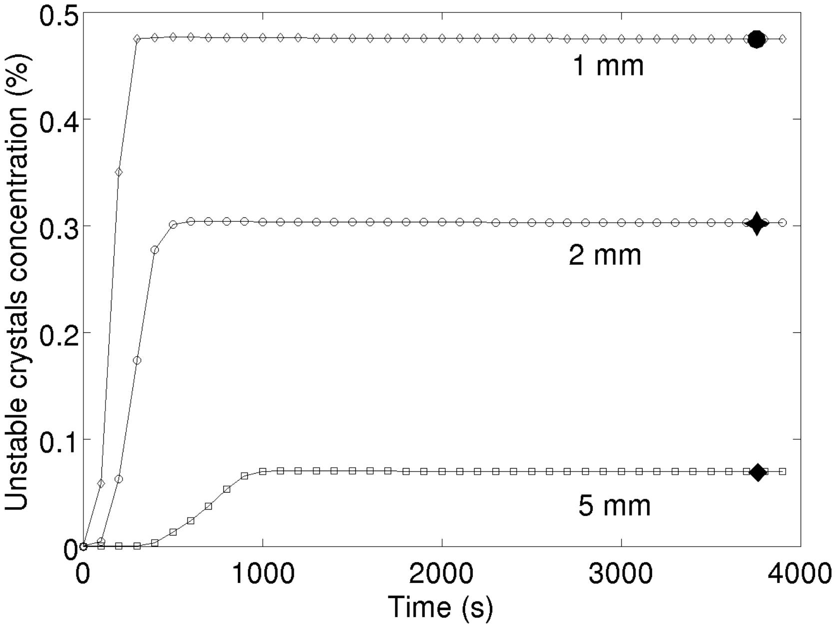

(b)

Figure 5.2: Example of the output of the finite element analysis describing the evolution of the concentration in *stable* (5.2(a)) and in *unstable* (5.2(b)) crystals during the cooling of a slab of chocolate on the Peltier stage using profile 1 (*cf.* figure 2.5(b)). Symbols can be used to compare with experimental data in figure 5.3.

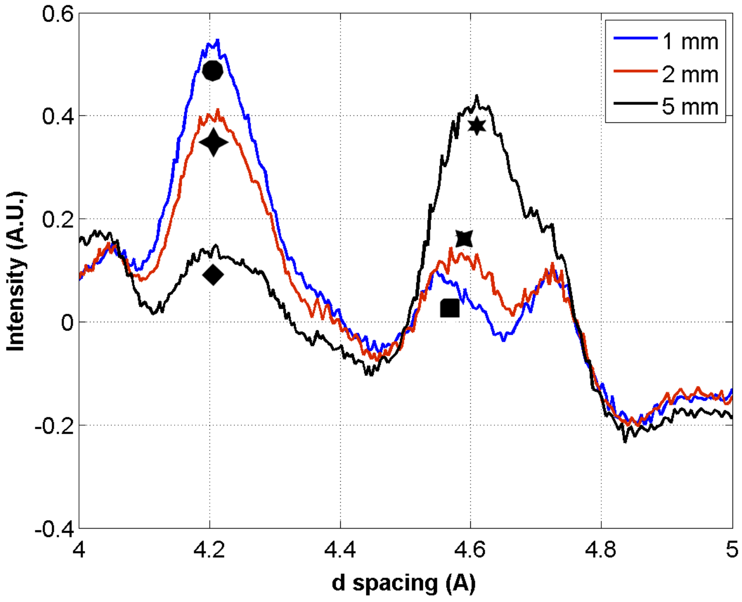

(a)

Figure 5.3: Evolution of the measured XRD intensity for different locations in the PCR cell (data collected at the Birmingham facility). Symbols can be used to compare with simulation data in figure 5.2.

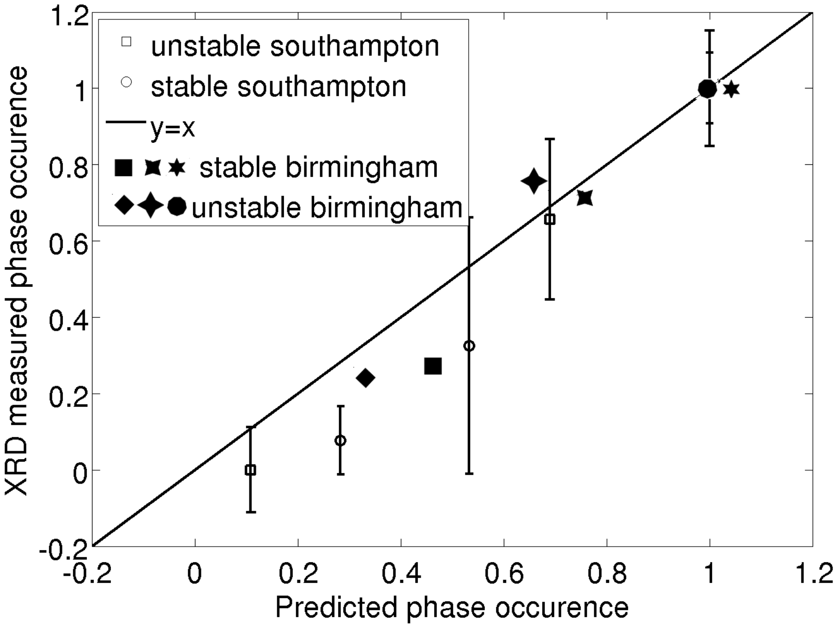

Figure 5.4: Comparison between the predicted and the actual (as measured using XRD) microstructure (data collected at the Southampton University EPSRC and the Birmingham University facilities).

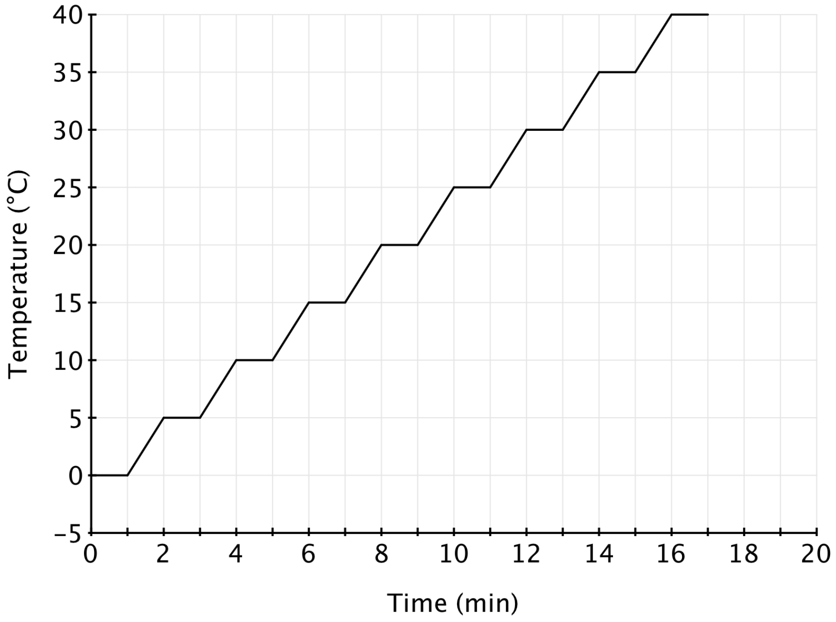

(a)

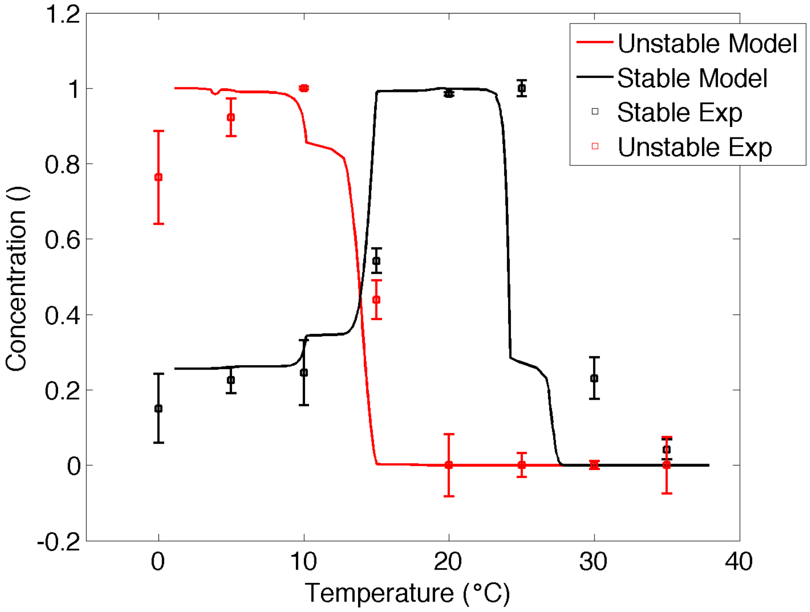

(b)

Figure 5.5: Temperature profile used to measure the evolution of the polymorphism during heating (5.5(a)) and comparison between the predicted and the experimental (as measured using XRD) concentration of *unstable* crystals and *stable* crystals (5.5(b)) in a sample originally cooled using profile 1 located at the contact with the Peltier stage.

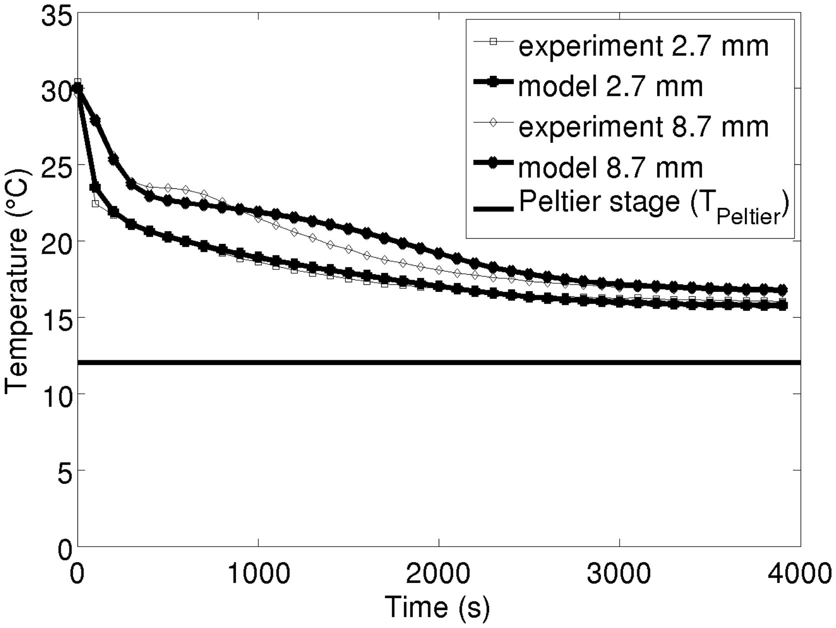

(a)

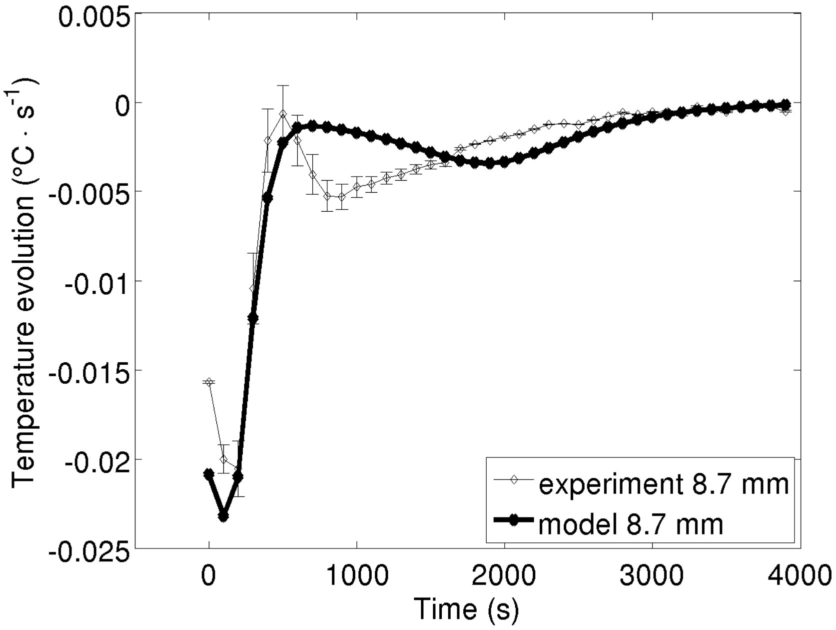

(b)

Figure 5.6: Experimental and simulation data compared for chocolate cooled using profile 2 (*cf.* figure 2.5(b)), temperature profiles (5.6(a)) and cooling rate at $8.7mm$ (5.6(b)).

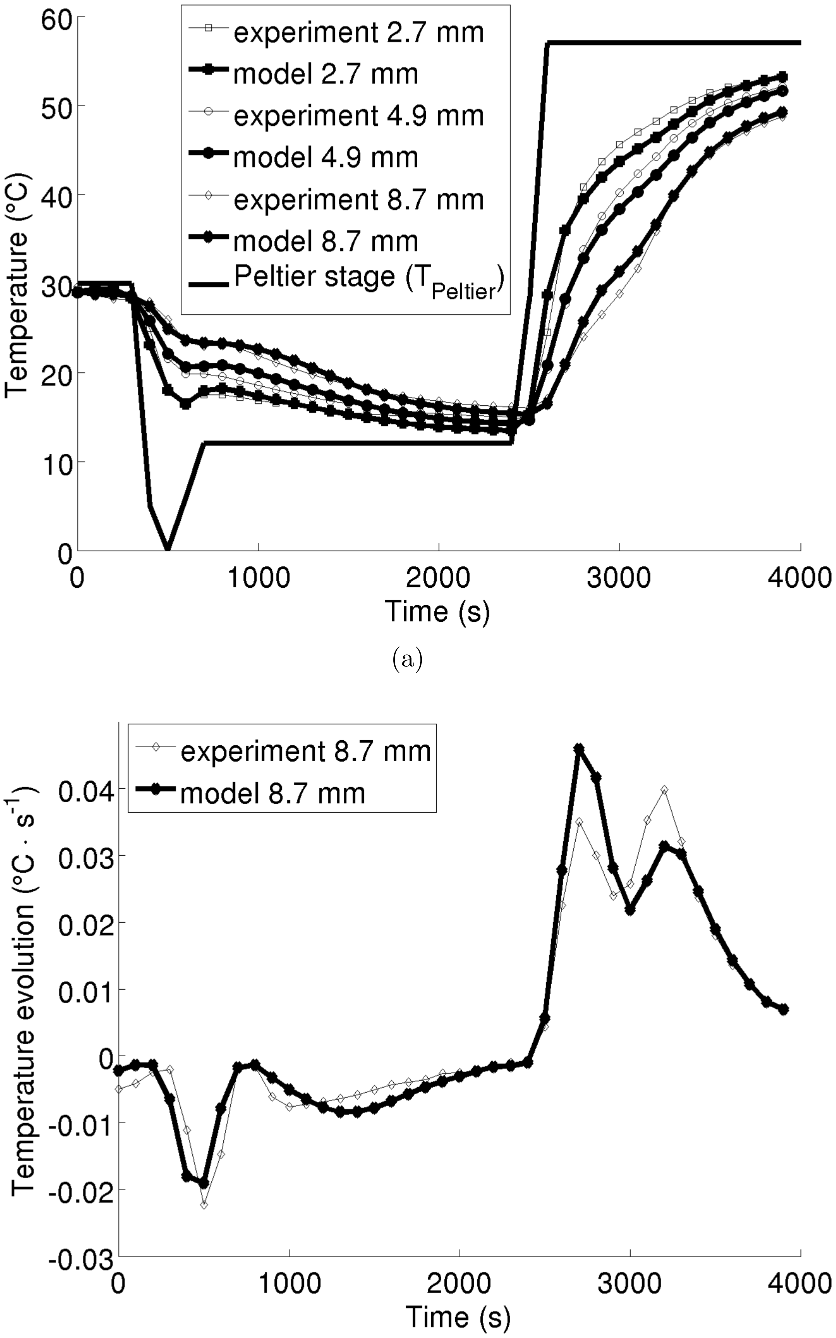

(a)

(b)

Figure 5.7: Experimental and simulation data compared for chocolate cooled using profile 3 (*cf.* figure 2.5(b)), temperature profiles (5.7(a)) and cooling rate at $8.7mm$ (5.7(b)).

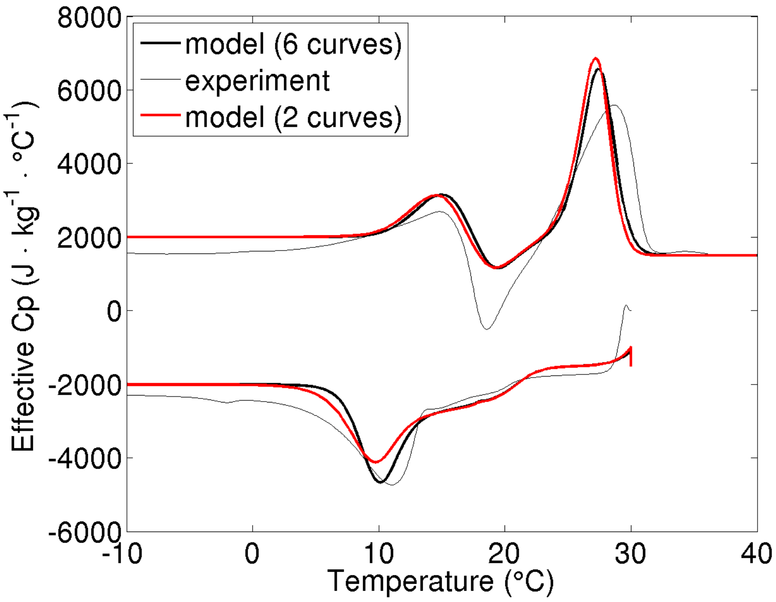

Figure 5.8: Experimental and simulation (6 DSC curves (−) and 2 DSC curves (−)) DSC data of milk chocolate cooled at $-5°\text{C} \cdot min^{-1}$ and reheated at $5°\text{C} \cdot min^{-1}$

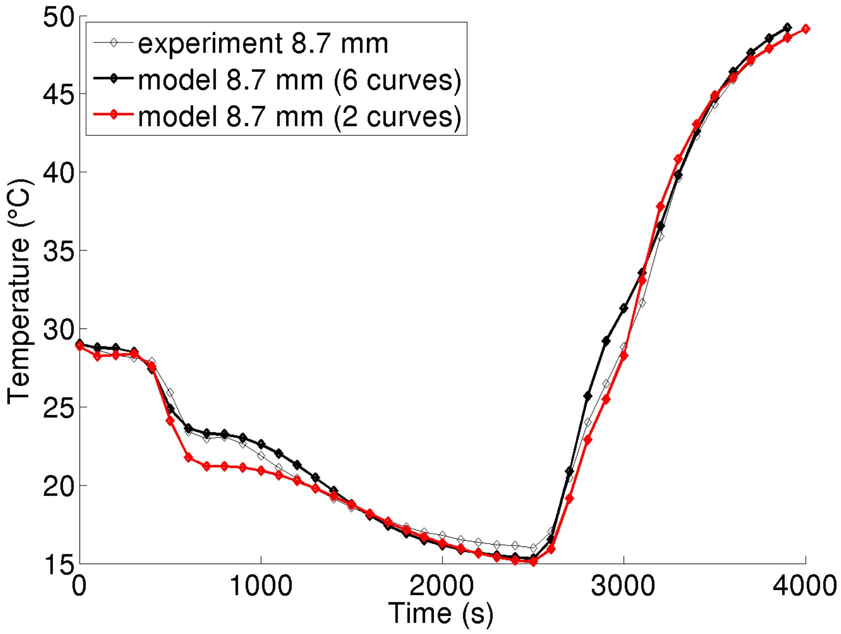

Figure 5.9: Comparison of experimental and modelled (6 DSC curves (−) and 2 DSC curves (−)) temperature profile at 8.7mm in chocolate cooled using profile 3 (*cf.* figure 2.5(b))

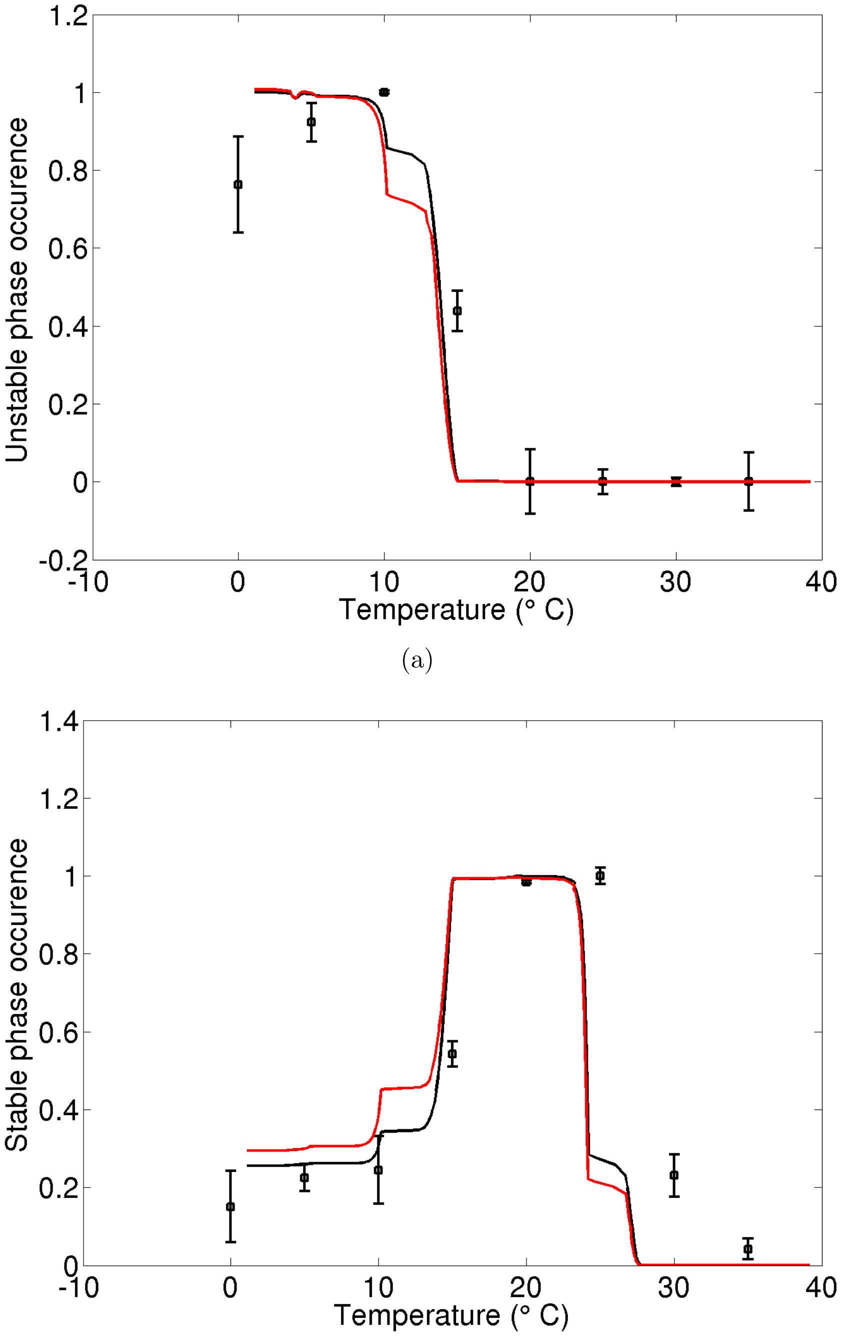

(a)

(b)

Figure 5.10: Comparison between the predicted (6 DSC curves (−) and 2 DSC curves (−)) and the experimental (as measured using XRD) concentration of *unstable* crystals (5.10(a)) and *stable* crystals (5.10(a)) in a sample originally cooled using profile 1 located at the contact with the Peltier stage.

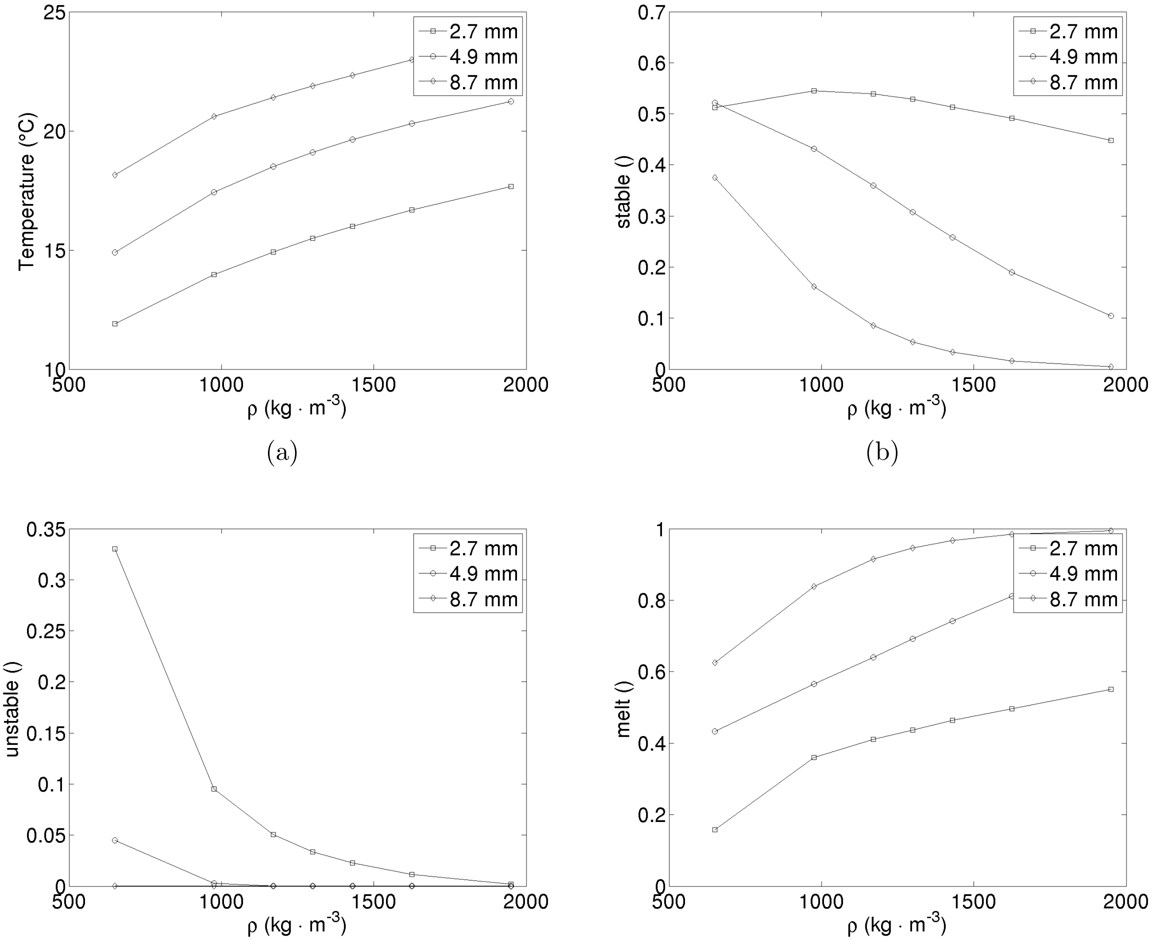

(a) (b)

(c) (d)

Figure 5.11: Influence of the variation of ρ on the temperature (5.11(a)), amount of *stable* crystals (5.11(b)), amount of *unstable* crystals (5.11(c)) and amount of *melt* material (5.11(d)) after $600s$ of profile 3 at $x = 2.7mm$, $x = 4.9mm$ and $x = 8.7mm$.

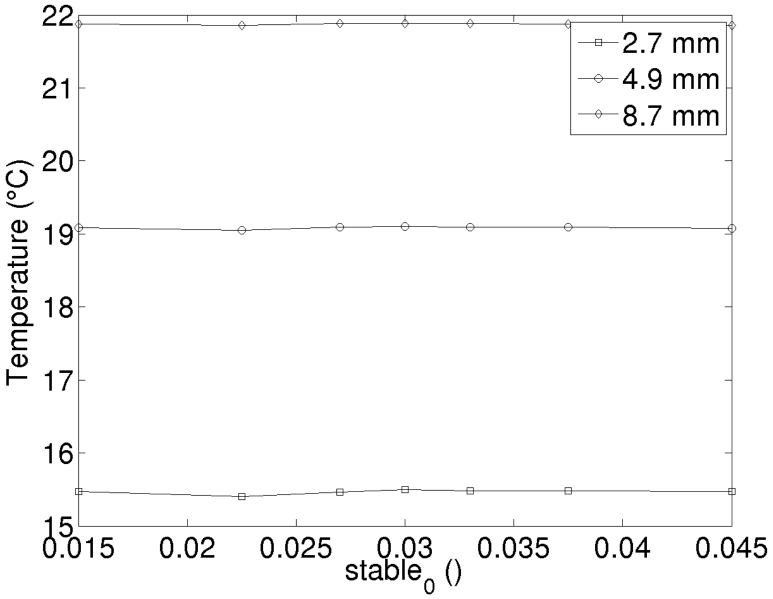

(a)

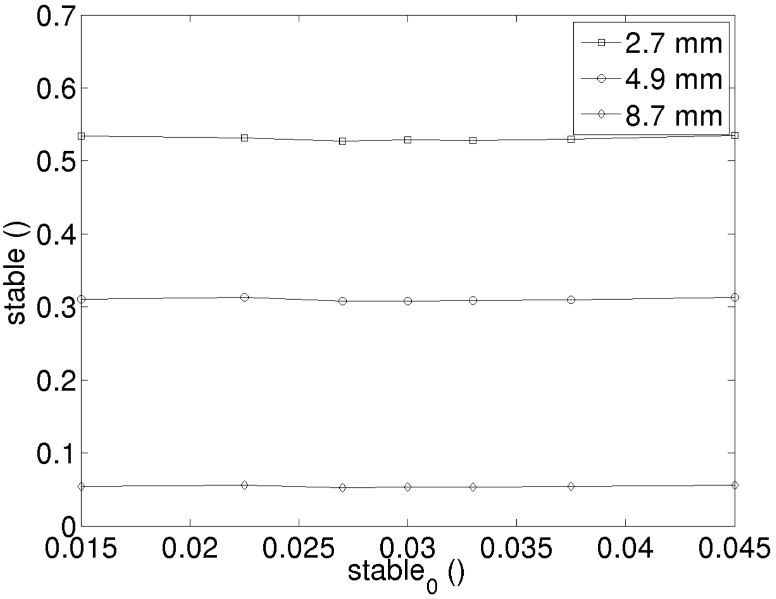

(b)

Figure 5.12: Influence of the variation of $[stable]_0$ on the temperature (5.12(a)), amount of *stable* crystals (5.12(b)) after $600s$ of profile 3 at $x = 2.7mm$, $x = 4.9mm$ and $x = 8.7mm$.

Table 5.1: Analysis of the error between the experimental and the simulated temperature profiles

	Profile 1	Profile 2	Profile 3
$RMSE(2.7mm)$	1.27	0.30	1.16
$MAX(2.7mm)$	2.07	1.07	2.45
$RMSE(4.9mm)$	0.84	–	1.28
$MAX(4.9mm)$	1.49	–	3.01
$RMSE(8.7mm)$	0.80	0.70	0.93
$MAX(8.7mm)$	1.98	1.42	1.81

Table 5.2: Predicted concentration and experimental peak area for *stable* and *unstable* crystals at different distances from the Peltier stage after cooling with profile 1

	$stable_{model}$	$unstable_{model}$	$stable_{exp}$	$unstable_{exp}$
$1mm$	0.52	0.48	0.0475	0.295
$2mm$	0.69	0.31	0.0684	0.2313
$5mm$	0.93	0.07	0.1024	0.0959

Table 5.3: Parameters used to model the phase change depending on the number of fitted DSC curves

Variable	Values for 6 curves (A)	Values for 2 curves (B)
K_{ms}	0.005 s^{-1}	0.0051 s^{-1}
K_{sm}	0.06 s^{-1}	0.077 s^{-1}
K_{mu}	0.08 s^{-1}	0.045 s^{-1}
K_{um}	0.06 s^{-1}	0.081 s^{-1}
K_{us}	10 s^{-1}	1.5 s^{-1}
K_{nuc}	0.0005 s^{-1}	0.0006 s^{-1}

Table 5.4: Analysis of the error between the experimental and the simulated temperature profiles depending on the number of fitted DSC curves to model the phase change

	Profile 3 - 6 curves (reference)	Profile 3 - 2 curves
$RMSE(2.7mm)$	1.16	1.37
$MAX(2.7mm)$	2.45	3.43
$RMSE(4.9mm)$	1.40	1.40
$MAX(4.9mm)$	3.01	3.76
$RMSE(8.7mm)$	0.93	0.91
$MAX(8.7mm)$	1.81	1.89

CHAPTER 6

APPLICATION OF THE MODEL TO INDUSTRIAL SYSTEMS

A model describing fat phase change coupled with heat transfer in chocolate has been developed and validated. In this chapter, the model will be applied to investigate industrial processes that involve rapid cooling. Typical examples include manufacturing of thin hollow shapes such as Easter eggs which can eventually be filled. As explained in chapter 1, traditional processes for the production of such shapes often lead to inconsistent products. Recently developed technologies such as FrozenCone (Aasted 2003) and ColdStamp (Steiner 2003) have been developed leading to much more controlled product shapes. This has enabled chocolate manufacturers to produce a range of 3D products having thin walls ($\approx 1-3mm$) which was not possible using previous technology. Typical production are up to 1 million eggs per day on certain production lines.

In the literature, rapid cooling is often associated with low melting point polymorphs (Stapley et al. 1999) and thus should be more likely to bloom during storage (Bricknell and Hartel 1998). An engineering paradox is encountered here since the products resulting from such manufacturing methods are perfectly acceptable; the question is how it arises.

A further understanding of rapid cooling chocolate manufacturing was thought to be a good example of a case study using the model.

6.1 Description of a typical rapid cooling process.

The process consists in a short application (typically $3s$) of a cold plunger to shape the product to the required geometry and then using conventional cooling tunnels to solidify the rest of the fat. This process can be described in more details as follows:

1. Freshly tempered chocolate is deposited in a polycarbonate mould.
2. A cold plunger (typically $T_{FC} = -10°\text{C}$) is stamped into the chocolate to give a shape to the chocolate during a short period of time, typically $t = 3s$ (step 1).
3. The plunger is taken off and the shells formed (see figure 6.1) are transported into a cooling tunnel at $\approx 12°\text{C}$ for about $10min$ (step 2).
4. After travelling through the first cooling tunnel, the shells can be filled with a cream or fondant at a typical temperature $T_{Filling} = 35°\text{C}$.
5. The filled shells then go through a second cooling tunnel at $\approx 12°\text{C}$ for about $10min$ to cool the filling rapidly (it could remelt the shells) (step 3).
6. The shells are reheated locally at the rim using infrared heaters and then the two halves are closed to form the complete eggs.
7. The closed eggs still surrounded by their moulds pass through a third cooling tunnel at $\approx 12°\text{C}$ for about $10min$ to finish to set the chocolate (step 4).
8. The eggs are demoulded and packaged before storage.

Each step of the process is represented in figure 6.2.

6.2 Modelling of step 1: Application of the plunger

6.2.1 Parameters used to model the application of the plunger

In an industrial context, most of the products manufactured using rapid cooling processes are Easter eggs. The egg shell geometry was simplified to a sphere to take advantage of axial symmetry (although a more realistic $3-D$ problem could be setup, this would involve greater computational complexity). The geometry chosen was typical of an actual product with a shell thickness $e_{shell} = 2.5mm$ (internal radius of $17mm$ and external radius of $19.5mm$). A commercial finite element code, COMSOL Multiphysics (London, UK), was used to solve the system of PDEs describing the problem. The system of equations used to model the industrial process is similar to the one developed for the PCR modelling described in section 4.

The first equation implemented in the model is the heat transfer equation 6.1.

$$\rho \cdot Cp \cdot \frac{\partial T}{\partial t} = \nabla \cdot (k \cdot \nabla T) + \dot{Q}_{source} \tag{6.1}$$

This was done using the transient conduction heat transfer `Application Mode` (T) and the following thermal properties (numerical values are shown in table 6.1):

Thermal conductivity $k = k_{solid} \cdot [unstable + stable] + k_{liquid} \cdot [melt]$.

Density ρ.

Specific heat capacity $Cp = Cp_{solid} \cdot [unstable + stable] + Cp_{liquid} \cdot [melt]$.

Source $\dot{Q}_{source} = \Delta H_{stable} \cdot \frac{\partial [stable]}{\partial t} + \Delta H_{unstable} \cdot \frac{\partial]unstable]}{\partial t}$.

Boundary conditions A Dirichlet boundary condition $T = T_{FC}$ was used on the boundaries in contact with the plunger (*i.e.* the temperature of the surface of the product is equal to the temperature of the plunger) and insulation or axisymmetry

$\nabla T \cdot n = 0$ elsewhere. These boundary conditions are specified on the geometry in figure 6.3.

Initial condition $T_{t=0} = T_0$ which is the temperature of the chocolate at the end of the tempering process.

The heat transfer equation is coupled to the phase change kinetics via the $\dot{Q}_{source}$ term. The evolution of the phases within each element of the mesh was described using the Convection Diffusion application mode, setting the diffusion rate to 0. This effectively enables solution of the PDE system 6.2 with a temperature dependence for the kinetic rates within each mesh element.

$$\begin{aligned}
\frac{\partial[stable]}{\partial t} &= k_{ms} \cdot [melt] \cdot [stable]^c + k_{us} \cdot [unstable] \cdot [stable]^c - k_{sm} \cdot [stable] \\
\frac{\partial[unstable]}{\partial t} &= k_{nuc} \cdot [melt] + k_{mu} \cdot [melt] \cdot [unstable]^c - k_{um} \cdot [unstable] \\
\frac{\partial[melt]}{\partial t} &= -k_{ms} \cdot [melt] \cdot [stable]^c + k_{sm} \cdot [stable] - k_{nuc} \cdot [melt] - k_{mu} \cdot [melt] \cdot [unstable]^c \\
&\quad +k_{um} \cdot [unstable]
\end{aligned} \tag{6.2}$$

For the *stable* phase:

Reaction rate $k_{ms} \cdot [melt] \cdot [stable]^c + k_{us} \cdot [unstable] \cdot [stable]^c - k_{sm} \cdot [stable]$.

Boundary conditions Insulation or axisymmetry $\nabla[stable] \cdot n = 0$.

Initial condition $[stable]_0$ which is the relative concentration in *stable* crystals of the chocolate at the end of the tempering process.

For the *unstable* phase:

Reaction rate $k_{nuc} \cdot [melt] + k_{mu} \cdot [melt] \cdot [unstable]^c - k_{um} \cdot [unstable] - k_{us} \cdot [unstable] \cdot [stable]^c$.

Boundary conditions Insulation or axisymmetry $\nabla[unstable] \cdot n = 0$.

Initial condition $[unstable]_0$ which is the relative concentration in *unstable* crystals of the chocolate at the end of the tempering process.

For the *melt* phase:

Reaction rate $-k_{ms} \cdot [melt] \cdot [stable]^c + k_{sm} \cdot [stable] - k_{nuc} \cdot [melt] - k_{mu} \cdot [melt] \cdot [unstable]^c + k_{um} \cdot [unstable]$.

Boundary conditions Insulation or axisymmetry $\nabla]melt] \cdot n = 0$.

Initial condition $[melt]_0$ which is the relative concentration in *melt* material of the chocolate at the end of the tempering process.

The different kinetic rates were calculated using the same step change equation as in the ODE system:

$$k_{ii} = \begin{cases} \frac{K_{ii}}{1-e^{+(T-T_{ii})}} & \text{for } k_{us}, k_{um} \text{ and } k_{sm} \\ \frac{K_{ii}}{1-e^{-(T-T_{ii})}} & \text{for } k_{mu} \text{ and } k_{ms} \end{cases} \tag{6.3}$$

$$k_{nuc} = \begin{cases} K_{nuc} \cdot (T_{nuc} - T) & (T < T_{nuc}) \\ 0 & (T \geq T_{nuc}) \end{cases}$$

The non structured mesh (2934 elements) was built using the mesh dependence analysis performed for the PCR geometry. The free mesh parameters of the COMSOL mesh module were set to `Normal` with a maximum mesh size of $0.1mm$ on the boundaries in contact with the plunger similar to the one used for the validation of the model on the Peltier stage geometry.

This mesh is presented in figure 6.3 with the boundary conditions used.

6.2.2 Predictions of temperature and polymorph concentrations using the model

Equations detailed above were solved using the $UMFPACK$ solver using the typical time and temperature used by manufacturers for this step $(t_{FC}, T_{FC}) = (3s, -10°\text{C})$. The result of the simulation for these processing conditions can be seen in figure 6.4.

On figure 6.4(a), one can see that the temperature at the end of the first step is quite heterogeneous. This is due to the ideal contact between the plunger and the chocolate and thus the temperature decreases rapidly at the interface, while the low thermal conductivity slows the heat transfer in the geometry.

In figure 6.4(c), one can see the freezing front of *unstable* crystals. Around 20% of the thickness of the shell is partially solidified with about 20% at the surface to 7% at $x = 0.2 \cdot e_{shell}$ of *unstable* crystals whilst the rest of the shell is still molten $(0.7 < [melt] < 0.97)$. Because of the relatively slow crystallisation kinetics (compared to heat transfer), phase change is only partial.

The mechanism of the process can be understood using the results from the simulation. During the application of the plunger, the high cooling rates form a thin *crust* of *unstable* and few *stable* crystals ($\approx 1\%$) at the inner surface of the chocolate (6.4(b)). These observations are consistent with the literature data that indicates that rapid cooling leads to *unstable* crystals (Stapley et al. 1999). This thin partially solid layer of chocolate at the surface does not allow the liquid material underneath to flow and therefore ensures the conservation of the shape of the product during the rest of the process.

Evolution of the temperature in the shell during the application of the plunger

During the application of the plunger, the temperature in the product is very heterogeneous (figure 6.5). This is typical of a situation of a large Biot number (Bi) detailed in equation 6.4.

$$Bi = \frac{h \cdot d}{k} \; (d = e_{shell}) \tag{6.4}$$

A typical heat transfer coefficient between a solid wall and a viscous food product is $h \approx 3000 W \cdot m^{-2} \cdot K^{-1}$ (Bimbenet 2002), which corresponds to $Bi \approx 25$, implying that the internal heat transfer is controlling the overall rate of heat transfer in this case. This is a typical situation in food engineering because of the small values of thermal conductivities in most foods compared to other materials such as metals, for example.

In figure 6.5(a), the evolution of temperature is presented at different locations along a normal to the surface corresponding to $1\%, 10\%, 25\%, 50\%, 75\%$ and 100% of the shell thickness ($e_{shell} = 2.5mm$) measured from the surface in contact with the plunger. One can see that the temperature at 1% of e_{shell} reaches the temperature of the plunger $T_{FC} = -10$°C very quickly ($\approx 0.5s$). On the other hand the temperature close to the mould is almost constant, with a temperature change of less than a degree. This is in agreement with the contour plots presented in figure 6.4 where the temperature at the end of the process is very heterogeneous. This also explains why only a thin layer of chocolate crystallises during the application of the plunger. As a result of the high cooling rate, these crystals are mainly *unstable*. In figure 6.5(b), one can see that at 1% of e_{shell} and 10% of e_{shell}, the crystallisation kinetics are very similar whereas the rest of the product is not crystallised.

Since little crystallisation occurs during this rapid cooling step, the contribution of the source term on the heat transfer model should be very small and the problem solved is essentially transient heat conduction. For such problems analytical solutions have been developed. Analytical solutions of the evolution of the dimensionless temperature U (see equation 6.5) for different geometries (Carslaw and Jaeger 1986, Incropera and DeWitt 2001) are a function of the Fourier time Fo (see equation 6.6).

$$U = \frac{T - T_0}{T_{FC} - T_0} \tag{6.5}$$

$$Fo = \frac{\alpha \cdot t}{d^2} \tag{6.6}$$

The analytical solution of heat conduction at a distance r from the center in a sphere of radius R ($Fo = \dfrac{\alpha \cdot t}{R^2}$ in this case) with the following conditions:

$$\begin{cases} T = T_0 & t = 0 \\ T(R) = T_{FC} & t > 0 \end{cases} \tag{6.7}$$

is:

$$U(r) = \sum\left(\frac{2 \cdot \sin\lambda_n - \lambda_n \cdot \cos\lambda_n}{\lambda_n - \cos\lambda_n \cdot \sin\lambda_n} \cdot \frac{\sin(\lambda_n \cdot \frac{r}{R})}{\lambda_n \cdot \frac{r}{R}} \cdot e^{-\lambda_n^2 \cdot Fo}\right) \tag{6.8}$$

where λ_n is the n^{th} root of the equation $Bi = 1 - \dfrac{\lambda}{\tan\lambda}$.

To test the hypothesis about heat conduction being the primary mechanism occurring during this step (radial heat diffusion with a fixed temperature boundary condition) there should be a linear relationship between $log(U)$ and Fo ($Fo = \dfrac{\alpha \cdot t}{e^2_{shell}}$ in this case), independent of r.

The natural (Napierian) logarithm $log(U)$ was plotted against the Fourier time Fo and the results are presented in figure 6.6. One can see that whether the plunger temperature is 0°C , −10°C , −20°C or −30°C the curves are very close (±0.2). The expected linear relationship is clearly seen in the graph and the different locations (same as in figure 6.5) have the same slope as expected. It is interesting to notice that when the temperature of the plunger decreases (0°C), the cooling rate is decreased and the curve starts to drift away from the prediction for heat conduction, whereas if the temperature of the plunger is very cold (−30°C) the relationship is more linear ($r^2 \approx 0.98$). This can be explained that for a colder plunger, the effect of the source term is less important compared to the heat conduction, as any generated heat is more absorbed by the heat sink. This is consistent with the observations made on figure 5.1(a) where the phase change plateau was not observed when a high cooling rate (profile 1) was applied in the PCR system. It can be explained as the high cooling rate drags heat away faster than heat is generated during the crystallisation.

This shows that the FEM solution for this problem is essentially conduction heat transfer and that little to no disturbance can be attributed to the phase change.

Prediction of the Solid Fat Content after application of the plunger

It would be of interest for the chocolate producers to obtain process design rules for rapid cooling manufacturing. This would involve estimating the required processing time as a function of processing parameters such as the temperature of the plunger (T_{FC}) and the thickness of the shell (e_{shell}). Analysis of the process so far revealed that only for industrial processing conditions ($T_{FC} = -10$°C ,$e_{shell} = 2.5mm$,$t = 3s$), only a small part ($\approx 20\%$) of the chocolate is partially solidified ($\approx 10\%$). Thus, the process leads to the formation of a *crust* holding the shape prescribed by the plunger. That a small amount of crystals increases the viscosity of chocolate enough to hold its shape is consistent with previous work (Bolliger, Zeng and Windhab 1999), where it was found that $\frac{\partial \eta}{\partial SFC} = 10 Pa \cdot s \cdot \%^{-1}$ for small values of Solid Fat Content (SFC (0 to 1.5%). Similar to conventional processes, the solidification of the majority of the cocoa butter still occurs in the cooling tunnels following the rapid cooling step.

Since these processing conditions have been successfully used in typical industrial lines, it will be assumed that a successful rapid cooling step will require a small percentage of the shell (20%) contains 10% of solid fat such as:

$$(unstable + stable)_{x=0.2 \cdot e_{shell}} \geq 0.1 \tag{6.9}$$

It was used to obtain equivalent processing conditions (t, T_{FC}) for step 1.

Conventional freezing of foods can be modelled by Planck's equation (James, Ketteringham, Palpacelli et al. 2009, Pham 1984) as follows:

$$t_f = \frac{\rho \cdot \Delta H}{\Delta T} \cdot \frac{x}{a} \cdot (\frac{1}{h} + \frac{x}{2 \cdot k}) \tag{6.10}$$

From this equation, one can see that the freezing time t_f is proportional to the density of the product ρ, the phase change enthalpy ΔH and the characteristic length of the product x. It is also inversely proportional to the temperature difference between the freezing point (crystallisation temperature of the *unstable* crystals in this case) and the surrounding media $\Delta T = T_{mu} - T_{FC}$ as well as the heat transfer coefficient h and the thermal conductivity k. A shape factor (a), takes different values depending whether the product is a slab $(a = 1)$, a cylinder $a = 2$ or a sphere $a = 3$ (again, this is considered to be the closest geometry to this case).

Since the Biot number (6.4) is large $(\frac{1}{h} \ll \frac{x}{2 \cdot k})$, a simpler form of the Planck's equation can be obtained 6.11.

$$t_f = \frac{\rho \cdot \Delta H}{2 \cdot a \cdot k} \cdot \frac{x^2}{\Delta T} \tag{6.11}$$

In figure 6.7, the amount of time required to solidify 10% of the cocoa butter (mainly as *unstable* crystals) is plotted against $\frac{x^2}{\Delta T}$ and a linear relationship is obtained as suggested by the simplified Planck's equation (6.11). The slope that can be calculated using the Planck equation is:

$$\frac{\rho \cdot \Delta H}{2 \cdot a \cdot k} = \frac{1300 \cdot 10\% \cdot 19000}{2 \cdot 3 \cdot 0.3} = 1.37 \cdot 10^6 \,^{\circ}\mathrm{C} \ \cdot s \cdot m^{-2}$$

whereas the slope obtained from the simulation as plotted on figure 6.7 is $1.5 \cdot 10^8 \,^{\circ}\mathrm{C} \ \cdot s \cdot m^{-2}$ or two orders of magnitude more. The error is a result the assumptions involved in the calculus of (6.10), *i.e.*

- the fact that the Planck equation was initially developed for the freezing of water, which is a pure phase, whereas a number of different solid phases exist for cocoa butter
- freezing occurs at a single temperature and does suppose that the initial temperature of the product is uniform

Since none of these assumptions is valid in our system, it is not surprising that the values obtained by theory and numerical experiments are different. It is interesting to note though that freezing time is still proportional to $\frac{x^2}{\Delta T}$.

As such, this semi-empirical relationship can be extremely useful for manufacturing purposes since initial trials on a new product geometry can be shortened by estimating the processing conditions. For example, if one wants to manufacture and egg with a thickness of $3.5mm$ with a plunger temperature $T_{FC} = -10$°C , 20% of the thickness or

$0.7mm$ have to have more than 10% solids, leading to:

$$\frac{x^2}{\Delta T} = \frac{0.0007^2}{10-(-10)} = 2.45E-8m^2 \cdot s^{-1}$$

and by reading graphically on figure 6.7:

$$t_f \approx 4.5s.$$

Similarly, if a shell of $5mm$ was to be manufactured with a plunger temperature $T_{FC} = 0$°C $, \frac{x^2}{\Delta T} = 1E-7m^2 \cdot s^{-1}$ and one could then read on the abacus $t_f = 15.5s$.

6.3 Modelling of step 2: Setting of the shells in the first cooling tunnel

After the rapid cooling process already discussed, the egg shells go through cooling tunnels. The objective of these cooling tunnels is to set the chocolate completely since ,as it has already been discussed, the rapid cooling process only prescribes the shape of the shell by cooling and partially freezing the geometry.

6.3.1 Model parameters used for the modelling of for the first cooling tunnel

To model this step the same set of equations as for step 1 were used. However due to the difference in processing, the properties of the transient conduction heat transfer `Application Mode` (T) were altered to match the process:

Thermal conductivity $k = k_{solid} \cdot [unstable + stable] + k_{liquid} \cdot [melt]$.

Density ρ.

Specific heat capacity $Cp = Cp_{solid} \cdot [unstable + stable] + Cp_{liquid} \cdot [melt]$

Source $\dot{Q}_{source} = \Delta H_{stable} \cdot \frac{\partial [stable]}{\partial t} + \Delta H_{unstable} \cdot \frac{\partial]unstable]}{\partial t}$.

Boundary conditions A Neumann boundary condition was used on the boundaries directly in contact with the air in the cooling tunnel (T_{tunnel},h_{tunnel}) and insulation or axisymmetry $\nabla T \cdot n = 0$ elsewhere. These boundary conditions are specified on the geometry in figure 6.8.

Initial condition T_0 which is the temperature of the chocolate at the end of step 1.

The `Application Modes` used to compute the concentrations in *stable*, *unstable* and *melt* were kept the same as for step 1 except that the initial values $[stable]_0$, $[unstable]_0$ and $[melt]_0$ were mapped to the solutions obtained at the end of step 1.

Because of the more gentle cooling, this step takes more time to complete than the rapid cooling step and a typical residence time in this tunnel is around $10min$. The different constants used to run the model are presented in table 6.2.

6.3.2 Predictions of the chocolate temperature and polymorphous structure in the first cooling tunnel

As one can see in figure 6.9, after $600s$ of processing, the temperature by the end of this step is uniform ($\approx$ 14°C) and most of the shell is solid and made of *stable* crystals. This is due to the gentle cooling over a long period of time. The Biot number is small ($Bi = \dfrac{h_{tunnel} \cdot e_{shell}}{k} = 0.25$), meaning that the heat flow is controlled by the external heat transfer. The model therefore conforms with what could be expected, that a slower cooling would lead to a more stable crystal structure.

The *unstable* crystals initially present at the surface because of the rapid cooling process transformed into *stable* crystals because of the conduction from warm melt underneath it providing the heat needed for the polymorphous transition, as shown on figure 6.10. Because of the two phenomena, the amount of *unstable* crystals at the end of this step is very low (less than 5%), as one can see in figure 6.9(c).

This analysis shows that this second cooling step is very important to ensure the final quality of the product and particularly its resistance to bloom, which is commonly associated with the transition of *unstable* crystals to *stable* crystals under uncontrolled conditions during storage.

6.4 Modelling of step 3: Injection of a filling and cooling in a tunnel

6.4.1 Model parameters used if a filling is injected in a set shell

After the shells have completely set, the filling is injected in the shells, for example a caramel filling. The filling was considered to have the physical properties of a sugar solution of 75°Bx. The specific heat capacity of this caramel filling would then be $Cp_{filling} = 2000 J \cdot kg^{-1} \cdot^{\circ} \mathrm{C}^{-1}$, the density $\rho_{filling} = 1500 kg \cdot m^{-3}$ and the thermal conductivity $k_{filling} = 0.32 W \cdot m^{-1} \cdot^{\circ} \mathrm{C}^{-1}$ according to the literature (Bubnik, Kadlec and Urban 1995, Hough, Moro and Luna 1986).

Heat transfer and phase change reactions were set in the same way as they were for step 2.

The different constants used to run the model including the values estimated for the filling are presented in table 6.3.

The geometry was modified to take account of the injection of the filling. It therefore consists of two parts, a chocolate shell and the filling, as shown in figure 6.11. The new geometry was remeshed using the same settings as for steps 1 and 2, increasing the number of elements from 2934 to 6266. The mesh and boundary conditions used can be seen in figure 6.11. The results from step 2 (as shown in figure 6.9) were used as the initial values for the chocolate shell in step 3. The temperature of the filling used is $T_{filling} = 35°\mathrm{C}$, and was assigned as the initial value over the new mesh created for the filling. However, when implementing this problem in COMSOL, the temperature for the new element was automatically set to $0K$.

The step was therefore first solved using this automatically set temperature for the filling of $0K$ for a very short time ($\approx 10^{-4}s$), so that the impact of this step on the temperature of the computational domain would be very small. Then the desired temperature $T_{filling}$ was used to replace the temperature value in all the elements where the temperature was found to be equal to $0K$ in the `fem.sol` structure. The details of the code needed for this manipulation is shown in Appendix B (lines 0489 to 0495).

6.4.2 Model predictions after a filling has been injected in a set shell

On figure 6.12, temperature contours are shown after $600s$ of processing. One can see that at the end of the process the temperature in the final product is quite heterogeneous and that most of the chocolate shell is still liquid. This is due to the increase in thermal mass brought by the filling compared to the chocolate shell ($\rho_{filling} \cdot V_{filling} \cdot Cp_{filling} = 61.7J \cdot ^{\circ}\mathrm{C}^{-1}\, vs.\, \rho_{shell} \cdot V_{shell} \cdot Cp_{shell} \approx 25J \cdot ^{\circ}\mathrm{C}^{-1}$), so the mass required to be cooled is not only more important but is also more resistant to temperature changes (high Cp). It is interesting to note that the contours are no longer radial, but parallel to the filling surface, which indicates that the problem is no longer 1-D as it was for the two first steps but truly axisymmetric. Moreover, the injection of the filling also decreases the surface available for cooling ($1.1E-3m^2\, vs.\, 2.1E-3m^2$ for the empty shell) that allowed the filling to partially melt the chocolate shell.

However, as it was shown during the modelling of the first step, 10% of solid fat content seems to be enough for the chocolate to hold this shape. It was though to be of interest to study the effect of the filling temperature on the microstructure of the chocolate shell. The cooling time was kept constant ($10min$), and the minimum solid fat content in the shell was estimated depending on the initial temperature of the filling. One can see that as if $T_{filling}$ is less than 36.5°C , the processing time of ten minutes is sufficient to cool the filling so that more than 10% of the fat is solid at the end of the cooling tunnel. If the filling is highly viscous and needs to be injected at a temperature higher than 36.5°C , then this case would need to be further examined by the manufacturer.

A way to solve such an issue would be to increase the cooling of the chocolate shell by using a more conductive metal mould. The same simulations were thus run by applying a heat flux boundary conditions on the boundary in contact with the mould ($h = h_{tunnel}$, $T = T_{tunnel}$). One can see that the amount of solid fat content is largely increased as expected from the extra cooling power coming from the mould side. The critical $T_{filling}$ temperature to keep more that 10% of the shell solid is increased to 44°C from 36.5°C for the insulating mould. This extra leverage could be very useful in order to use highly viscous fillings that need to be heated in order to flow easily during processing.

Because the chocolate has been partially remelted during this third step, it is required that the shells are closed during the first step to expose the moulds to the air flow in order to cool the chocolate shells directly and not through the filling.

6.5 Modelling of step 4: Setting after closure of the egg

In the last step, the moulds are closed and the egg shells are stuck to one another form the filled Easter eggs. As a result of the partial remelt due to the hot filling in the precedent step, it is important to make sure that the eggs are completely solid at the end of this process to facilitate demoulding.

6.5.1 Model parameters for the final cooling tunnel (closed eggs)

Similar processing conditions were used to the problem described before, but boundary conditions were modified to reflect the closure of the moulds as shown in figure 6.14. The external heat transfer coefficient $h_{tunnel+mould}$ was also modified to take account of the resistance of the polycarbonate mould, since the heat is now dissipated through the moulds (see equation 6.12).

$$h_{tunnel+mould} = \frac{1}{\dfrac{1}{h_{tunnel}} + \dfrac{e_{mould}}{k_{mould}}} \tag{6.12}$$

With a value of $e_{mould} = 3mm$ and $k_{mould} = 0.24W \cdot m^{-1} \cdot degC^{-1}$, the overall value for the heat transfer coefficient is $h_{tunnel+mould} = 22W \cdot m^{-2} \cdot degC^{-1}$.
The different constants used to run the model are presented in table 6.4.

6.5.2 Model predictions for the final cooling tunnel (closed eggs)

Figure 6.15(a), shows temperature contours after $600s$ of cooling in the cooling tunnel. One can see that the temperature is almost homogenous by the end of the process. This leads to a shell which is mostly solid ($SFC > 75\%$) as seen on figure 6.15(b), which should prove sufficient for demoulding. Figure 6.15(c) shows that level of *unstable* crystals is very low ($\approx 10^{-4}$) and should give a good heat resistance to the chocolate manufactured during this process. The filling is still relatively warm in the center ($T \approx 20°C$), but this temperature is not high enough to allow the melting of the *stable* crystals in the shell. The storage of the eggs manufactured using the process presented here should not prove difficult. Indeed the *unstable* crystals generated during the rapid cooling are transformed into *stable* crystals and the final product is only made of *stable* crystals, which have a high melting point, are less likely to melt (or bloom) during typical storage temperatures ($15 - 20°C$).

6.6 Temperature and crystal concentration profiles predicted at different locations

The main outcome of this work is the understanding of phase change during the process and its kinetics, allowing control the structure of the final product.

Three different locations, all at $x = 0.125mm$ from the surface in contact with (*i*) the plunger and then (*ii*) the filling, were used to follow the temperature and the concentration in stable, unstable and melt during the process. The three locations were located at $(r, z) = (0, 0.002375)$ $(0.0121092, 0.0073908)$ $(0.0165415, 0.0150677)$, which corresponds to angles of $0, 45, 70°$ from the axis of symmetry (see figure 6.16). These locations being all close to the surface where the heat flux changes most during the process, they are more likely the showcase the history of the structure during the process.

On figures 6.17(a) and 6.17(b), one can see the plot of the predictions for the stable and melt phases at the locations detailed in figure 6.16. The unstable crystals are not plotted as they are completely melted at the end of step 2 and not recrystallised subsequently. One can note that the overall process is a succession of crystallisation (step 1, 2 and 4) and melting (step 3).One can see that around $t = 1000s$ there is the largest difference between the three points $(0.16, 0.25$ and $0.65)$, corresponding to the effect of the filling melting partially the chocolate. As expected, the closer to the surface of the filling, the higher the *stable* fraction is. This is due to the higher rate of cooling close to the surface resulting in a colder filling preventing it to melt the chocolate. Reciprocally, further away form the surface, chocolate is almost completely molten. Chocolate slowly recrystallises in *stable* crystals during step 4, to produce solid and demouldable shells at the end of the process.

On figure 6.17(c), one can see that the high differences in crystalline structure do not correspond to high temperature differences. Temperatures predicted are very similar for the steps 1 and 2 (±0.5°C). This is not surprising as the geometry and boundary conditions are symmetric (cf 6.4(a) and 6.9(a)). When the filling is injected, the problem is no longer symmetric (cf 6.12(a)). This creates a slightly higher difference (±2°C) between the temperature predicted during step 3 and during step 4 subsequently. It is important to notice that these differences of temperature are rather small, this can be explained by the fact that the steady state for the phase change is never reached, acting like a buffer stabilising the temperature in the phase change region (≈ 23°C).

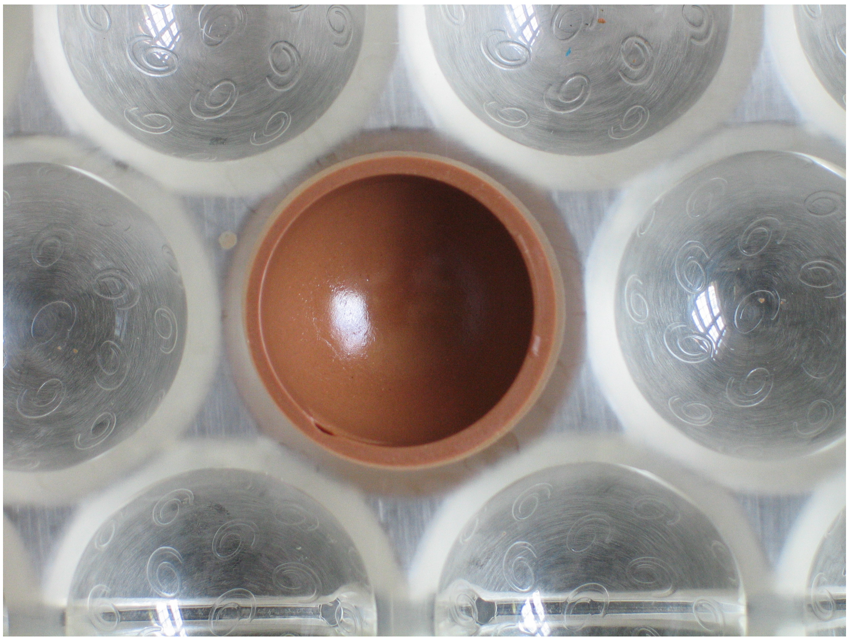

Figure 6.1: Chocolate shell in its polycarbonate mould after application of the plunger

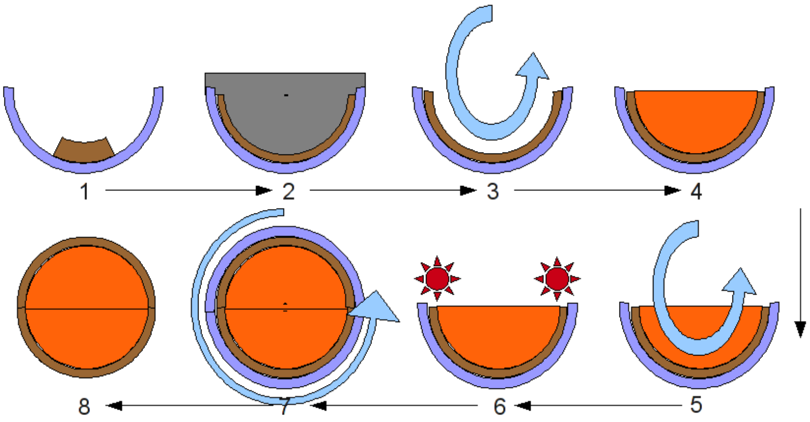

Figure 6.2: Unit operations of a typical rapid cooling process

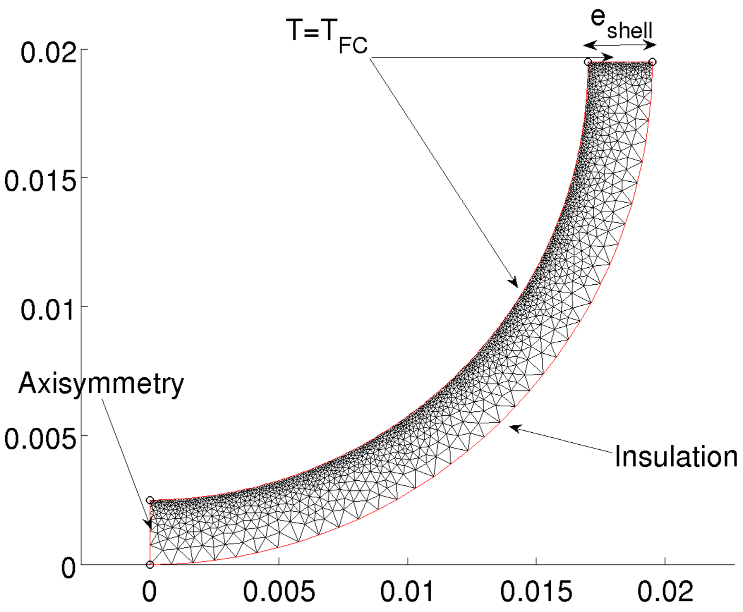

Figure 6.3: Mesh and boundary conditions used for the numerical simulation of step 1.

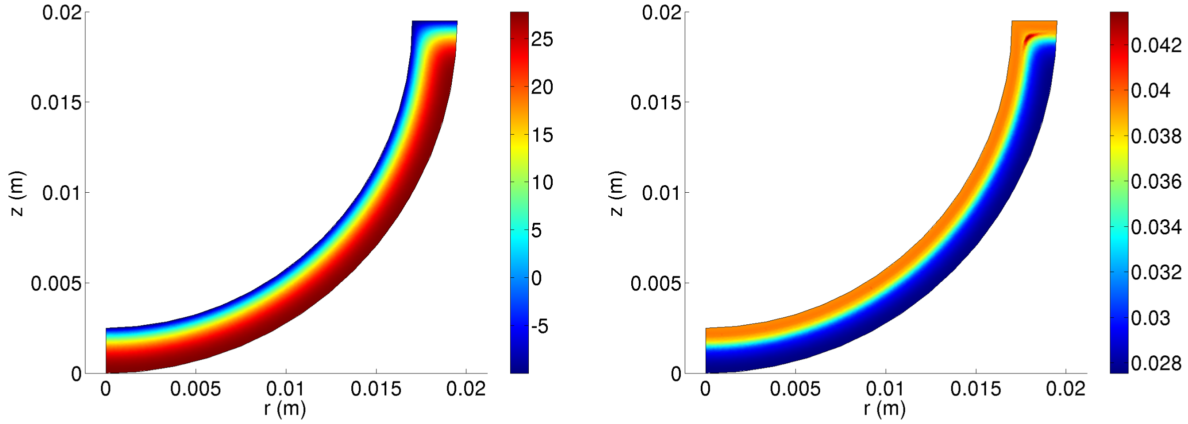

(a) Temperature °C (b) stable

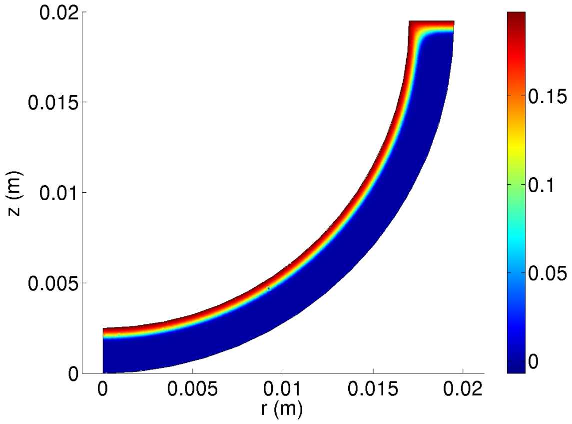

(c) unstable

Figure 6.4: Results of the simulation after application of the rapid cooling head for temperature (6.4(a)),*stable* crystals concentration (6.4(b)),and the *unstable* crystals concentration (6.4(c)) with $(t_{FC}, T_{FC}) = (3s, -10°\text{C})$

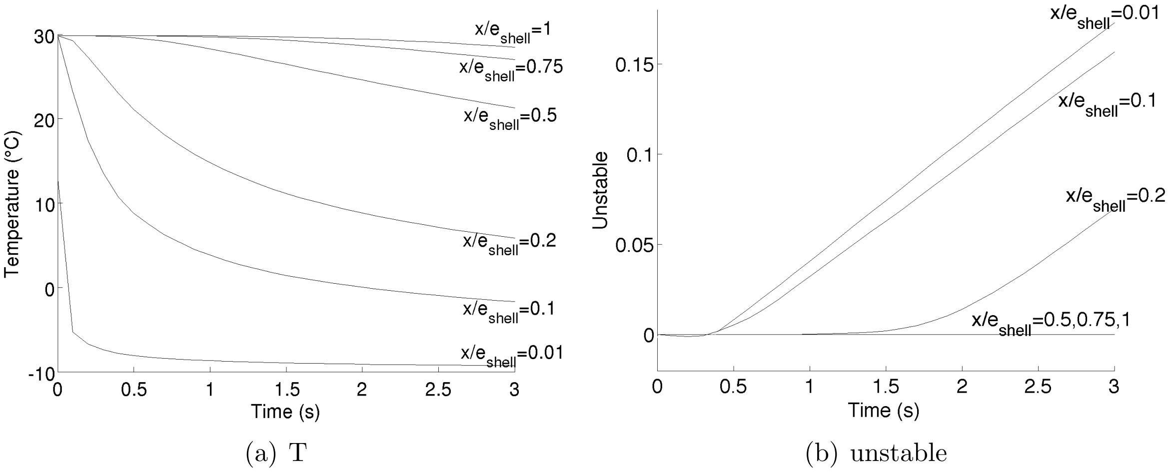

(a) T (b) unstable

Figure 6.5: Evolution of the temperature and unstable concentration at different locations $(\frac{x}{e_{shell}} \in 0.01, 0.1, 0.2, 0.5, 0.75, 1)$ during application of the plunger $(3s, -10°\text{C})$.

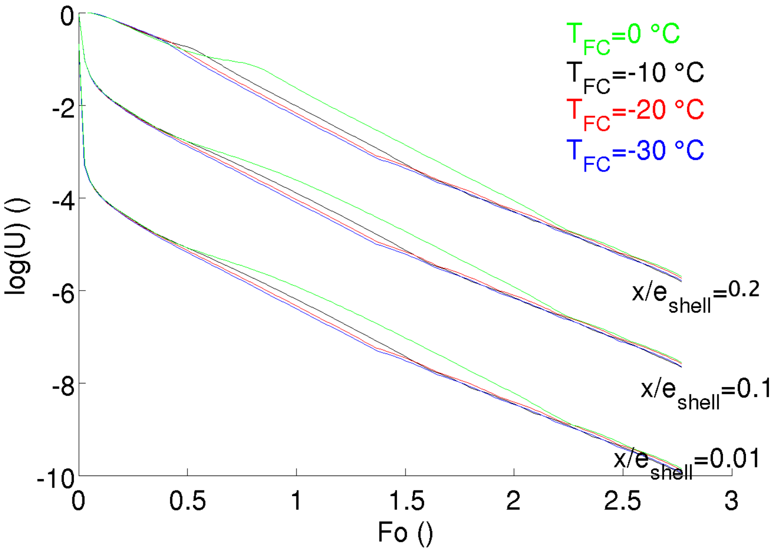

Figure 6.6: Evolution of the dimensionless temperature U against the dimensionless Fourier time Fo, with $e_{shell} = 2.5mm$ and $T_{FC} = 0$°C , $T_{FC} = -10$°C , $T_{FC} = -20$°C and $T_{FC} = -30$°C

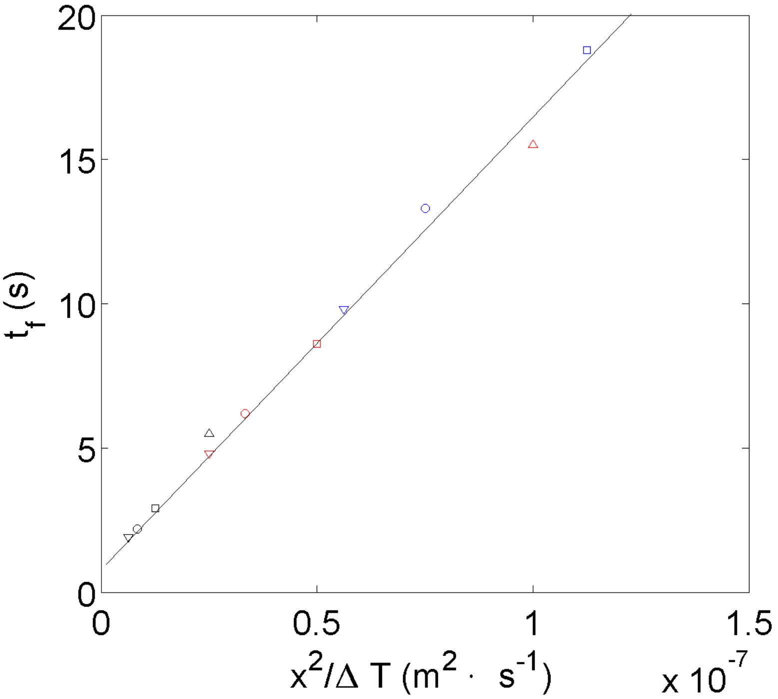

Figure 6.7: Evolution of the plunger application time required to obtain 10% solids at the location x measured from the surface of contact between the plunger and the chocolate. A linear relationship $t_f \propto \dfrac{x^2}{\Delta T}$ is suggested by Planck's equation (6.11). The numerical data was obtained for different processing conditions: $T_{FC} = 0$°C ($\triangle$), $T_{FC} = -10$°C ($\square$), $T_{FC} = -20$°C ($\bigcirc$), $T_{FC} = -30$°C ($\bigtriangledown$) and geometries: $e_{shell} = 2.5mm$ (–), $e_{shell} = 5mm$ (–), $e_{shell} = 7.5mm$ (–).

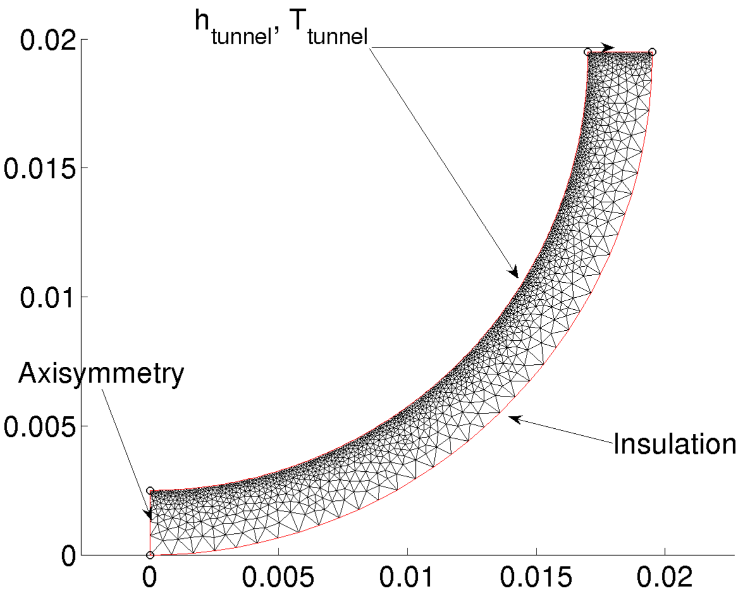

Figure 6.8: Mesh and boundary conditions used for the numerical simulation of step 2.

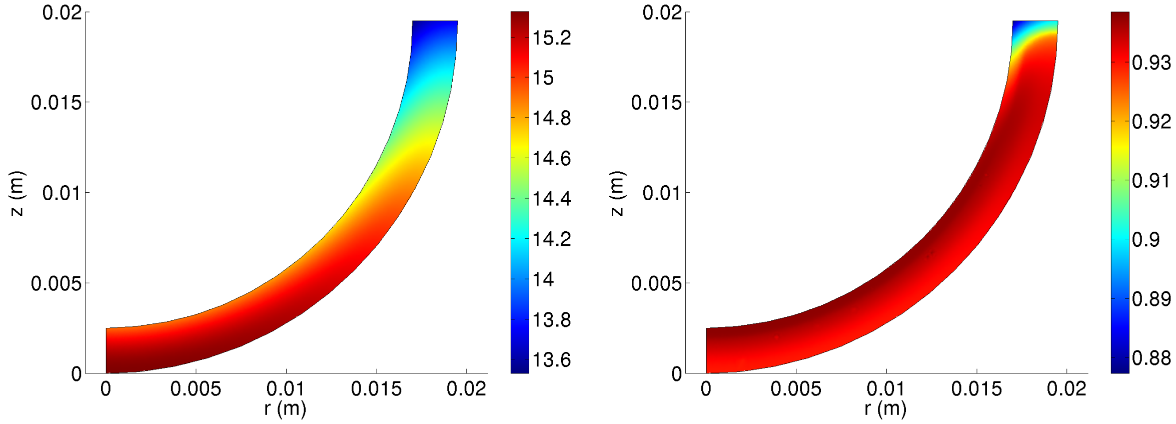

(a) Temperature (b) stable

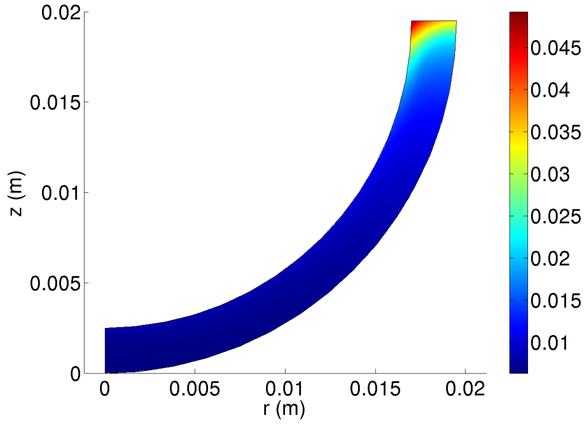

(c) unstable

Figure 6.9: Results of the simulation after processing ($h_{tunnel} = 30W \cdot m^{-2} \cdot ^{\circ}C^{-1}$,$T_{tunnel} = 12^{\circ}C$ and $time = 600s$) for temperature (6.9(a)),*stable* crystals concentration (6.9(b)),and the *unstable* crystals concentration (6.9(c))

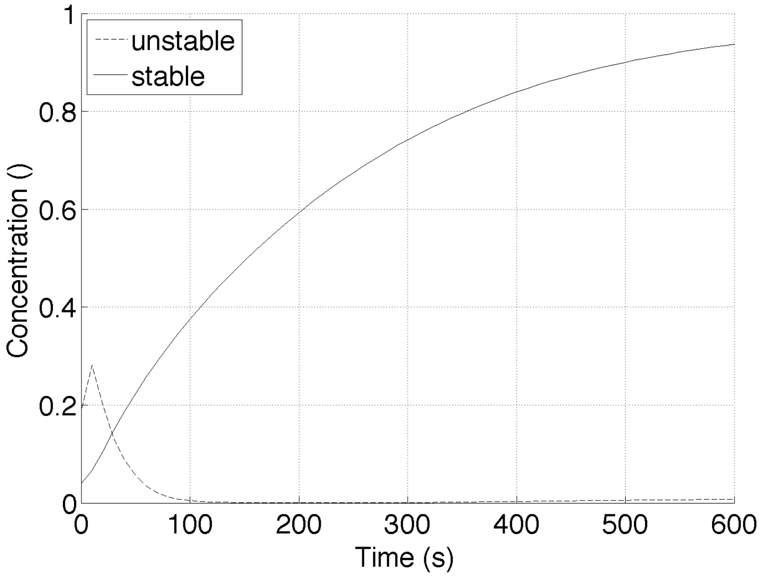

Figure 6.10: Polymorphous transition of unstable to stable ($t < 100s$) during step 2 (location 5% of e_{shell}).

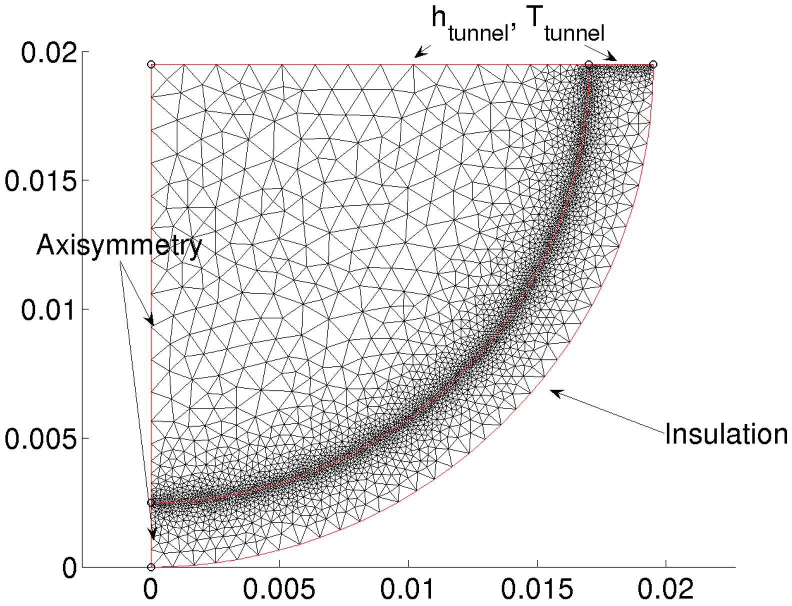

Figure 6.11: Mesh and boundary conditions used for the numerical simulation of step 3.

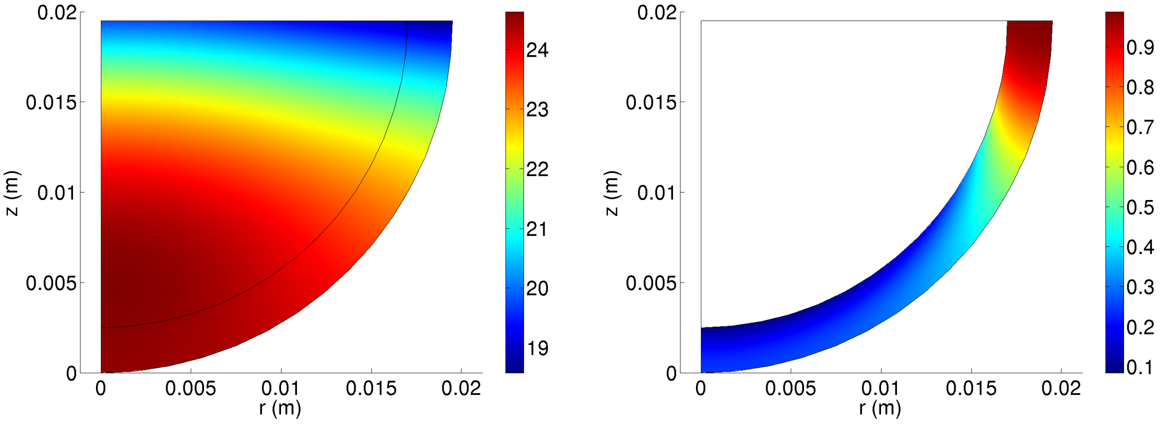

(a) Temperature (b) stable

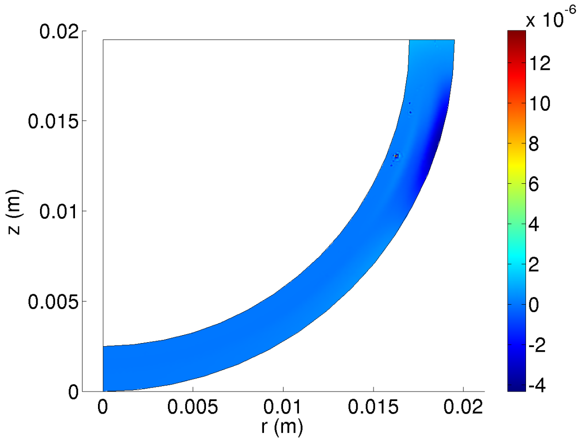

(c) unstable

Figure 6.12: Results of the simulation after processing ($h_{tunnel} = 30W \cdot m^{-2} \cdot ^{\circ}C^{-1}$,$T_{tunnel} = 12^{\circ}C$ and $time = 600s$) for temperature (6.12(a)),*stable* crystals concentration (6.12(b)),and the *unstable* crystals concentration (6.12(c))

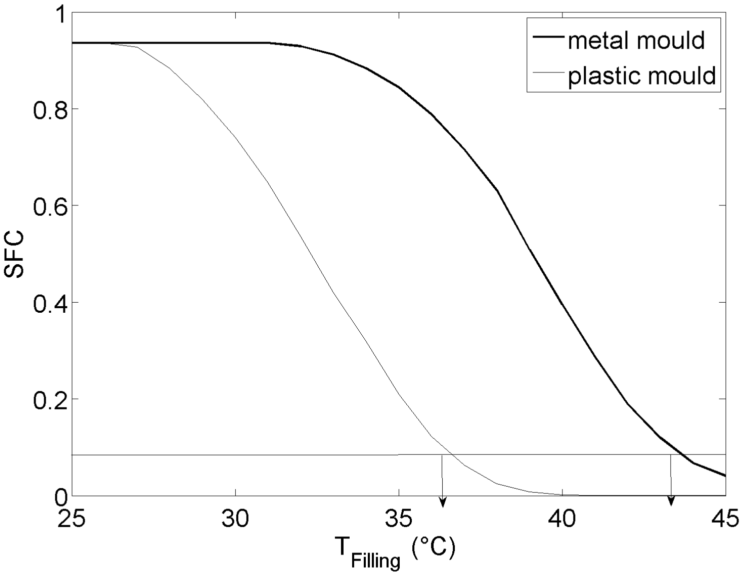

Figure 6.13: Effect of the temperature ($T_{filling}$) of the filling on the minimum SFC value during processing

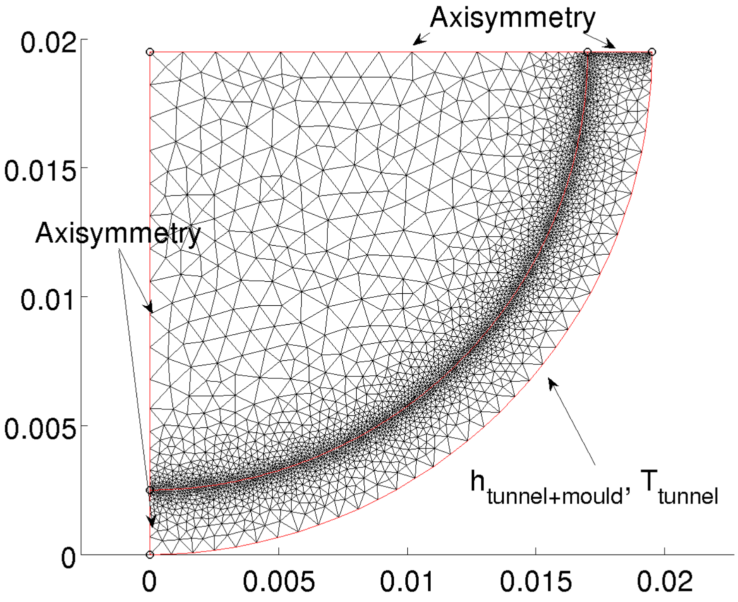

Figure 6.14: Mesh and boundary conditions used for the numerical simulation of step 4.

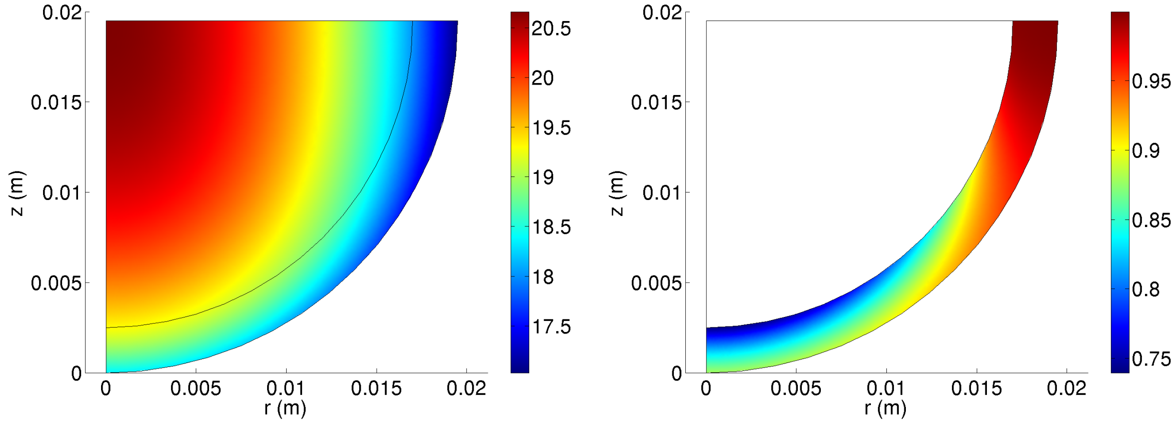

(a) Temperature (b) stable

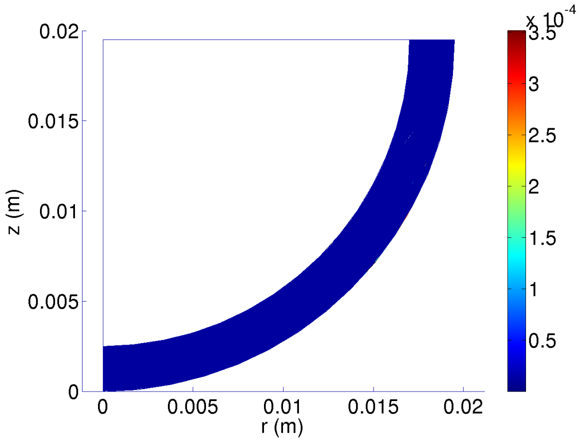

(c) unstable

Figure 6.15: Results of the simulation after processing ($h_{tunnel+mould} = 22W \cdot m^{-2} \cdot^{\circ} \mathrm{C}^{-1}$,$T_{tunnel} = 12°\mathrm{C}$ and $time = 600s$) for temperature (6.15(a)),*stable* crystals concentration (6.15(b)),and the *unstable* crystals concentration (6.15(c)) with $(t_{FC}, T_{FC}) = (3s, -10°\mathrm{C})$

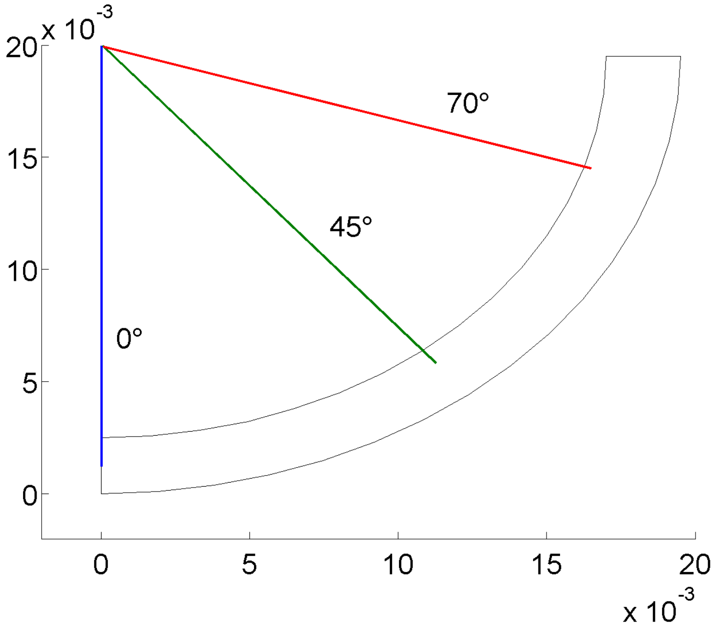

Figure 6.16: Locations of the three points used to evaluate the changes in the structure for simulation of the overall process (see figure 6.17)

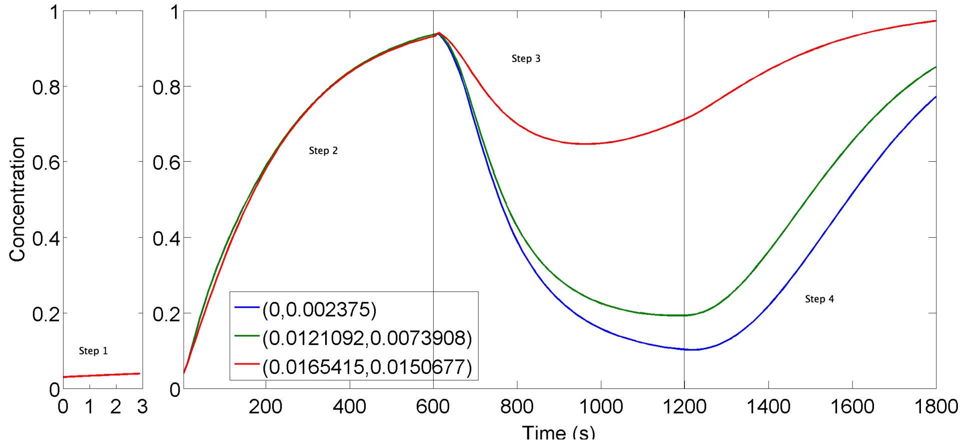

(a) stable

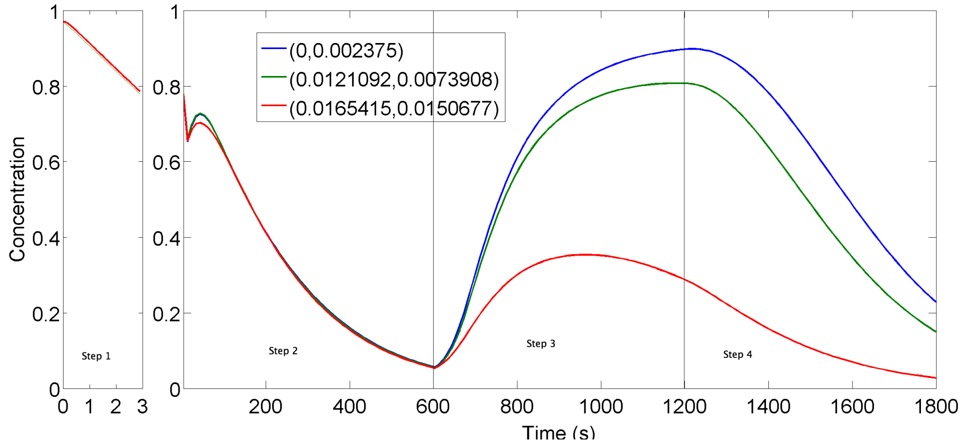

(b) melt

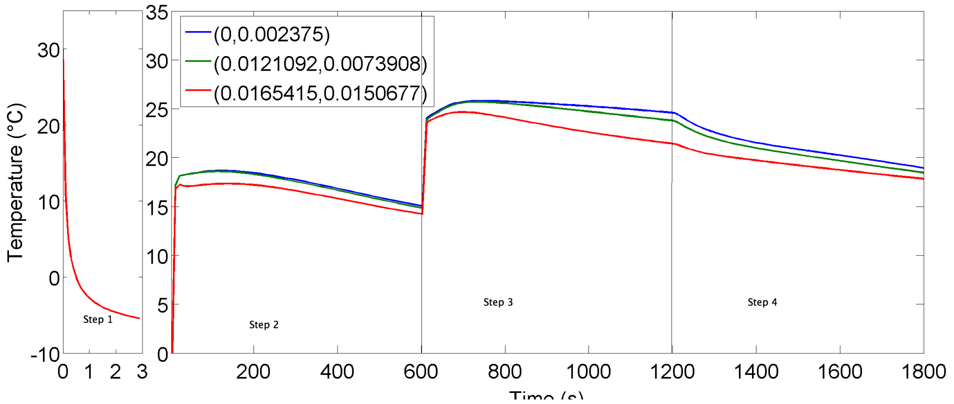

(c) Temperature

Figure 6.17: Results of the simulation during the overall process for temperature (6.17(c)), *stable* and *melt* concentrations (6.17(a) and 6.17(b)).

Table 6.1: Values of the different parameters used to model step 1.

Constant	Value
ρ	$1300 kg \cdot m^{-3}$
k_{solid}	$0.25 W \cdot m^{-1} \cdot ^{\circ}\mathrm{C}^{-1}$
k_{liquid}	$0.35 W \cdot m^{-1} \cdot ^{\circ}\mathrm{C}^{-1}$
Cp_{solid}	$2000 J \cdot kg^{-1} \cdot ^{\circ}\mathrm{C}^{-1}$
Cp_{liquid}	$1500 J \cdot kg^{-1} \cdot ^{\circ}\mathrm{C}^{-1}$
ΔH_{stable}	$22000 J \cdot kg^{-1}$
$\Delta H_{unstable}$	$19000 J \cdot kg^{-1}$
T_0	$30^{\circ}\mathrm{C}$
T_{FC}	$-10^{\circ}\mathrm{C}$
$stable_0$	0.03
$unstable_0$	0
$melt_0$	0.97
K_{ms}	$0.005 s^{-1}$
K_{sm}	$0.06 s^{-1}$
K_{mu}	$0.08 s^{-1}$
K_{um}	$0.06 s^{-1}$
K_{us}	$10 s^{-1}$
K_{nuc}	$0.0005 s^{-1}$

Table 6.2: Values of the different parameters used to model step 3.

Constant	Value
ρ	$1300 kg \cdot m^{-3}$
k_{solid}	$0.25 W \cdot m^{-1} \cdot ^{\circ}\mathrm{C}^{-1}$
k_{liquid}	$0.35 W \cdot m^{-1} \cdot ^{\circ}\mathrm{C}^{-1}$
Cp_{solid}	$2000 J \cdot kg^{-1} \cdot ^{\circ}\mathrm{C}^{-1}$
Cp_{liquid}	$1500 J \cdot kg^{-1} \cdot ^{\circ}\mathrm{C}^{-1}$
ΔH_{stable}	$22000 J \cdot kg^{-1}$
$\Delta H_{unstable}$	$19000 J \cdot kg^{-1}$
T_{tunnel}	12°C
h_{tunnel}	$30 W \cdot m^{-2} \cdot ^{\circ}\mathrm{C}^{-1}$
K_{ms}	$0.005 s^{-1}$
K_{sm}	$0.06 s^{-1}$
K_{mu}	$0.08 s^{-1}$
K_{um}	$0.06 s^{-1}$
K_{us}	$10 s^{-1}$
K_{nuc}	$0.0005 s^{-1}$

Table 6.3: Values of the different parameters used to model step 3.

Constant	Value
ρ	$1300kg \cdot m^{-3}$
k_{solid}	$0.25W \cdot m^{-1} \cdot^{\circ} \mathrm{C}^{-1}$
k_{liquid}	$0.35W \cdot m^{-1} \cdot^{\circ} \mathrm{C}^{-1}$
Cp_{solid}	$2000J \cdot kg^{-1} \cdot^{\circ} \mathrm{C}^{-1}$
Cp_{liquid}	$1500J \cdot kg^{-1} \cdot^{\circ} \mathrm{C}^{-1}$
ΔH_{stable}	$22000J \cdot kg^{-1}$
$\Delta H_{unstable}$	$19000J \cdot kg^{-1}$
T_{tunnel}	12°C
h_{tunnel}	$30W \cdot m^{-2} \cdot^{\circ} \mathrm{C}^{-1}$
$T_{filling}$	35°C
$Cp_{filling}$	$2000J \cdot kg^{-1} \cdot^{\circ} \mathrm{C}^{-1}$
$\rho_{filling}$	$1500kg \cdot m^{-3}$
$k_{filling}$	$0.32W \cdot m^{-1} \cdot^{\circ} \mathrm{C}^{-1}$
K_{ms}	$0.005s^{-1}$
K_{sm}	$0.06s^{-1}$
K_{mu}	$0.08s^{-1}$
K_{um}	$0.06s^{-1}$
K_{us}	$10s^{-1}$
K_{nuc}	$0.0005s^{-1}$

Table 6.4: Values of the different parameters used to model step 4.

Constant	Value
ρ	$1300kg \cdot m^{-3}$
k_{solid}	$0.25W \cdot m^{-1} \cdot^{\circ} \mathrm{C}^{-1}$
k_{liquid}	$0.35W \cdot m^{-1} \cdot^{\circ} \mathrm{C}^{-1}$
Cp_{solid}	$2000J \cdot kg^{-1} \cdot^{\circ} \mathrm{C}^{-1}$
Cp_{liquid}	$1500J \cdot kg^{-1} \cdot^{\circ} \mathrm{C}^{-1}$
ΔH_{stable}	$22000J \cdot kg^{-1}$
$\Delta H_{unstable}$	$19000J \cdot kg^{-1}$
T_{tunnel}	12°C
$h_{tunnel+mould}$	$22W \cdot m^{-2} \cdot^{\circ} \mathrm{C}^{-1}$
$T_{filling}$	35°C
$Cp_{filling}$	$2000J \cdot kg^{-1} \cdot^{\circ} \mathrm{C}^{-1}$
$\rho_{filling}$	$1500kg \cdot m^{-3}$
$k_{filling}$	$0.32W \cdot m^{-1} \cdot^{\circ} \mathrm{C}^{-1}$
K_{ms}	$0.005s^{-1}$
K_{sm}	$0.06s^{-1}$
K_{mu}	$0.08s^{-1}$
K_{um}	$0.06s^{-1}$
K_{us}	$10s^{-1}$
K_{nuc}	$0.0005s^{-1}$

CHAPTER 7

CONCLUSIONS AND FUTURE WORK

Consumer acceptance of chocolate is partially driven by its texture which can be related to the crystal structure (crystal size and polymorphism) developed during processing, thus controlling and understanding processing conditions is critical. It is known that the cooling rate applied during solidification is the main factor controlling the polymorphic state of fats. A fast cooling rate ($> 5°C \cdot min^{-1}$), typically leads to *unstable* crystals (low melting point) and is therefore widely not used, despite offering the possibilities to increasing process capabilities of existing equipment in a plant. Traditional chocolate processing therefore uses moderate cooling ($< 2°C \cdot min^{-1}$) methods such as forced convection in cooling tunnels, giving high melting point polymorphs which are attractive to the consumers.

However recent developments in the equipment for chocolate manufacturing use very high cooling rates ($> 50°C \cdot min^{-1}$) for short times and still produce acceptable chocolate with high yields ($\approx 10^6$ units per day). Such equipment usually consists of a plastic mould similar to traditional cooling coupled with the action of a cold (e.g. $-10°C$) metallic anti-mould setting the surface of the chocolate almost instantly.

Obtaining an understanding of this new rapid cooling processes was the main objective of this work.

A mathematical model describing the phase change kinetics of fats was successfully developed by clustering the polymorphs into two groups of *unstable* (I,II,III and IV) and *stable* (V,VI) species. This simplification allowed the kinetic parameters of the model to be fitted to DSC data obtained over a range of cooling rates relevant to chocolate processing ($0.5 - 20$°C $\cdot\, min^{-1}$). Initial DSC data also demonstrated polymorphous transitions from *unstable* to *stable* crystals only if the material initially contained some *stable* crystals. Such transitions were therefore incorporated in the model.

The model developed to describe crystallisation and melting kinetics was coupled to the heat transfer equation. The phase change kinetics were used to calculate the heat source and the temperature was used to calculate the kinetic rates, resulting in a fully coupled two-way model. This allowed the prediction of the temperature field and phase concentration of *unstable* and *stable* during a typical process.

Since the kinetics of phase change were fitted to DSC data, an independent method to validate the phase concentrations was necessary. XRD has been widely used for cocoa butter crystal structure determination but, because of the overlap between the sucrose and the cocoa butter XRD patterns (particularly around 4.56Å, location of the main *stable* peak), there was no technique available to directly identify the state of cocoa butter in chocolate.

This issue was resolved by using a new XRD technique, consisting of subtracting the pattern measured at 40°C (sucrose XRD pattern) from the pattern measured at −30°C (sucrose and cocoa butter XRD patterns). This measurement technique was validated using pure cocoa butter, dark and milk chocolate processed under similar conditions. The method was also used to measure polymorphous transitions in pure cocoa butter and milk chocolate and quantitative measurements (concentration of the different phases) were obtained by integrating the area under the XRD peaks related to the *stable* (4.56Å) and *unstable* (4.19Å) crystals.

The XRD method already presented was used to validate the different phases concentration during heating of rapidly cooled chocolate to validate polymorphous transition and melting predictions or at the end of a solidification process to validate the crystallisation kinetics predictions. The model was also found to compare favorably with the collected XRD data.

To validate the temperature predictions, a rig (PCR) was developed around a Peltier stage for accurate temperature control at the boundary and the use of accurately positioned thermocouples to measure the evolution of the temperature at different locations during the process. A wide range of processing conditions were used to validate the model. The model was found to compare well (typically within $1-2°\text{C}$) with the experimental data.

The model was then used to investigate industrial relevant geometries (Easter eggs). The impact of the injection of a warm filling was studied and its effect on the remelting of the chocolate already set. During the rapid cooling step (similar to the FrozenCone process), only a thin layer (to maintain the prescribed shape) of the shell is partially crystallised (typically 20% of the thickness) with *unstable* crystals (typically 10%) due to the high cooling rates. These *unstable* crystals transform into *stable* crystals later on during the process explaining the good quality of the final products, which contain only *stable* crystals at the end of the process.

In most food processes, a relationship between the time, the temperature and a structure parameter is an attractive opportunity to find equivalent processes leading to a similar structure. The model was therefore used to develop a rapid cooling process abacus ($t_f = f(\frac{x^2}{\Delta T})$, similar to Planck's original work) allowing the estimation of the processing time required for the rapid cooling step depending on the thickness of the shell and the temperature of the plunger. The use of this abacus could prove very useful in the future to expand the process to larger geometries.

Future work on this project could focus on blooming phenomena when the temperature is raised above the form V (*stable*) polymorph melting point. Indeed, if the model predicts an almost entirely *stable* chocolate at the end of the chocolate process modelled, there has been no validation of the resistance to bloom of this chocolate. This would require a shelf life study in controlled temperature conditions.

Moreover, the model could be extended to include more polymorphs, and further XRD study could use the subtraction method to differentiate the different polymorphs lumped in *stable* and *unstable*. This will allow a more detailed explanation of the phenomena occurring during the process.

In addition, the same approach would need to be applied to more formulations, including variations in fat content or fat composition, to be able to predict the processing conditions to apply to more confectionery products.

Finally, an interesting addition to the model would be a fluid dynamics application, where the flow properties of the fluid could be coupled with the phase change kinetics and the heat transfer equations. This would allow further understanding of the stability of the shells just after the application of the cold plunger.

APPENDIX A

MATLAB CODE FOR THE DSC MODEL FITTING

The ODE system is described 4.2 is described in the function `kineticsdsc.m`:

```
function [dXdt]=kineticsdsc(t,X,Ti,dTdt,K)
%The ODE system

T=Ti+dTdt*t;
X=real(X);
% Constants
Tms=21;
Tsm=28;
Tmu=10;
Tum=18;
Tus=25;
power=1/10;
% Kinetic parameters
Kms=K(1)./(1+exp(1*(T-Tms)));
Ksm=K(2)./(1+exp(1*(Tsm-T)));
Kmu=K(3)./(1+exp(1*(T-Tmu)));
```

```
Kum=K(4)./(1+exp(0.5*(Tum-T)));
Kus=K(5)./(1+exp(1*(Tus-T)));
Knuc=K(6).*(Tum-T).*((Tum-T>0));
% Equations
dXdt=[-Kms*X(1).^(2/2).*X(2).^power...
    -Kmu*X(1).^(2/2).*X(3).^power...
    +Ksm*X(2)+Kum*X(3)-Knuc.*X(1);...textcolorcomment %dm/dt
    -Ksm*X(2)...
    +Kms*X(1).*X(2).^power...
    +Kus*X(3).*X(2).^power;...textcolorcomment %ds/dt
    -Kum*X(3)...
    +Kmu*X(1).*X(3).^power...
    -Kus*X(3).*X(2).^power...
    +Knuc.*X(1)]; %du/dt
```

The heat source associated with the phase change is calculated using the built-in function `ode23.m` within the function `heatdsc.m`:

```
function [T,cpeff,X,endphase]=heatdsc(Ti,Tf,dT,dTdt,initphase,K)

tmax=(Tf-Ti)/dTdt;
dt=dT/dTdt;
T=Ti:dT:Tf;
% Integration of the ODE system
[t,X]=ode23(@kineticsdsc,[0:dt:tmax],initphase,[],Ti,dTdt,K);

X=real(X);

m=X(:,1);
```

```
s=X(:,2);
u=X(:,3);

endphase=[m(end);s(end);u(end)];

dmdt=[0;diff(m)/dt];
dsdt=[0;diff(s)/dt];
dudt=[0;diff(u)/dt];

cpm=1500;
cpsu=2000;
dhs=22000;
dhu=19000;
cp=cpsu*(s+u)+cpm*m;
% Evaluation of effective Cp
cpeff=(-sign(dTdt).*dsdt.*dhs./dTdt-sign(dTdt).*dudt.*dhu./dTdt)..
       +sign(dTdt).*cp;
```

Comparison with experimental data is provided by the function `dsc.m`:

```
function [ssq]=dsc(dTdt1,file1,dTdt2,file2,K)
%K=[0.005,0.06,0.08,0.06,10,0.0005]; % values for model
% Cooling
Ti=30;
Tf=-9.9;
dT=-0.01;
T=[];cr=[];cpeff=[];
initphase=[0.97,0.03,0];
[Tcool,cpeffcool,Xcool,endphasecool]=...
```

```
heatdsc(Ti,Tf,dT,dTdt1,initphase,K);
T=[T;Tcool’];
cr=[cr;ones(size(Tcool’))*i];
cpeff=[cpeff;cpeffcool];
% Heating
Ti=Tf;
Tf=39.9;
dT=0.1;
initphase=endphasecool;
[Theat,cpeffheat,Xheat,endphaseheat]=...
heatdsc(Ti,Tf,dT,dTdt2,initphase,K);
T=[Tcool Theat];
cpeff=[cpeffcool;cpeffheat];
X=[Xcool;Xheat];
% load of experimental data
data1=importdata(file1);
if isstruct(data1),
data1=data1.data;
end
Texp1=data1(:,1);
cpexp1=data1(:,2);
data2=importdata(file2);
if isstruct(data2),
data2=data2.data;
end
Texp2=data2(:,1);
cpexp2=data2(:,2);
Texp=[Texp1;Texp2];
```

```
cpexp1=interp1(Texp1,cpexp1,Tcool);
cpexp2=interp1(Texp2,cpexp2,Theat);
cpexp=[cpexp1';cpexp2']*1000;
%Sum of squares
ssq=sum((cpexp-cpeff).^4);
```

The error between the experimental and the predicted data for several cooling rates is calculated using the function `optimize.m`:

```
function [err]=optimize(K)

[ssq05]=dsc(-0.5/60,'cryst055.txt',5/60,'melt055.txt',K)
[ssq1]=dsc(-1/60,'cryst15.txt',5/60,'melt15.txt',K)
[ssq2]=dsc(-2/60,'cryst25.txt',5/60,'melt25.txt',K)
[ssq5]=dsc(-5/60,'cryst55.txt',5/60,'melt55.txt',K)
[ssq10]=dsc(-10/60,'cryst105.txt',5/60,'melt105.txt',K)
[ssq20]=dsc(-20/60,'cryst205.txt',5/60,'melt205.txt',K)
% Error between the model and the experimental data
err=mean([ssq05,ssq1,ssq2,ssq5,ssq10,ssq20])
```

The error calculated from `optimize.m` is minimized using the built-in function `fminbnd.m` within the script `scriptoptim.m`

```
% script to optimize the DSC model
% Minimisation of the error
Ki=[0.005,0.05,0.05,0.05,5,0.0001]; % initial value
% reference : [0.005,0.06,0.08,0.06,10,0.0005]
Ko=fmincon(@(K) optimize(K),Ki,[],[],[],[],...
   [0.001 0.001 0.001 0.001 0.001 0.00001],...
```

```
    [0.1 0.1 0.1 0.1 20 0.1])
```

APPENDIX B

MATLAB CODE FOR SOLVING THE EASTER EGG PROCESS USING THE FINITE ELEMENT METHOD IN COMSOL MULTIPHYSICS

The code used to described the overall Easter egg process is described in the following script:

```
% COMSOL Multiphysics Model M-file
flclear fem

% Geometry of the Easter egg shell
carr={curve2([0,0.0195,0.0195],[0,0,0.0195],...
  [1,0.7071067811865475,1]), ...
  curve2([0.0195,0.017],[0.0195,0.0195],[1,1]), ...
  curve2([0.017,0.017,0],[0.0195,0.0025,0.0025],...
  [1,0.7071067811865475,1]), ...
  curve2([0,0],[0.0025,0],[1,1])};
g1=geomcoerce(’solid’,carr);

```

```
% Constants
fem.const = {'Kms','0.005', ...
  'Ksm','0.06', ...
  'Kmu','0.08', ...
  'Kum','0.06', ...
  'Kus','10', ...
  'Knuc','0.0005', ...
  'Tref','273', ...
  'Tms','21+Tref', ...
  'Tsm','28+Tref', ...
  'Tmu','10+Tref', ...
  'Tum','18+Tref', ...
  'Tus','25+Tref', ...
  'Ti','30+Tref', ...
  'TFC','-10+Tref', ...
  'Ttunnel','12+Tref', ...
  'htunnel','30', ...
  'Text','23+Tref', ...
  'hext','7', ...
  'Trad','400+Tref', ...
  'power','1/10', ...
  'kliq','0.35', ...
  'ksol','0.25', ...
  'Cpliq','1500', ...
  'Cpsol','2000', ...
  'dHstable','22000', ...
  'dHunstable','19000', ...
  'rho','1300', ...
```

```
  'Cpfilling','2000', ...
  'kfilling','0.32', ...
  'rhofilling','1500', ...
  'Tfilling','35+Tref', ...
  'htunnelmould','22'};

% Global expressions
fem.globalexpr = {'kms','Kms./(1+exp(1*(T-Tms)))', ...
  'kus','Kus./(1+exp(1*(Tus-T)))', ...
  'ksm','Ksm./(1+exp(1*(Tsm-T)))', ...
  'kum','Kum./(1+exp(0.5*(Tum-T)))', ...
  'kmu','Kmu./(1+exp(1*(T-Tmu)))', ...
  'knuc','Knuc*(Tum-T).*((Tum-T>0))', ...
  'dsdt',['-ksm*stable+kms*melt*stable.^power' ...
          '+kus*unstable*stable.^power'], ...
  'dudt',['-kum*unstable+kmu*melt*unstable.^power' ...
          '-kus*unstable*stable.^power+knuc*melt'], ...
  'dmdt',['-kms*melt*stable.^power-kmu*melt*unstable.^power' ...
          '+ksm*stable+kum*unstable-knuc*melt'], ...
  'k','kliq*melt+ksol*(stable+unstable)', ...
  'Cp','Cpliq*melt+Cpsol*(stable+unstable)', ...
  'Q','rho_ht*(unstablet*dHunstable+stablet*dHstable)'};

% Analyzed geometry
clear s
s.objs={g1};
s.name={'CO1'};
s.tags={'g1'};
```

```

fem.draw=struct('s',s);
fem.geom=geomcsg(fem);

% Initialize mesh
fem.mesh=meshinit(fem, ...
                  'hauto',5, ...
                  'hmaxedg',[2,0.0001,4,0.0001]);

% (Default values are not included)

% Application mode 1
clear appl
appl.mode.class = 'HeatTransfer';
appl.mode.type = 'axi';
appl.module = 'CHEM';
appl.assignsuffix = '_ht';
clear bnd
bnd.type = {'q0','T','ax'};
bnd.T0 = {0,'TFC',0};
bnd.ind = [3,2,1,2];
appl.bnd = bnd;
clear equ
equ.C = 'Cp';
equ.init = 'Ti';
equ.k = 'k';
equ.Q = 'Q';
equ.rho = 'rho';
```

```
equ.ind = [1];
appl.equ = equ;
fem.appl{1} = appl;

% Application mode 2
clear appl
appl.mode.class = 'FlConvDiff';
appl.mode.type = 'axi';
appl.dim = {'stable'};
appl.assignsuffix = '_cd';
clear prop
clear weakconstr
weakconstr.value = 'off';
weakconstr.dim = {'lm2'};
prop.weakconstr = weakconstr;
appl.prop = prop;
clear bnd
bnd.type = 'N0';
bnd.ind = [1,1,1,1];
appl.bnd = bnd;
clear equ
equ.D = 0;
equ.init = 0.03;
equ.R = 'dsdt';
equ.ind = [1];
appl.equ = equ;
fem.appl{2} = appl;

```

```
% Application mode 3
clear appl
appl.mode.class = 'FlConvDiff';
appl.mode.type = 'axi';
appl.dim = {'unstable'};
appl.name = 'cd2';
appl.assignsuffix = '_cd2';
clear prop
clear weakconstr
weakconstr.value = 'off';
weakconstr.dim = {'lm3'};
prop.weakconstr = weakconstr;
appl.prop = prop;
clear bnd
bnd.type = 'N0';
bnd.ind = [1,1,1,1];
appl.bnd = bnd;
clear equ
equ.D = 0;
equ.R = 'dudt';
equ.ind = [1];
appl.equ = equ;
fem.appl{3} = appl;

% Application mode 4
clear appl
appl.mode.class = 'FlConvDiff';
appl.mode.type = 'axi';
```

```
appl.dim = {'melt'};
appl.name = 'cd3';
appl.assignsuffix = '_cd3';
clear prop
clear weakconstr
weakconstr.value = 'off';
weakconstr.dim = {'lm4'};
prop.weakconstr = weakconstr;
appl.prop = prop;
clear bnd
bnd.type = 'N0';
bnd.ind = [1,1,1,1];
appl.bnd = bnd;
clear equ
equ.D = 0;
equ.init = 0.97;
equ.R = 'dmdt';
equ.ind = [1];
appl.equ = equ;
fem.appl{4} = appl;
fem.sdim = {'r','z'};
fem.frame = {'ref'};
fem.border = 1;
fem.outform = 'general';
clear units;
units.basesystem = 'SI';
fem.units = units;

```

```
% ODE Settings
clear ode
clear units;
units.basesystem = 'SI';
ode.units = units;
fem.ode=ode;
% Multiphysics
fem=multiphysics(fem);

% Extend mesh
fem.xmesh=meshextend(fem);

% Solve problem
fem.sol=femtime(fem, ...
                'solcomp',{'T','unstable','stable','melt'}, ...
                'outcomp',{'T','unstable','stable','melt'}, ...
                'tlist',[0:0.1:3], ...
                'tout','tlist', ...
                'tsteps','strict', ...
                'complex','on');

% Save current fem structure for restart purposes
fem1=fem;

% (Default values are not included)

% Application mode 1
clear appl
```

```
appl.mode.class = ’HeatTransfer’;
appl.mode.type = ’axi’;
appl.module = ’CHEM’;
appl.assignsuffix = ’_ht’;
clear bnd
bnd.type = {’q0’,’q’,’ax’};
bnd.Tinf = {0,’Ttunnel’,0};
bnd.h = {0,’htunnel’,0};
bnd.ind = [3,2,1,2];
appl.bnd = bnd;
clear equ
equ.C = ’Cp’;
equ.init = ’Ti’;
equ.k = ’k’;
equ.Q = ’Q’;
equ.rho = ’rho’;
equ.ind = [1];
appl.equ = equ;
fem.appl{1} = appl;

% Application mode 2
clear appl
appl.mode.class = ’FlConvDiff’;
appl.mode.type = ’axi’;
appl.dim = {’stable’};
appl.assignsuffix = ’_cd’;
clear prop
clear weakconstr
```

```
weakconstr.value = 'off';
weakconstr.dim = {'lm2'};
prop.weakconstr = weakconstr;
appl.prop = prop;
clear bnd
bnd.type = 'N0';
bnd.ind = [1,1,1,1];
appl.bnd = bnd;
clear equ
equ.D = 0;
equ.init = 0.03;
equ.R = 'dsdt';
equ.ind = [1];
appl.equ = equ;
fem.appl{2} = appl;

% Application mode 3
clear appl
appl.mode.class = 'FlConvDiff';
appl.mode.type = 'axi';
appl.dim = {'unstable'};
appl.name = 'cd2';
appl.assignsuffix = '_cd2';
clear prop
clear weakconstr
weakconstr.value = 'off';
weakconstr.dim = {'lm3'};
prop.weakconstr = weakconstr;
```

```
appl.prop = prop;
clear bnd
bnd.type = 'N0';
bnd.ind = [1,1,1,1];
appl.bnd = bnd;
clear equ
equ.D = 0;
equ.R = 'dudt';
equ.ind = [1];
appl.equ = equ;
fem.appl{3} = appl;

% Application mode 4
clear appl
appl.mode.class = 'FlConvDiff';
appl.mode.type = 'axi';
appl.dim = {'melt'};
appl.name = 'cd3';
appl.assignsuffix = '_cd3';
clear prop
clear weakconstr
weakconstr.value = 'off';
weakconstr.dim = {'lm4'};
prop.weakconstr = weakconstr;
appl.prop = prop;
clear bnd
bnd.type = 'N0';
bnd.ind = [1,1,1,1];
```

```
appl.bnd = bnd;
clear equ
equ.D = 0;
equ.init = 0.97;
equ.R = ’dmdt’;
equ.ind = [1];
appl.equ = equ;
fem.appl{4} = appl;
fem.sdim = {’r’,’z’};
fem.frame = {’ref’};
fem.border = 1;
fem.outform = ’general’;
clear units;
units.basesystem = ’SI’;
fem.units = units;

% ODE Settings
clear ode
clear units;
units.basesystem = ’SI’;
ode.units = units;
fem.ode=ode;
% Multiphysics
fem=multiphysics(fem);

% Extend mesh
fem.xmesh=meshextend(fem);

```

```
% Solve problem
fem.sol=femtime(fem, ...
                'init',fem1.sol, ...
                'solcomp',{'unstable','T','stable','melt'}, ...
                'outcomp',{'unstable','T','stable','melt'}, ...
                'tlist',[0:10:10*60], ...
                'tout','tlist', ...
                'tsteps','strict', ...
                'complex','on');

% Save current fem structure for restart purposes
fem2=fem;

% Geometry of the filling
carr={curve2([0,0.017,0.017],...
  [0.0025000000000000005,0.0025,0.0195],...
  [1,0.7071067811865475,1]), ...
  curve2([0.017,0],[0.0195,0.0195],[1,1]), ...
  curve2([0,0],[0.0195,0.0025000000000000005],[1,1])};
g2=geomcoerce('solid',carr);

% Analyzed geometry
clear s
s.objs={g1,g2};
s.name={'CO1','CO2'};
s.tags={'g1','g2'};

fem.draw=struct('s',s);
```

```
fem.geom=geomcsg(fem);

% Initialize mesh
fem.mesh=meshinit(fem, ...
                  'hauto',5, ...
                  'hmaxedg',[4,0.0001,6,0.0001]);

% Application mode 1
clear appl
appl.mode.class = 'HeatTransfer';
appl.mode.type = 'axi';
appl.module = 'CHEM';
appl.assignsuffix = '_ht';
clear bnd
bnd.type = {'ax','q0','q','cont'};
bnd.Tinf = {0,0,'Ttunnel','Ttunnel'};
bnd.h = {0,0,'htunnel','htunnel'};
bnd.ind = [1,1,3,3,2,4];
appl.bnd = bnd;
clear equ
equ.C = {'Cp','Cpfilling'};
equ.init = {'Ti','Tfilling'};
equ.k = {'k','kfilling'};
equ.Q = {'Q',0};
equ.rho = {'rho','rhofilling'};
equ.ind = [1,2];
appl.equ = equ;
fem.appl{1} = appl;
```

```

% Application mode 2
clear appl
appl.mode.class = ’FlConvDiff’;
appl.mode.type = ’axi’;
appl.dim = {’stable’};
appl.assignsuffix = ’_cd’;
clear prop
clear weakconstr
weakconstr.value = ’off’;
weakconstr.dim = {’lm2’};
prop.weakconstr = weakconstr;
appl.prop = prop;
clear bnd
bnd.type = {’N0’,’cont’};
bnd.ind = [1,2,2,1,1,1];
appl.bnd = bnd;
clear equ
equ.D = {0,1};
equ.init = {0.03,0};
equ.R = {’dsdt’,0};
equ.usage = {1,0};
equ.ind = [1,2];
appl.equ = equ;
fem.appl{2} = appl;

% Application mode 3
clear appl
```

```
appl.mode.class = 'FlConvDiff';
appl.mode.type = 'axi';
appl.dim = {'unstable'};
appl.name = 'cd2';
appl.assignsuffix = '_cd2';
clear prop
clear weakconstr
weakconstr.value = 'off';
weakconstr.dim = {'lm3'};
prop.weakconstr = weakconstr;
appl.prop = prop;
clear bnd
bnd.type = {'N0','cont'};
bnd.ind = [1,2,2,1,1,1];
appl.bnd = bnd;
clear equ
equ.D = {0,1};
equ.R = {'dudt',0};
equ.usage = {1,0};
equ.ind = [1,2];
appl.equ = equ;
fem.appl{3} = appl;

% Application mode 4
clear appl
appl.mode.class = 'FlConvDiff';
appl.mode.type = 'axi';
appl.dim = {'melt'};
```

```
appl.name = 'cd3';
appl.assignsuffix = '_cd3';
clear prop
clear weakconstr
weakconstr.value = 'off';
weakconstr.dim = {'lm4'};
prop.weakconstr = weakconstr;
appl.prop = prop;
clear bnd
bnd.type = {'N0','cont'};
bnd.ind = [1,2,2,1,1,1];
appl.bnd = bnd;
clear equ
equ.D = {0,1};
equ.init = {0.97,0};
equ.R = {'dmdt',0};
equ.usage = {1,0};
equ.ind = [1,2];
appl.equ = equ;
fem.appl{4} = appl;
fem.sdim = {'r','z'};
fem.frame = {'ref'};
fem.border = 1;
fem.outform = 'general';
clear units;
units.basesystem = 'SI';
fem.units = units;

```

```
% ODE Settings
clear ode
clear units;
units.basesystem = 'SI';
ode.units = units;
fem.ode=ode;
% Multiphysics
fem=multiphysics(fem);

% Extend mesh
fem.xmesh=meshextend(fem);

% Mapping current solution to extended mesh
init = asseminit(fem,'init',fem2.sol,'xmesh',fem0.xmesh);

% Solve problem
fem.sol=femtime(fem, ...
                'init',init, ...
                'solcomp',{'T','unstable','stable','melt'}, ...
                'outcomp',{'T','unstable','stable','melt'}, ...
                'tlist',[0:0.0001:0.0001], ...
                'tout','tlist', ...
                'tsteps','strict', ...
                'complex','on');

% Save current fem structure for restart purposes
fem3=fem;

```

```
% Trick that replaces all zeros with Tfilling
a=fem3.sol.u;
b=a(:,1);
c=a(:,2);
ind=find(b==0);
c(ind)=35+273; % Tfilling
fem3.sol=femsol(c);


% Application mode 1
clear appl
appl.mode.class = ’HeatTransfer’;
appl.mode.type = ’axi’;
appl.module = ’CHEM’;
appl.assignsuffix = ’_ht’;
clear bnd
bnd.type = {’ax’,’q0’,’q’,’cont’};
bnd.Tinf = {0,0,’Ttunnel’,’Ttunnel’};
bnd.h = {0,0,’htunnel’,’htunnel’};
bnd.ind = [1,1,3,3,2,4];
appl.bnd = bnd;
clear equ
equ.C = {’Cp’,’Cpfilling’};
equ.init = {’Ti’,’Tfilling’};
equ.k = {’k’,’kfilling’};
equ.Q = {’Q’,0};
equ.rho = {’rho’,’rhofilling’};
equ.ind = [1,2];
```

```
appl.equ = equ;
fem.appl{1} = appl;

% Application mode 2
clear appl
appl.mode.class = ’FlConvDiff’;
appl.mode.type = ’axi’;
appl.dim = {’stable’};
appl.assignsuffix = ’_cd’;
clear prop
clear weakconstr
weakconstr.value = ’off’;
weakconstr.dim = {’lm2’};
prop.weakconstr = weakconstr;
appl.prop = prop;
clear bnd
bnd.type = {’N0’,’cont’};
bnd.ind = [1,2,2,1,1,1];
appl.bnd = bnd;
clear equ
equ.D = {0,1};
equ.init = {0.03,0};
equ.R = {’dsdt’,0};
equ.usage = {1,0};
equ.ind = [1,2];
appl.equ = equ;
fem.appl{2} = appl;

```

```
% Application mode 3
clear appl
appl.mode.class = 'FlConvDiff';
appl.mode.type = 'axi';
appl.dim = {'unstable'};
appl.name = 'cd2';
appl.assignsuffix = '_cd2';
clear prop
clear weakconstr
weakconstr.value = 'off';
weakconstr.dim = {'lm3'};
prop.weakconstr = weakconstr;
appl.prop = prop;
clear bnd
bnd.type = {'N0','cont'};
bnd.ind = [1,2,2,1,1,1];
appl.bnd = bnd;
clear equ
equ.D = {0,1};
equ.R = {'dudt',0};
equ.usage = {1,0};
equ.ind = [1,2];
appl.equ = equ;
fem.appl{3} = appl;

% Application mode 4
clear appl
appl.mode.class = 'FlConvDiff';
```

```
appl.mode.type = 'axi';
appl.dim = {'melt'};
appl.name = 'cd3';
appl.assignsuffix = '_cd3';
clear prop
clear weakconstr
weakconstr.value = 'off';
weakconstr.dim = {'lm4'};
prop.weakconstr = weakconstr;
appl.prop = prop;
clear bnd
bnd.type = {'N0','cont'};
bnd.ind = [1,2,2,1,1,1];
appl.bnd = bnd;
clear equ
equ.D = {0,1};
equ.init = {0.97,0};
equ.R = {'dmdt',0};
equ.usage = {1,0};
equ.ind = [1,2];
appl.equ = equ;
fem.appl{4} = appl;
fem.sdim = {'r','z'};
fem.frame = {'ref'};
fem.border = 1;
fem.outform = 'general';
clear units;
units.basesystem = 'SI';
```

```
fem.units = units;

% ODE Settings
clear ode
clear units;
units.basesystem = ’SI’;
ode.units = units;
fem.ode=ode;
% Multiphysics
fem=multiphysics(fem);

% Extend mesh
fem.xmesh=meshextend(fem);

% Mapping current solution to extended mesh
init = asseminit(fem,’init’,fem3.sol,’xmesh’,fem0.xmesh);

% Solve problem
fem.sol=femtime(fem, ...
                ’init’,init, ...
                ’solcomp’,{’T’,’unstable’,’stable’,’melt’}, ...
                ’outcomp’,{’T’,’unstable’,’stable’,’melt’}, ...
                ’tlist’,[0:10:10*60], ...
                ’tout’,’tlist’, ...
                ’tsteps’,’strict’, ...
                ’complex’,’on’);

% Save current fem structure for restart purposes
```

```
fem4=fem;

% (Default values are not included)

% Application mode 1
clear appl
appl.mode.class = 'HeatTransfer';
appl.mode.type = 'axi';
appl.module = 'CHEM';
appl.assignsuffix = '_ht';
clear bnd
bnd.type = {'ax','q','cont'};
bnd.Tinf = {0,'Ttunnel','Ttunnel'};
bnd.h = {0,'htunnelmould','htunnel'};
bnd.ind = [1,1,1,1,2,3];
appl.bnd = bnd;
clear equ
equ.C = {'Cp','Cpfilling'};
equ.init = {'Ti','Tfilling'};
equ.k = {'k','kfilling'};
equ.Q = {'Q',0};
equ.rho = {'rho','rhofilling'};
equ.ind = [1,2];
appl.equ = equ;
fem.appl{1} = appl;

% Application mode 2
clear appl
```

```
appl.mode.class = 'FlConvDiff';
appl.mode.type = 'axi';
appl.dim = {'stable'};
appl.assignsuffix = '_cd';
clear prop
clear weakconstr
weakconstr.value = 'off';
weakconstr.dim = {'lm2'};
prop.weakconstr = weakconstr;
appl.prop = prop;
clear bnd
bnd.type = {'N0','cont'};
bnd.ind = [1,2,2,1,1,1];
appl.bnd = bnd;
clear equ
equ.D = {0,1};
equ.init = {0.03,0};
equ.R = {'dsdt',0};
equ.usage = {1,0};
equ.ind = [1,2];
appl.equ = equ;
fem.appl{2} = appl;

% Application mode 3
clear appl
appl.mode.class = 'FlConvDiff';
appl.mode.type = 'axi';
appl.dim = {'unstable'};
```

```
appl.name = 'cd2';
appl.assignsuffix = '_cd2';
clear prop
clear weakconstr
weakconstr.value = 'off';
weakconstr.dim = {'lm3'};
prop.weakconstr = weakconstr;
appl.prop = prop;
clear bnd
bnd.type = {'N0','cont'};
bnd.ind = [1,2,2,1,1,1];
appl.bnd = bnd;
clear equ
equ.D = {0,1};
equ.R = {'dudt',0};
equ.usage = {1,0};
equ.ind = [1,2];
appl.equ = equ;
fem.appl{3} = appl;

% Application mode 4
clear appl
appl.mode.class = 'FlConvDiff';
appl.mode.type = 'axi';
appl.dim = {'melt'};
appl.name = 'cd3';
appl.assignsuffix = '_cd3';
clear prop
```

```
clear weakconstr
weakconstr.value = 'off';
weakconstr.dim = {'lm4'};
prop.weakconstr = weakconstr;
appl.prop = prop;
clear bnd
bnd.type = {'N0','cont'};
bnd.ind = [1,2,2,1,1,1];
appl.bnd = bnd;
clear equ
equ.D = {0,1};
equ.init = {0.97,0};
equ.R = {'dmdt',0};
equ.usage = {1,0};
equ.ind = [1,2];
appl.equ = equ;
fem.appl{4} = appl;
fem.sdim = {'r','z'};
fem.frame = {'ref'};
fem.border = 1;
fem.outform = 'general';
clear units;
units.basesystem = 'SI';
fem.units = units;

% ODE Settings
clear ode
clear units;
```

```
units.basesystem = 'SI';
ode.units = units;
fem.ode=ode;
% Multiphysics
fem=multiphysics(fem);

% Extend mesh
fem.xmesh=meshextend(fem);

% Solve problem
fem.sol=femtime(fem, ...
                'init',fem4.sol, ...
                'solcomp',{'unstable','T','stable','melt'}, ...
                'outcomp',{'unstable','T','stable','melt'}, ...
                'tlist',[0:10:10*60], ...
                'tout','tlist', ...
                'tsteps','strict', ...
                'complex','on');

% Save current fem structure for restart purposes
fem5=fem;
```

APPENDIX C

PUBLICATIONS OF THIS WORK

Peer reviewed articles

1. Le Révérend, B. J. D., Fryer, P. J. and Bakalis, S. Modelling crystallization and melting kinetics of cocoa butter in chocolate and application to confectionery manufacturing Soft Matter, 2009, 5, 891-902
2. Le Révérend, B. J. D., Fryer, P. J., Coles, S. and Bakalis, S. A method to qualify and quantify the crystalline state of cocoa butter in industrial chocolate Journal of the American Oil Chemists' Society, 2009, accepted, in press

Book Chapter

1. Le Révérend, B. J. D., Bakalis, S. and Fryer, P. J. in Aguilera, J. M. and Lillford, P. (ed.) Food Materials Science, Structured Chocolate Products, Springer, 2008, 525-547

Presentations and posters

1. Bakalis, S., Le Révérend, B. J. D. and Fryer, P. J. Crystallisation and phase change in chocolate, ZDS Shoko Teknik, 2007
2. Legros, A. Le Révérend, B. J. D., Pinschower, K., Bakalis, S., Wells, M. and Fryer, P. J. IUFoST Measurement of chocolate contraction during solidification IUFoST, 2007
3. Le Révérend, B. J. D., Bakalis, S. and Fryer, P. J. 98th AOCS Annual Meeting Computational Modelling of the Cooling Process during Chocolate Manufacturing, AOCS, 2007
4. Le Révérend, B. J. D., Bakalis, S. and Fryer, P. J. 99th AOCS Annual Meeting Computational Modelling of Chocolate Production, AOCS, 2008
5. Le Révérend, B. J. D., Bakalis, S., Smart, I. and Fryer, P. J. ISFRS 2009 Measuring and modeling the structure of chocolate ETH Zurich, 2009

LIST OF REFERENCES

Aasted, L. (2003) Method and apparatus for the production of shells of fat-containing, chocolate-like masses under pressure build-up, patent 1472229. http://www.patentstorm.us/patents/6641386/claims.html.

Aasted Microverk (NO DATE) **Tempermeter PC 2 Manual**. Aasted Microverk.

Afoakwa, E.O., Paterson, A., Fowler, M. et al. (NO DATE) Effects of tempering and fat crystallisation behaviour on microstructure, mechanical properties and appearance in dark chocolate systems. **Journal of Food Engineering**, In Press, Corrected Proof.

Aguilera, J.M., Michel, M. and Mayor, G. (2004) Fat migration in chocolate: diffusion or capillary flow in a particulate solid? -a hypothesis paper. **Journal of Food Science**, 69 (7): 167–174

Ali, A., Selamat, J., Man, Y.B.C. et al. (2001) Effect of storage temperature on texture, polymorphic structure, bloom formation and sensory attributes of filled dark chocolate. **Food Chemistry**, 72: 491–497

Alwis, A.A.P.D. and Fryer, P.J. (1990) A finite-element analysis of heat generation and transfer during ohmic heating of food. **Chemical Engineering Science**, 45 (6): 1547–1559

Anonymous (2008) Bragg's law. http://en.wikipedia.org/wiki/Bragg%27s_law.

Avrami, M. (1939) Kinetics of phase change. i general theory. **The Journal of Chemical Physics**, 7 (12): 1103–1112

Avrami, M. (1940) Kinetics of phase change. ii transformation-time relations for random distribution of nuclei. **The Journal of Chemical Physics**, 8 (2): 212–224

Avrami, M. (1941) Granulation, phase change, and microstructure kinetics of phase change. iii. **The Journal of Chemical Physics**, 9 (2): 177–184

Bassani, F., Liedl, G.L. and Wyder, P. (eds.) (2004) **Encyclopedia of Condensed Matter Physics**. Elsevier Academic Press.

Beckett, S.T. (1989) **Industrial chocolate: manufacture and use**. RSC publishing.

Beckett, S.T. (2002) **The Science of Chocolate**. RSC publishing.

Bimbenet, J.J. (2002) **Génie des procédés alimentaires. Des bases aux applications**, 1 ed. Dunod. chap. Lois de Fourier et de Fick, pp. 179–194

Bolliger, S., Breitschuh, B., Stranzinger, M. et al. (1998) Comparison of precrystallization of chocolate. **Journal of Food Engineering**, 35 (3): 281–297

Bolliger, S., Zeng, Y. and Windhab, E. (1999) In-line measurement of tempered cocoa butter and chocolate by means of near-infrared spectroscopy. **Journal of the American Oil Chemists' Society**, 76 (6): 659–667

Bragg, W. (1913) The structure of some crystals as indicated by their diffraction of x-rays. **Proceeding of the Royal Socitey of London Series A-Containing Papers**, 89 (610): 248–277

Bragg, W. (1923) The diffraction of x-rays with crystals. nobel reading. **Zeitshrift fur Physikalische Chemie–Stochiometrie**, 104 (5/6): 337–348

Bragg, W. (1929) Diffraction of x-rays by two-dimensional crystal lattice. **Nature**, 124: 125–125

Bragg, W. and Thomson, J. (1914) The diffraction of short electromagnetic waves by a crystal. **Proceeding of the Cambridge Philosophical Society**, 17: 43–57

Braipson-Danthine, S. and Deroanne, C. (2004) Influence of sfc, microstructure and polymorphism on texture (hardness) of binary blends of fats involved in the preparation of industrial shortenings. **Food Research International**, 37 (10): 941–948

Bricknell, J. and Hartel, R. (1998) Relation of fat bloom in chocolate to polymorphic transition of cocoa butter. **Journal of the American Oil Chemists' Society**, 75 (11): 1609–1615

Bubnik, Z., Kadlec, P. and Urban, D. (1995) **Sugar Technologists Manual**. Bartens, A.

Buchgraber, M., Androni, S. and Anklam, E. (2007) Determination of cocoa butter equivalents in milk chocolate by triacylglycerol profiling. **Journal of Agricultural and Food Chemistry**, 55 (9): 3284–3291

Buchgraber, M., Ulberth, F. and Anklam, E. (2004) Interlaboratory evaluation of injection techniques for triglyceride analysis of cocoa butter by capillary gas chromatography. **Journal of Chromatography A**, 1036 (2): 197–203

Carslaw, H.S. and Jaeger, J.C. (1986) **Conduction of Heat in Solids**, 2 ed. Oxford University Press, USA.

Cebula, D. and Smith, K. (1991) Differential scanning calorimetry of confectionery fats. pure triglycerides: Effects of cooling and heating rate variation. **Journal of the American Oil Chemists' Society**, 68 (8): 591–595

Chapman, G., Akehurst, E. and Wright, W. (1971) Cocoa butter and confectionery fats. studies using programmed temperature x-ray diffraction and differential scanning calorimetry. **Journal of the American Oil Chemists' Society**, 48 (12): 824–830

Chocovison (NO DATE) **Revolation 2 Manual**. Chocovison.

Davis, T.A. (2004) Algorithm 832: Umfpack v4.3—an unsymmetric-pattern multifrontal method. **ACM Trans. Math. Softw.**, 30 (2): 196–199

Davis, T.A. and Duff, I.S. (1997) An unsymmetric-pattern multifrontal method for sparse lu factorization. **SIAM Journal on Matrix Analysis and Applications**, 18 (1): 140–158

Davis, T.R. and Dimick, P.S. (1986) Solidification of cocoa butter. **Proc. PMCA Prod. Conf.**, 40: 104–108

Decloux, M. (2002) **Génie des procédés alimentaires. Des bases aux applications**, 1 ed. Dunod. chap. Crystallization, pp. 179–194

Dimick, P. and Manning, D. (1987) Thermal and compositional properties of cocoa butter during static crystallization. **Journal of the American Oil Chemists' Society**, 64 (12): 1663–1669

Duck, W. (1964) The measurement of unstable fat in finished chocolate. **The Manufacturing Confectioner**, 35 (6): 67–72

Edmondson, P., Grammatika, M., Fryer, P. et al. (2005) Modelling of heat transfer, mass transfer and flavour development in chocolate crumb. **Food and Bioproducts Processing**, 83 (2): 89–98

European Parliament (2000) **Directive 2000/36/EC of the European Parliament and of the Council of 23 June 2000 relating to cocoa and chocolate products intended for human consumption**.

evitherm (2008) Calorimetric methods. http://evitherm.athena.as/.

Fessas, D., Signorelli, M. and Schiraldi, A. (2005) Polymorphous transitions in cocoa butter - a quantitative DSC study. **Journal of Thermal Analysis and Calorimetry**, 82 (3): 691–702

Field-Museum (NO DATE) Chocolate - all about chocolate - history of chocolate. http://www.fieldmuseum.org/Chocolate/history.html.

Foubert, I. (2003) **Modelling isothermal cocoa butter crystallization: Influence of temperature and chemical composition**. Ph.D. thesis, University of Ghent.

Foubert, I., Dewettinck, K., Janssen, G. et al. (2006) Modelling two-step isothermal fat crystallization. **Journal of Food Engineering**, 75 (4): 551–559

Foubert, I., Dewettinck, K. and Vanrolleghem, P.A. (2003a) Modelling of the crystallization kinetics of fats. **Trends in Food Science and Technology**, 14 (3): 79–92

Foubert, I., Vanrolleghem, P., Thas, O. et al. (2004) Influence of chemical composition on the isothermal cocoa butter crystallization. **Journal of Food Science**, 69 (9): E478–E487

Foubert, I., Vanrolleghem, P.A. and Dewettinck, K. (2003b) A differential scanning calorimetry method to determine the isothermal crystallization kinetics of cocoa butter. **Thermochemica Acta**, 400: 131–142

Foubert, I., Vanrolleghem, P.A., Thas, O. et al. (2005) "96th aocs annual meeting." Salt Lake City, UT, USA.

Foubert, I., Vanrolleghem, P.A., Vanhoutte, B. et al. (2002) Dynamic mathematical model of the crystallization kinetics of fats. **Food Research International**, 35 (10): 945–956

Fourier, J.B.J. (1822) **Théorie analytique de la chaleur**. Paris: Firmin Didot.

Franke, K. (1998) Modelling the cooling kinetics of chocolate coatings with respect to final product quality. **Journal of Food Engineering**, 36 (4): 371–384

Gartling, D.K. and Reddy, J. (1994) **The Finite Element Method in Heat Transfer and Fluid Dynamics**, 1 ed. CRC-Press.

Guthrie, S.E., Mazzanti, G. and Idziak, S.H.J. (2005) X-ray phase identification of chocolate is possible without the removal of sugar. **European Journal of Lipid Science Technology**, 107: 656–659

Hartel, R.W. and Bricknell, J. (1998) Relation of fat bloom in chocolate to polymorphic transition of cocoa butter. **Journal of the American Oil Chemists' Society**, 75 (11): 1609–1616

Heiney, P. (2007) **DataSqueeze manual**.

Himawan, C., Starov, V.M. and Stapley, A.G. (2006) Thermodynamic and kinetic aspects of fat crystallization. **ECIC-XVII, XVIIth European Chemistry at Interfaces Conference, 27 June-1 July, 2005, Department of Chemical Engineering, Loughborough University**, 122 (1-3): 3–33

Hooft, R.W.W. (1998) **The Bruker AXS "Collect" program suite**. Bruker Nonius.

Hough, G., Moro, O. and Luna, J. (1986) Thermal conductivity and heat capacity of dulce de leche, a typical argentine dairy product. **Journal of Dairy Science**, 69 (6): 1518—1522

Huyghebaert, A. and Hendrickx, H. (1971) Polymorphism of cocoa butter, shown by differential scanning calorimetry. **Lebensmittel-Wissenschaft und-Technologie**, 4: 59–63

Incropera, F.P. and DeWitt, D.P. (2001) **Fundamentals of Heat and Mass Transfer**, 5th edition ed. John Wiley & Sons.

James, C., Ketteringham, L., Palpacelli, S. et al. (2009) **Predictive Modeling and RiskAssessment**. chap. Prediction of Heat Transfer During Food Chilling, Freezing, Thawing, and Distribution, pp. 55–78

Kloek, W., Walstra, P. and van Vliet, T. (2000) Crystallization kinetics of fully hydrogenated palm oil in sunflower oil mixtures. **Journal of the American Oil Chemists' Society**, 77 (4): 389–398

Kudasheva, D.S., Lai, J., Ulman, A. et al. (2004) Structure of carbohydrate-bound polynuclear iron oxyhydroxide nanoparticles in parenteral formulations. **Journal of Inorganic Biochemistry**, 98 (11): 1757–1769

Larsson, K. (1966) Classification of glyceride crystal forms. **Acta Chemica Scandinavia**, 20 (8): 2255–2260

Le Maguer, M. (1986) **Food Engineering and Process Applications: Transport Phenomena**. Elsevier Applied Science.

Le Révérend, B.J.D., Bakalis, S. and Fryer, P.J. (2008) **Food Materials Science**. Springer. chap. Structured Chocolate Products, pp. 525–547

Lees, R. and Jackson, E. (1979) **Sugar Confectionery and Chocolate Manufacture**, new impression ed. L.Hill.

Linkam Scientific Instruments Ltd (NO DATE) **Linksys 32 Control Software Manual**. Linkam Scientific Instruments Ltd.

Loisel, C., Keller, G., Lecq, G. et al. (1997a) Tempering of chocolate in a scraped surface heat exchanger. **Journal of Food Science**, 62 (4): 773–780

Loisel, C., Keller, G., Lecq, G. et al. (1998) Phase transitions and polymorphism of cocoa butter. **Journal of the American Oil Chemists' Society**, 75 (4): 425–439

Loisel, C., Lecq, G., Ponchel, G. et al. (1997b) Fat bloom and chocolate structure studied by mercury porosimetry. **Journal of Food Science**, 62 (4): 781–788

Lonchampt, P. and Hartel, R.W. (2004) Fat bloom in chocolate and compound coatings. **European Journal of Lipid Science and Technology**, 106: 241–274

Lonchampt, P. and Hartel, R.W. (2006) Surface bloom on improperly tempered chocolate. **European Journal of Lipid Science and Technology**, 108 (2): 159–168

Lovegren, N., Gray, M. and Feuge, R. (1976) Polymorphic changes in mixtures of confectionery fats. **Journal of the American Oil Chemists' Society**, 53 (2): 83–88

Lutton, E. (1950) Review of the polymorphism of saturated even glycerides. **Journal of the American Oil Chemists' Society**, 27 (7): 276–281

Malkin, T. and Meara, M.L. (1939) 22. an x-ray and thermal examination of the glycerides. part iv. symmetrical mixed triglycerides, ch(o[middle dot]cor[prime or minute])(ch2[middle dot]o[middle dot]cor)2. **Journal of the Chemical Society (Resumed)**, pp. 103–108

Mazzanti, G., Guthrie, S.E., Marangoni, A.G. et al. (2007) A conceptual model for shear-induced phase behavior in crystallizing cocoa butter. **Crystal Growth & Design**, 7 (7): 1230–1241

Mazzanti, G., Marangoni, A.G. and Idziak, S.H.J. (2005) Modeling phase transitions during the crystallization of a multicomponent fat under shear. **Physical Review**, 71 (041607): 1–12

Md.Ali, A. and Dimick, P. (1994) Thermal analysis of palm mid-fraction, cocoa butter and milk fat blends by differential scanning calorimetry. **Journal of the American Oil Chemists' Society**, 71 (3): 299–302

Merken, G.V. and Vaeck, S.V. (1980) Etude du polymorphisme du beurre de cacao par calorimétrie dsc. **Lebensmittel-Wissenschaft und-Technologie**, 13: 314–317

Metin, S. and Hartel, R.W. (2005) **Bailey's Industrial Oil and Fat Products**. John Wiley and Sons. chap. Crystallization of Fats and Oils, pp. 45–76

Min, D. (2008) The Ohio State University.

Nicolaï, B.M., Verboven, P. and Scheerlink, N. (2001) **Food Process Modelling**. chap. Modelling of heat and mass transfer, pp. 60–87

Ollivon, M. (2004) Chocolate, a mysteriously appealing food. **European Journal of Lipid Science and Technology**, 106: 205–206

Ozisik, M.N. (1994) **Finite Difference Methods in Heat Transfer**, 1 ed. CRC-Press.

Perkin Elmer (1987) **DSC 7 Manual**. Perkin Elmer.

Pham, Q. (1984) Extension to planck's equation for predicting freezing times of foodstuffs of simple shapes. **International Journal of Refrigeration**, 7 (6): 377–383

Rousseau, D. and Smith, P. (2008) Microstructure of fat bloom development in plain and filled chocolate confections. **Soft Matter**, 4 (8): 1706–1712

Sato, K. (2001) Crystallization behaviour of fats and lipids - a review. **Chemical Engineering Science**, 56: 2255–2265

Schenk, H. and Peschar, R. (2004) Understanding the structure of chocolate. **Radiation Physics and Chemistry**, 71 (3-4): 829–835

Seguine, C.S. (1991) Tempering-the inside story. **Manufacturing Confectioner**, pp. 117–125

Sonoda, T., Takata, Y., Ueno, S. et al. (2004) Dsc and synchrotron-radiation x-ray diffraction studies on crystallization and polymorphic behavior of palm stearin in bulk and oil-in-water emulsion states. **Journal of the American Oil Chemists' Society**, 81 (4): 365–373

Stapley, A.G.F., Tewkesbury, H. and Fryer, P.J. (1999) The effects of shear and temperature history on the crystallization of chocolate. **Journal of the American Oil Chemists' Society**, 76 (6): 677–685

Steiner, U. (2003) Production of consumable shell-shaped articles from a fatty material containing cacao or a chocolate-type substance patent wo/2004/068963. http://www.wipo.int/pctdb/en/wo.jsp?wo=2004068963.

Szydlowska-Czerniak, A., Karlovits, G., Lach, M. et al. (2005) X-ray diffraction and differential scanning calorimetry studies of beta' to beta transitions in fat mixtures. **Food Chemistry**, 92: 133–141

Tewkesbury, H., Stapley, A.G.F. and Fryer, P.J. (2000) Modelling temperature distributions in cooling chocolate moulds. **Chemical Engineering Science**, 55 (16): 3123–3132

Tremeac, B., Datta, A.K., Hayert, M. et al. (2007) Thermal stresses during freezing of a two-layer food. **International Journal of Refrigeration**, 30 (6): 958–969

Vaisey-Genser, M., Vane, B.K. and Johnson, S. (1989) Graininess, crystal size and firmness of stored canola oil margarines. **Journal of Texture Studies**, 20 (3): 347–361

van Boekel, M.A.J.S. and Tijskens, L.M.M. (2001) **Food Process Modelling**. chap. Kinetic modelling, pp. 35–60

Walter, P. and Cornillon, P. (2001) Influence of thermal conditions and presence of additives on fat bloom in chocolate. **Journal of the American Oil Chemists' Society**, 78 (9): 927–932

Wichchukit, S., Zorrilla, S.E. and Singh, R.P. (2001) Contact heat transfer coefficient values during double-sided contact cooking of hamburger patties. **Journal of Food Processing and Preservation**, 25 (3): 207–221

Wille, R. and Lutton, E. (1966) Polymorphism of cocoa butter. **Journal of the American Oil Chemists' Society**, 43 (8): 491–496

Yasuyoshi, K. and Hartel, R.W. (2008) "99th aocs annual meeting." Seattle, WA, USA: AOCS.